FINITE ELEMENT ANALYSIS OF ELASTIC BEHAVIOR OF SUCTION CAISSON

A Dissertation

by

YUZE ZHANG

Submitted to the Office of Graduate and Professional Studies of
Texas A&M University
in partial fulfillment of the requirements for the degree of

DOCTOR OF PHILOSOPHY

Chair of Committee,	Charles P. Aubeny
Committee Members,	Zenon Medina-Cetina
	Marcelo Sanchez
	Jerome Schubert
Head of Department,	Robin Autenrieth

August 2016

Major Subject: Civil Engineering

ABSTRACT

As the demand on energy increases rapidly, exploration and production in deep water and facilities in shallow water are in imperative need. Suction caissons are most commonly used as anchoring system for offshore floating structures and are used as foundations for coastal wind turbines in relatively shallow water. For a long time, suction caisson loaded in soft clay such as in Gulf of Mexico are considered rigid due to the stiffness being stronger than soft clay.

The objective of this study is to investigate the elastic behavior of suction caissons in soft clay. A new 3-D finite element analysis method using coupled caisson-springs model is introduced. The properties of springs are developed based on a 2-D continuum finite element analysis and scaled to 3-D scenario. Computer program ABAQUS is used for the numerical analysis for the coupled caisson-springs model.

Results show that elastic behavior of caissons is quite different with a rigid caisson particularly under small displacement. Taking the advantage of the newly developed model, the structural response of the caisson is also assessed.

ACKNOWLEDGEMENTS

I would like to express my sincere thanks to Dr. Aubeny for his kind advice and guidance throughout the research. I would especially like to thank him for bringing me to this offshore wind tower project, and leading me into the field of finite element study of offshore caisson foundations.

I would also extend my gratitude to Dr. Medina-Cetina and Dr. Sanchez for their comments and feedbacks throughout the course of this research.

Thanks also go the staff of the supercomputing facility for their continuing support.

Finally, special thanks to my parents for their unconditional support, and my wife, Beibei Dong, for her encouragement, patience and love.

TABLE OF CONTENTS

Page

LIST OF FIGURES

LIST OF TABLES

CHAPTER I

INTRODUCTION

Background

With the increasing demand of energy, exploring the offshore is becoming a necessity to maintain the energy consumption. As a result, offshore structures have developed for over 70 years to cope with this increasing demand. The early offshore structures were designed as fixed structures which the top was supported by the steel jacket, or concrete gravity base, founded on the seabed (Figure 1a). These fixed structures are typically used at water depth less than 350 m. Compliant tower, another type of fixed structure, which can tolerate larger horizontal deformations, can make them feasible for water depth up to 600 m.

As water depth keeps increasing, fixed structure will not be economical because of its increased substructure loads and high material cost. In this case, floating structure is a better option to accommodate greater water depth. In such system, the structure is floating at the sea surface, and stabled by steel cables connected to anchors founded in seafloor. Current applications are used in mooring for tension leg platform (TLP), semisubmersible, spars, and so on (Figure 1b).

No matter what types of structures are used, they all need to be fixed on the soil by anchors to sustain the loadings from waves, currents, winds, etc. Typical anchors used for stabilization include piles, suction caissons, and drag anchors. This research is focusing on the behavior of suction caisson.

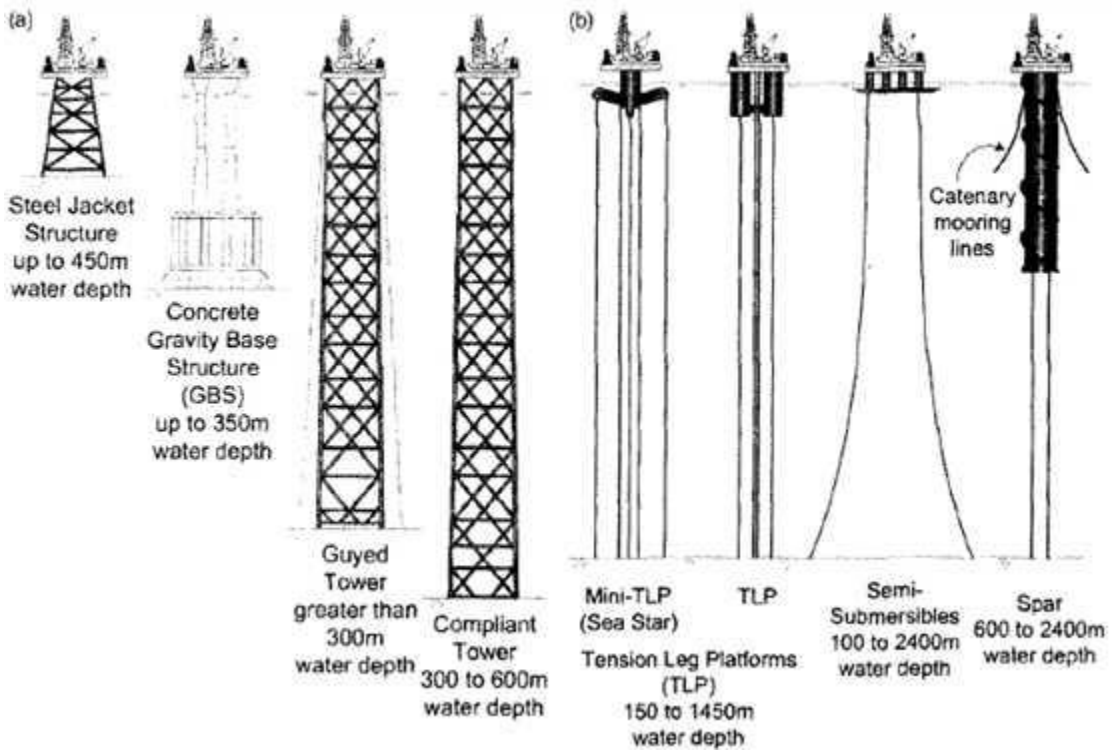

Figure 1.1 (a) Fixed structure; (b) Floating structures (Schneider & Senders, 2010)

The Concept of Suction Caissons

Caissons are large cylindrical structures (Figure 2), serviced as foundations or mooring anchors. They are constructed with the top sealed with valve-controlled vent, and the bottom open. They have been reported to apply in both sands and clay, with different aspect ratio from less than one to ten. The advantages of suction caisson foundation include larger capacity than embedded anchors, less seafloor disturbance, being able to reuse. From installation point of view, they require lower cost of manufacturing and installation equipment, and more time efficient. The installation of

the caisson can generally completed by two steps. Initially, the caisson is set vertically, partially penetrated into the seafloor driven by its own weight with the vent open. Then, a suction is applied within the caisson to force the water out through the valve, and cause the caisson to sink further until the full penetration achieved. After installation and prior to loading in service, it has to need a period of time for the surrounding soil that is disturbed during installation to regain the strength. Then, caisson is connected to structure from the top or side of the caisson.

Figure 1.2 Suction Caissons (Delmar)

Problem Statement

Many studies have been conducted to investigate the load capacity of suction caisson. Luke et al. (2003) carried ten pullout tests in the normally consolidated kaolinite to quantify the axial capacity of caisson, and found the axial capacity was considerably

larger in the vent sealed case. A simplified theory for predicting the axial capacity of suction caisson was developed by Houlsby et al. (2005). Vásquez et al. (2010) conducted a numerical study of the caisson axial capacity and resulted in a good agreement with the laboratory tests, except the pore water pressure measured near the caisson tip, which may be caused by the insufficiently fine mesh. Clukey and Morrison (1993) reported based on the combined centrifuge test and analytical study that the uplift capacity is contributed by the suction at the bottom of the caisson. Coffman et al. (2004) conducted nine horizontal load tests in the normally consolidated clay, and found that the maximum horizontal capacity occurred when the loading points were at two-thirds and three-quarters of the embedded length. Villalobos et al. (2009) conducted an experimental test using a three-degree-of-freedom loading rig to investigate the caisson response under combined loads with low vertical loads, and found that the moment and/or horizontal capacity can be mobilized under tensile loads. A simplified analytical solution of estimating horizontal capacity of suction caisson was presented by Aubeny et al. (2003) using an upper bound plasticity formulation. Gong et al. (2011) conducted a three dimensional elasto-plastic finite element analysis of caisson under combined vertical-horizontal-torsional (V-H-T) loads, and found that the bearing capacity in V-T and H-T spaces increased with aspect ratio.

In spite of numerous researches conducted in the suction caisson behavior, very little was focused on investigations of the compliance effect on the load-displacement relationship, particularly for the relatively small displacement. In addition, from the structural perspective, soil reaction stresses along the caisson are always the practical

information that structural engineers would need in the caisson design, and hope to get from geotechnical engineers. However, little was studied on this since geotechnical researches are always focusing on the ultimate capacity.

Research Scope

Traditionally, for pile analysis, beam-column methodology captures elastic behavior due to bending moments but neglects the cross-section deformation, or called ovalization. The traditional pile analysis can be simulated by a single spring connected to the pile capturing capacity as shown in Figure 1.3 (a), but cannot capture the response around the caisson. This study fills this gap by modeling the caisson connected to springs around the caisson circumference as illustrated in Figure 1.3 (b). The purpose of this research is to investigate the elastic behavior on the load-displacement relationship characterize circumferential response like deformation and soil stress, and assess the caisson structural response by a new methodology of a 3-D finite element analysis which greatly increase the time efficiency.

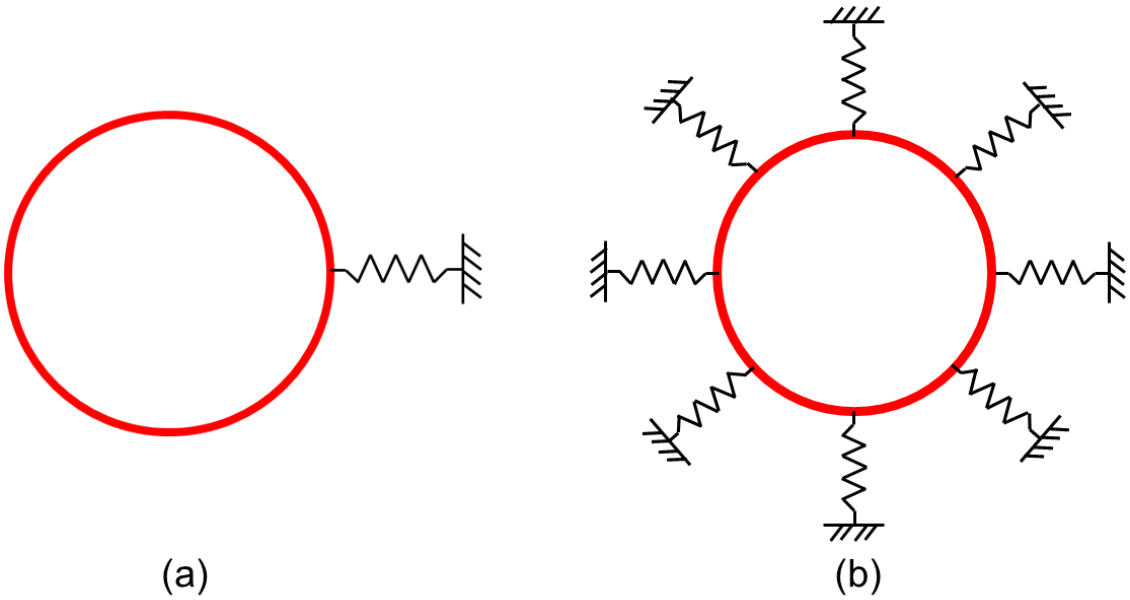

Figure 1.3 (a) Traditional beam-column single spring analysis; (b) Caisson-springs model

This dissertation investigates the above problems using Finite Element Methods to simulate caisson and soil responses. The soil is modeled by soil springs based on the 2-D finite element analysis, and is representative of soil profile from the Gulf of Mexico. The studies are conducted for caissons with aspect ratio of 5 and 3 and with rigid and flexible caisson, under loadings at different load attachment points. The objective is to study elastic behavior of caisson capacity and structural response of caisson.

Organization

There are six chapters in this dissertation, including the introduction in this chapter, and are organized as follows: literature review with brief caisson history,

installation of caisson, and previous work in both experimental and numerical researches in Chapter II; the fundamentals of mechanics in Chapter III; the methodology of soil spring development in Chapter IV; the results and discussions of finite element study are discussed in Chapter V; and finally the conclusions and recommendations in Chapter VI.

CHAPTER II

LITERATURE REVIEW

Suction caissons, also referred as to suction anchors, suction piles, suction buckets, and bucket foundations. A suction caisson is an upturned circular bucket embedded in soils, typically applied as a foundation to sustain the large tensional and lateral loadings due to currents and waves that is beyond the capability of gravity foundation. It is a new form of offshore foundation that has a number of advantages over the traditional driven pile foundation, mainly due to its easy installation process and capability of removal and reuse. It is investigated by many researchers, and applied for the first time in the North Sea in 1981. Its development is prompted by the oil and gas exploration in the great water depth in mid 1980s. Up to 2002, there are recorded 485 suction caissons installed in over 50 different places around the world in the depth up to 2000 m. From then on, the use of suction caissons is rising rapidly.

Caisson History

The concept of suction caisson was initially the anchor used to immobilize mobile military field equipment by applying the vacuum. It was first introduced in the literature by Goodman et al. (1961), and performed excellent anchorage in clays and silts. Brown and Nacci (1971) verified the feasibility of vacuum anchors on sand using large-scale model test (10 inch OD). After that, under the background of proliferation of offshore oil industry, there were a lot of researches conducted on capacity of suction

anchors on different soils in 1970s' and 1980s' including Bemben et al. (1973), Wang et al. (1975, 1977, 1978), Helfrich et al. (1976), Wilson (1978), Wilson et al. (1980), Hogervorst (1980), and Sahota and Wilson (1982).

Hogervorst (1980) first conducted full-scale test on suction caisson to evaluate both the suction emplacement and the load carrying capacities in sand and hard clay. Suction caissons of 3.8 m diameter and between 5 to 10 m long were tested. The study demonstrated that the suction method was feasible in both sand and clay, and that the carrying capacities could be reasonably accurately predicted. Hogervorst also concluded that the competitiveness of suction caisson increased rapidly over traditional driven piles in deep water.

The first commercial application of suction caisson was the installation of twelve caisson for Shell in Gorm field, North Sea in 1981, and was reported by Senepere and Auvergne in 1982. The suction caissons were serviced as Catenary Anchors Leg Mooring (CALM) to secure buoy devices, and installed on soils consisting of 6 m sand layer underlain by 1 to 2 m soft clay then by stiff clay at a water depth of 40 m. This installation required only light craft, and demonstrated the high reliability of suction piles. The authors also concluded that the suction pile was a proven alternative to traditional driven piles.

Large-scale offshore test of suction piles used for foundation of the Gulfaks C gravity platform was reported by Tjelta et al., 1986. The test structure, consisting of two steel cylinders with length of 23 m and diameter of 6.5 m, attached to each other by concrete panel, was penetrated 22 m into clay at more than 200 m water depth. The test

proved the feasibility of penetrating long concrete skirts into soft to still clay by dead weight and suction.

Installation of Caissons

Suction caissons can be installed in a great variety of soil condition and in a wide range of water depth. Installation of suction caissons is considered easier and less costly than the pile driving. Installation equipment typically ranges from pre-installed pump-modules on the anchor with an umbilical cord running back to the installation vessel to simpler Remotely Operated Vehicles (ROV) mounted and operated equipment with a minimum of monitoring equipment (Tjelta, 2001). Close monitoring and predefined project specifications are required to achieve successful installation and satisfactory performance.

Installation Techniques

Suction caissons can be either lift-installed from crane vessels or launched over the stern of an Anchor Handler Tug (Tjelta, 2001). Crane vessels can lift the caisson vertically, and apply the installation. Crane vessels can be load with a large number of caisson and do no need assistant vessels; however, the daily cost is high (Sparrevik, 1998). When an Anchor Handler Tug is used, the caisson is skidded horizontally off the stern of the tug, and deployed and oriented by an assistant vessel. This method limits the number of caisson installation per trip. Availability of installation vessels, logistics, and

cost rather than the anchor itself will often dictate which installation method is preferred (Tjelta, 2001).

It is important to realize that project specification may have a significant impact on installation technique and monitoring philosophy (Tjelta, 2001). A very strict installation criteria will require more instrumentation and data acquisition equipment. The parameters monitored typically includes: position, orientation and tile, penetration depth, and pressure difference between inside and outside of the caisson (Sparrevik, 1998, Colliat et al., 1998, Dendani and Colliat, 2002, El-Gharbawy et al., 1999, and Audibert et al., 2003). Some other parameter may also be monitored, such as water flow rate through the pump (Audibert et al., 2003), total pressure (Colliat et al., 1998), and clearance inside the caisson (Colliat et al., 1998).

Installation tolerances have an impact on caisson holding capacity. General guidelines for tolerance are ± 10° on tilting and ± 10° on heading (Sparrevik, 1998, Dendani and Colliat, 2002). A 5°-10° limitation on both tilting and heading are suggested by Tjelta, 2001. A ± 5° tolerance on both tilting and heading are reported in Na Kika Floating Development System located in the Mississippi Canyon Area of the Gulf of Mexico (Newlin, 2003).

Penetration Resistance

The penetration resistance of the caisson is the sum of skin and tip resistance. The calculation of the penetration resistance should be based on the soil measurement obtained from in-situ testing. However, there remain some uncertainties in converting

resistance from one case to another due to the differences in caisson geometry, soil properties, penetration rate, etc. (Hogervorst, 1980). Hogervorst (1980) assumed that the internal and external frictions are equal, and used the following formula to estimate the penetration resistance:

$$R = \pi D\left(2k_f \int_0^h f dz + k_p \bar{q}_{ch} t \right) \quad \text{.....(2.1)}$$

where,

D=diameter of pile

k_f=empirical coefficient relating f to skin friction

f=local friction as measured by the penetrometer

h=penetrated depth

k_p=empirical coefficient relating q_c to end resistance

$\bar{q}_{ch}$=average cone resistance of identified strata

t=thickness of pile rim

Andréasson et al. (1988) conducted five model tests with a seven-cell model foundation in soft clay in the vicinity of Gothenburg. The authors reported a bearing capacity factor of 7, and friction factor ranging from 0.2 to 0.4 applied to the fall cone shear strength of 15 kPa. The higher penetration rate of 20 to 30 mm/min fell close to lower friction factor while the slower penetration rate of 3 mm/min resulted in higher friction factor of 0.4.

Colliat et al. (1998) reported a field model penetration test with a 1.37 m diameter and 5 m long caisson at the Nkossa site in the Gulf of Guinea. The soil profile

consisted of sandy clay underlain by normally consolidated clay. The undrained shear strength of soil was determined by unconsolidated and undrained UU triaxial test. The adhesion factor α was found to be 0.3. The authors also reported a full scale test with a diameter between 4 m to 5 m, and length between 12.3 m to 13 m. The measured penetration resistances were in perfect agreement with the predicted range of resistance.

Whittle and Germaine (1998) conducted laboratory tests on normally consolidated Boston Blue Clay using the Caisson Element Test (CET) cell. The CET cell comprised a miniature cylindrical caisson with an outside diameter of 5.1 cm and a wall thickness of 0.15 cm. The model had separate caisson cap and wall that allowed the independent measurement of displacement and load on caisson cap and wall. The caisson was installed at a constant rate of δ_w=0.3 mm/min. The measured wall force increased almost linearly after the tip penetration of 0.7 cm, and was described by the following:

$$F_w=F_0+f_w'\delta_w \quad \text{.....(2.2)}$$

where,

F_w=wall force

F_0=10.3±0.2 kg

f_w'=1.45±0.2 kg/cm

The intercept F_0 was used to calculate the bearing capacity factor N_c. The bearing capacity factor was calculated to be 16.3 assuming an undrained shear strength ratio from triaxial compression of S_{uTC}/σ_{vc}'=0.32. The slope f_w' was used to calculate the skin friction factor β. The skin friction factor was calculated to range from 0.053 to 0.071.

House and Randolph (2001) conducted a series of centrifuge model tests with smooth-sided and internally stiffened caisson in normally consolidated and over-consolidated clay. House and Randolph proposed the following theoretical equation to calculate the underpressure for installing stiffened caisson:

$$\Delta p_{caisson} = \frac{\left(N_c S_u + \gamma' l\right)A_{tip} + \alpha_e \overline{S_u} A_e - W_{cais} + F_q + F_\tau}{A_{plug}} \quad \text{.....(2.3)}$$

where,

$\Delta p_{caisson}$=theoretical installation pressure

N_c=bearing capacity factor

S_u=undrained shear strength

γ'=effective unit weight of soil

l=embedded caisson length

A_{tip}=tip area of caisson

A_{plug}=cross sectional area of soil plug

A_e=external area of caisson shaft in contact with soil

α_e=external skirt friction factor

W_{cais}=submerged caisson weight

F_q=total stiffener bearing resistance

F_τ=total stiffener internal frictional resistance

They concluded that there was little difference for required underpressure for installing the stiffened and smooth caisson. They also concluded that the lower measured resistance of stiffened caisson compared to the theoretical estimation was due to the

possible incomplete soil flow around the stiffener. The caisson installation were modeled well by applying an average factor of 0.4 on inside and outside of the caisson. They also indicated that the internal friction is lower than the external friction based on analyses of the plug stability during pullout of a caisson with no setup time.

Cao et al. (2002) conducted eight centrifuge tests for suction caissons in kaolin clay. The caisson was first penetrated under its self-weight, and then an active suction was applied at the top of caisson after a time period (5 to 20 seconds). The penetration resistance was monitored and recorded for both stages. The friction coefficient α was then back calculated with the following equations for self-weigh penetration stage and suction penetration stage:

Self-weight stage: $\alpha_{sw} = \left(C_{sw} - LCR - \left(N_c S_u + \gamma' h\right)A_t\right)/\left(\overline{S_u} A_s\right)$ .....(2.4)

Suction stage: $\alpha_s = \left(C_{sw} + S - LCR - \left(N_c S_u + \gamma' h\right)A_t\right)/\left(\overline{S_u} A_s\right)$.....(2.5)

where,

α_{sw}=friction coefficient at self-weight stage

α_s=friction coefficient at suction stage

C_{sw}=submerged weight of the caisson

LCR=load cell reading

N_c=bearing capacity factor

S_u=undrained shear strength of clay

γ'=buoyant unit weight of the soil

h=penetration depth

A_t=annular base area of steel at the base of the caisson

A_s=total surface area along the caisson's wall

The authors found that the average friction coefficient during self-weight stage decreased from about 0.6 at the mudline to about 0.15 at 160 mm. This reduction indicated that the rate of soil resistance increase with depth was lower than the rate of soil shear strength increase. This may be caused by the disturbance of the surrounding soil over the penetration process. The friction coefficient during suction stage increased from about 0.15 at 160 mm to about 0.27 over the penetration depth when suction was applied. This was believed to be due to the active suction on the soil inside the caisson and/or the soil-caisson set-up that occurred during the time period between the end of penetration stage and the beginning of suction application.

Newlin (2003b) reported the installation performance of Na Kika suction piles in the Mississippi Canyon Area of the Gulf of Mexico. The penetration resistance was predicted using the adhesion factor α, which was defined as the inverse of the soil sensitivity. The upper bound and lower bound sensitivities were taken as the average and 95 percent non-exceedance sensitivities obtained from laboratory tests and were 2.35 and 3.55 respectively. The corresponding α factor ranges from 0.28 to 0.43. The measured underpressure was reported to concur with the predicted range.

Rauch et al. (2003) conducted 17 laboratory tests in normally consolidated kaolinite to study the installation resistance. The caisson was made with a anodized aluminum tube with a 0.81 mm thickness, a 100 mm diameter, and a 910 mm length. Seven installations were inserted completely using dead weight, and ten others were inserted using dead weight to about one-fourth of the length, followed by insertion to full

depth using an applied suction. The total resistance was directly measured. The end bearing resistance was estimated from the following formula assuming a shape factor of 1.0 and a maximum depth factor of 1.5:

$$Q_t=(7.7S_u+\sigma_v)A_t \quad (2.6)$$

where,

Q_t=end bearing resistance

S_u=undrained shear strength

σ_v=total vertical stress

A_t=cross sectional area of the caisson tip

The friction resistance on exterior and interior caisson wall was then calculated by subtracting the end bearing force from the total resistance. The corresponding average friction factor α was calculated from the following formula:

$$\alpha = \frac{Q_{soil} - Q_t}{(A_{si} + A_{se})S_{u,avg}} \quad (2.7)$$

where,

Q_{soil}=total soil resistance

A_{si}=interior surface area of caisson in contact with the soil

A_{se}=exterior surface area of caisson in contact with the soil

$S_{u,avg}$=average undrained shear strength

For dead weight installation, α averaged 0.22; with suction insertion, α averaged 0.28. The mechanism for the increased resistance during suction installation was not

clear and may result from multiple effects. One possible explanation was that suction may cause more soil enter the interior of the caisson than would occur during dead weight insertion. Thus, the disturbance on the outside may be diminished and significant amounts of consolidation may have occurred to cause increased exterior effective stresses.

Chen and Randolph (2004) conducted a series of centrifuge tests on caissons in normally consolidated clay. The caissons were installed by jacking and by suction, and the results were compared. The penetration resistance during installation was expressed as:

$$A_{base}\Delta p = \sum_{i=1}^{n}\left(N_{ci}S_{ui} + z_i\gamma'\right)A_{tip_i} + \alpha\bar{S}_u\left(A_{ext} + A_{i-b}\right) + \tau_{i-a}A_{i-a} \quad \text{.....(2.8)}$$

where,

A_{base}=gross cross sectional area of the caisson

Δp=net installation pressure applied

N_{ci}=bearing capacity factor for i^{th} surface

S_{ui}=local undrained shear strength for i^{th} surface

γ'=effective unit weight of soil

z_i=embedded depth of i^{th} surface

A_{tipi}=area of bearing surface (caisson tip or stiffener)

A_{ext}=external area of caisson shaft in contact with soil

$A_{i\text{-}b}$=internal area of the caisson shaft in contact with soil

$A_{i\text{-}a}$=area of internal shaft above upper edge of pad-eye stiffener

τ_{i-a}=nominal friction of 0.5 kPa for internal shaft above pad-eye

α=interface friction factor

By applying a bearing capacity factor of N_c of 7.5, and the above formula, the friction factor α could be back calculated. The estimated friction factors were very similar with the similar clay shear strength installed by jacking and by suction. An average value of 0.39 was reported for the former and 0.36 for the later, respectively. In general, the friction factor varied from 0.3 to 0.45 for normally consolidated clay, with an average value of 0.37. The authors also found that there was no essential difference between penetration resistance by jacking and by suction.

Penetration Limits

In soft clays, long caisson is preferred to provide sufficient capacity. Increasing penetration depth leads to higher side friction, tip resistance, and thus higher capacity due to the increasing soil strength with depth. In addition, high aspect ratio caisson is easier to handle, more robust (Tjelta, 2001), and thus is economical to have large depth to diameter ratio (Andersen et al., 2005).

During the caisson installation, the initial penetration is determined by the submerged self-weight of the caisson. The additional penetration will be achieved by applying a pressure difference at the top of the caisson. The underpressure required to advance the caisson can be calculated by equating the total thrust and the penetration resistance. The required underpressure can therefore be formulated as:

$$\Delta p_{caisson} = \frac{\left(N_c S_u + \gamma' l\right) A_{tip} + \alpha_e \overline{S_u} A_e - W_{cais}}{A_{plug}} \quad \text{.....(2.9)}$$

However, if the applied pressure exceeds a certain limit, the soil plug failure occurs inside the caisson, and no more penetration can be achieved. Andersen et al. (2005) presented the allowable underpressure with respect to large soil heave by bearing capacity consideration:

$$\Delta u_a = N_c S_{u,tip}^{av} + A_{inside} \alpha S_u^{D\bar{S}S} / A_{in} \quad \text{.....(2.10)}$$

where,

N_c=bearing capacity factor

$S_{u,tip}^{av}$ =average undrained shear strength at skirt tip level

A_{inside}=inside skirt wall area

α=adhesion factor, assumed equal to the inverse of the sensitivity of the soil

$S_{u,tip}^{av}$ =average direct simple shear strength over penetration depth

A_{in}=plan view inside area where underpressure is applied

The ratio of A_{inside}/A_{in} is proportional to the caisson aspect ratio. Therefore, besides the bearing capacity factor, adhesion factor, and soil strength, the allowable underpressure is also a function of aspect ratio.

Allersma et al. (1997) carried out small centrifuge tests to simulate the behavior of suction piles in dense sand. The test showed that a pile with aspect ratio of 4 could be penetrated without any problem. The authors also found that the relation between the pressure difference, the pile diameter, and caisson length, and the wall thickness appeared to be linear.

El-Gharbawy et al. (1999) successfully installed model caissons with aspect ratios ranging between 2 to 12, and full-scale caisson with an aspect ratio of 5.

House et al. (1999) presented a theoretical critical aspect ratio based on the upheaval of the soil plug (Eq. 2.11), and indicated that the caisson may be installed with an aspect ratio over 10. However, the caisson installation tests conducted in normally and slightly overconsolidated kaolin clay suggested a much lower aspect ratio in the region of 5 to 7.

$$\left(\frac{l}{d}\right)_{limit} \approx \frac{1}{4\alpha_0}\left\{N_c + \left[N_c^2 + \frac{32W\alpha_0}{\pi k d^3}\right]^{\frac{1}{2}}\right\} \quad \text{.....(2.11)}$$

where,

l=embedded caisson length

d=caisson diameter

α_0=external friction factor

N_c=bearing capacity factor

W=submerged caisson weight

k=shear strength factor

Tjelta (2001) presented some guidance on aspect ratio. The aspect ratio over 1.5 was not recommended in dense sand. In soft clay, however, a higher aspect ratio may be preferable since for the same weight of an anchor this would provide larger penetration and thus reach stronger clay strata. For high aspect ratio anchors, this number was limited by penetration refusal which depended on soil sensitivity and pile/soil interface

friction, and was believed to be around 20. However, the highest known aspect ratio was 9 used for riser support anchors.

Sparrevik (2002) studied four suction piles, with diameter of 6.4 m, 3.2 m, 1.6 m, and 0.8 m, each with 35 mm skirt-wall thickness and a length of 35 m. The tests were conducted in very soft clay and stiffer clay (a three time stronger soil). The author found that the aspect ratio is very high (38) for the pile with smallest diameter in very soft clay, and decrease with larger diameter piles. The aspect ratio decreased significantly in a stiffer clay, being 22, 13, and 8 for the smaller diameter piles.

Andersen et al. (2005) conducted three centrifuge tests in normally consolidated kaolin clay. The authors showed that the suction anchors could be penetrated by underpressure to reach the aspect ratio of about 12.4 to 14.5. The authors also found that when penetration depth reached about half of the maximum penetration depth, the volume of soil entering inside the anchor increased more than the volume of soil displaced by the skirt.

Experimental Studies on Suction Caissons

There are many experimental studies conducted including both field tests and laboratory tests. Experimental studies are conducted in both sandy and clay material. The lateral, vertical, and inclined capacity, penetration resistance, caisson aspect ratio, etc. are well investigated in these literatures. Some of these studies are reviewed in this section.

Field Tests

Hogervorst (1980) conducted full-scale field tests of which two with sandy soils and one with hard clay. Suction piles with diameter of 3.8 m and length of 5 m and 10 m were tested to investigate the lateral and axial load capacities. The lateral pile stiffness, β, was 0.19, which was considered infinitely stiff. The analytical approaches in previous literature were based on equilibrium condition, and shown as follow:

$$Q = \int_0^H p dz$$

where,

p=lateral soil pressure on pile

z=depth below the seabed

H=caisson length

According to Broms (1964), the maximum allowable lateral pile load in this case was:

$$Q = \frac{\gamma' D H^3 \tan^2\left(45 + \frac{\phi}{2}\right)}{2(a+H)}$$

where,

γ'=underwater unit weight of sand

D=diameter of pile

φ=angle of internal friction of sand

a=distance from pulling point to sand surface

The test results showed a reasonable agreement with calculated allowable lateral resistance.

As the pile was provided with an internal friction reducer, only the external friction was contributed to the axial capacity. The analytical friction resistance was expressed as follow:

$$F_s = \pi D \int_0^H f dz$$

Where,

f=unit skin friction

It was known that the skin friction in sandy soil was 50% lower in tension than in compression. This difference was not found in clay. The test results showed a slight underestimation of the theoretical values.

El-Gharbawy et al. (1999) performed six suction anchor installations in the Gulf of Mexico with water depth ranging from 4000 feet to 6000 feet. The suction anchors were first penetration by their own weight, and followed by suction. Self-weight penetration rate was observed to range from 7.6 to 12.7 mm/sec, and accounted for at least one-half the installation distance. The final installation suction pressure ranged between 34.5 and 138 kPa. The relationship between the required suction pressure and penetration distance was shown in Figure 2.1.

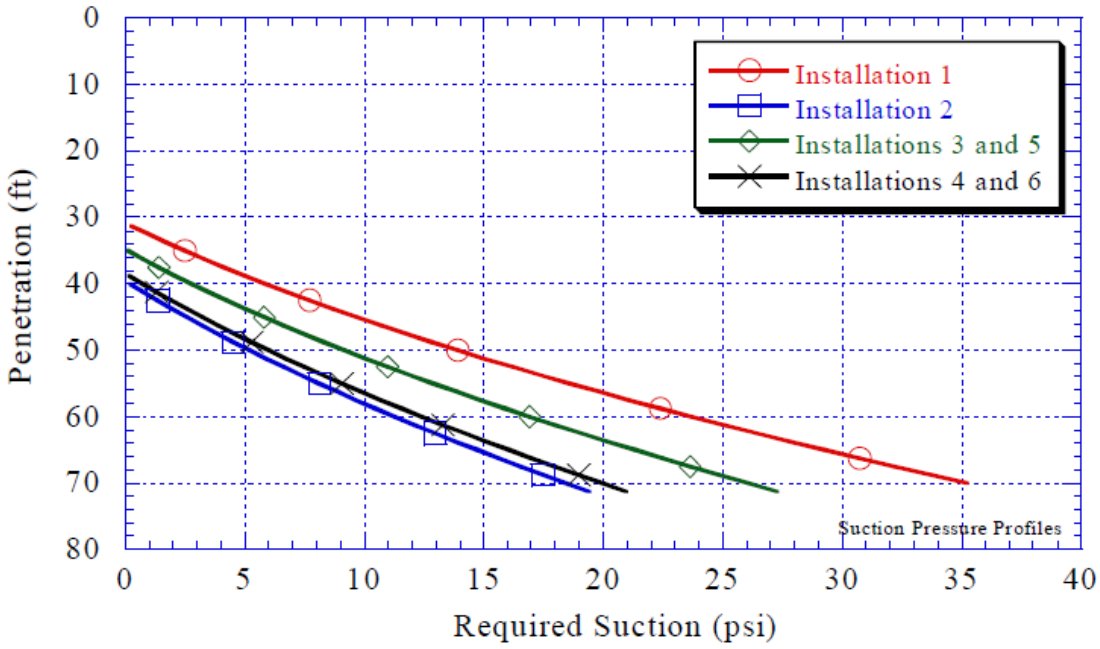

Figure 2.1 Required suction pressure profile for suction anchor installations (El-Gharbawy et al., 1999)

Cho et al. (2002) conducted a series of field tests with a total of seven piles with diameters ranging from 0.7 m to 2.5 m and lengths of either four or five meters. The suction piles were made of steel and concrete, and were penetrated in an average water depth of 15 meters in the Okpa harbor located along the southern coast of Korea. The data were collected to validate the "mobilized soil cohesion ratio", β, which was defined as:

$$\beta = \frac{c_m}{S_u}$$

where,

c_m=mobilized soil cohesion necessary for equilibrium between the external force and the pile bearing capacity

S_u=fully available soil undrained shear strength

The authors found that the values of β had an almost linear relationship with the normalized equivalent external pressure, and ranging from 0.1 to 0.35. The β value approached zero as the normalized equivalent external pressure decreased. The data points were grouped in two separate curves, which was distinguished by the pile type or pile thickness.

Cho et al. (2002) similarly conducted three filed tests of suction piles in sand. The pile was made of steel, was 2.3 m long, 1.5 m in diameter, and 0.64 cm thick. Similar to the "mobilized soil cohesion ratio" for clay, the density of sand at the pile tip and inside the pile may reduce due to pile installation, and therefore result in the decrease of soil friction angle, and thus the pile capacity. The mobilized effective soil friction angle ratio, α, was defined as:

$$\alpha = \frac{\tan\phi_m^{'}}{\tan\phi^{'}}$$

where,

$\varphi_m{}^{'}$=mobilized effective soil friction angle necessary for the equilibrium between external force and the pile bearing capacity

$\varphi^{'}$=fully available effective soil friction angle

The authors introduced an coefficient, X, which was defined as:

$$X = \frac{p_s + F_b / A}{\gamma_b D_p} \frac{D}{D_{p-\max}}$$

where,

p_s=applied suction pressure

F_b=buoyant weight of the pile and the surcharge

γ_b=soil buoyant unit weight

A=area of soil plug inside the pile

D_p=penetration depth

$D_{p\text{-}max}$=the maximum penetration depth

By applying the coefficient X, the relationship betweenα and X was shown in Figure 2.2.

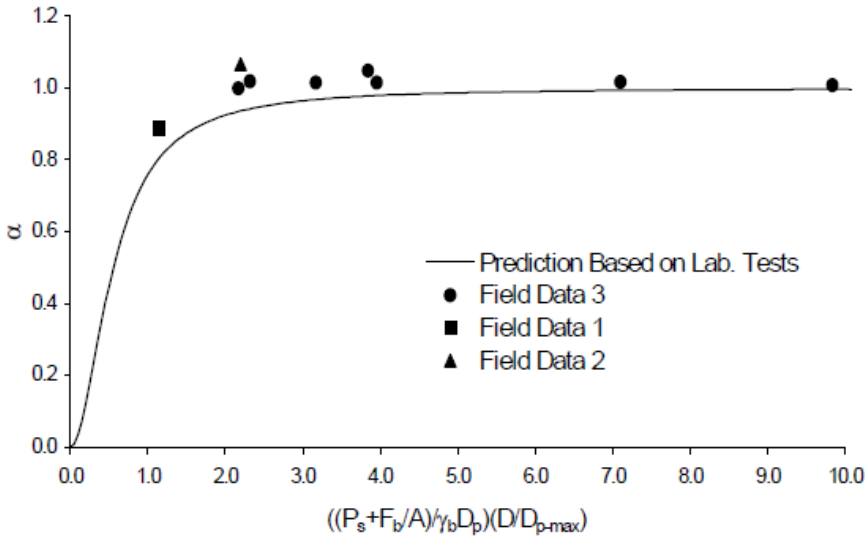

Figure 2.2 Variation of mobilized effective friction angle ratio with X (Cho et al., 2002)

Cho et al. (2003) conducted three field suction pile pullout tests in the Okpo harbor. The suction pile had a diameter of 0.5 m, 1 m, and 1.5 m, and a length of 5 m. The suction piles were installed by applying suction pressure first, and the pullout tests

were conducted after a minimum of three days of installation. The pullout tests showed that the piles did not move until approximate one half of the ultimate load was reached. The ultimate load was reached at the displacement of about 11 cm. The water pressure near the pile inside top decreased during the pulling out. It was noted that the water pressure increased immediately after the ultimate load was reached. This might be due to the relative displacement between pile inside wall and the soil.

Jeanjean (2006) presented results of installation and retrieval of suction anchors in the Gulf of Mexico. The tests included two main suction applications: permanent and temporary mooring foundations. For temporary mooring application, the pile diameter was 9.55 feet and 12 feet, wall thickness was 1.0 and 1.5 inch. For permanent mooring application, the pile diameter was 18 feet, wall thickness ranged from 1.5 inch to 2.0 inch at the padeye. The author found that the suction anchor would reach 90% consolidation after about 30 days. The best fit friction factor is between 0.7 and 0.75 at 90% consolidation.

Colliat et al. (2007) reported installation of suction piles in 1300 m of water in three oil field offshore Angola. Site A and B were floating production storage and off-loading (FPSO) piles with diameter of 8.0 m and wall thickness of 25 mm. Site A and C were riser tower foundations with similar pile dimension. The authors found a much lower penetration resistance of the suction piles in Site A, which was attributed to: a) the effect of pain on the pile resulting in a friction resistance up to three times lower than that along non-pained steel; b) the effect of ring stiffeners on the internal friction

resistance due to soil remolding; c) the underestimated sensitivity of clay due to the use of upper bound adhesion factor and clay strength in penetration analyses.

Colliat and Colliard (2011) performed a series of filed test of suction piles in water depth ranging from 700 m to 1300 m offshore Angola and Congo. The diameters of the piles ranged from 3.8 m to 8.0 m. The penetration was up to 20.5 m. The installations were conducted by self-weight first and followed by suction. The self-weight penetration was found to be 50% to 67% of final penetration depth. After the installation, the extraction tests were conducted after various set-up times, ranging from 1 day to 3.5 years. The authors found that the increase in resistance was from 35%-45% in one week to 70% in one month, and very little between one month to 3.5 years.

Laboratory Tests

Larsen (1989) conducted a total of 15 model tests of suction anchors, 11 of which were in sand, 2 in clay, and 2 in kaolin. The suction anchors was 104 mm, 204 mm, and 305 mm in diameter, and all 450 mm long, and all 1.5 mm thick of wall. The installation was accomplished by applying a pressure. It was found that when the pressure grew sufficiently high, the effective stress of soil inside the anchor became zero, and thus the penetration resistance reduced. The static load and oscillating load were then applied on the anchors, and the load-displacement curves for two tests were shown in Figure 2.3 and 2.4. The author also found that the ultimate pulling capacity was 30% to 60% higher than the theoretical values. This may due to that a) the calculation method aiming for practical purposes was very conservative; b) the calculation method only took into

consideration the horizontal stressed outside the anchor, and neglected the bottom friction; c) the size scale effects were not precluded. The horizontal displacement at failure was less than 20 mm for static load test, and was 25 mm to 30 mm for oscillating load tests. The author also found that the vertical displacement at failure was proportional to the anchor diameter and that the angular motion at failure was between 3 to 6 degrees. The ultimate pulling capacity in clay was found to be in good agreement with the calculated value with static load tests.

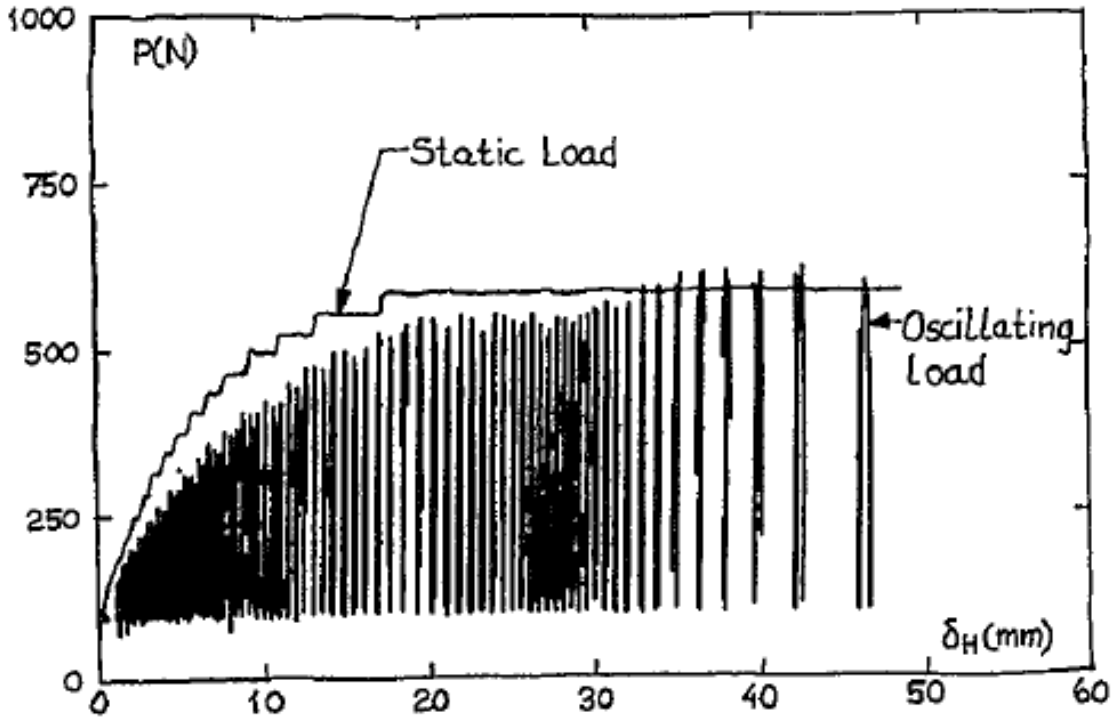

Figure 2.3 Static-and-oscillating load-displacement curves for model anchor (d=104 mm) (Larsen, 1989)

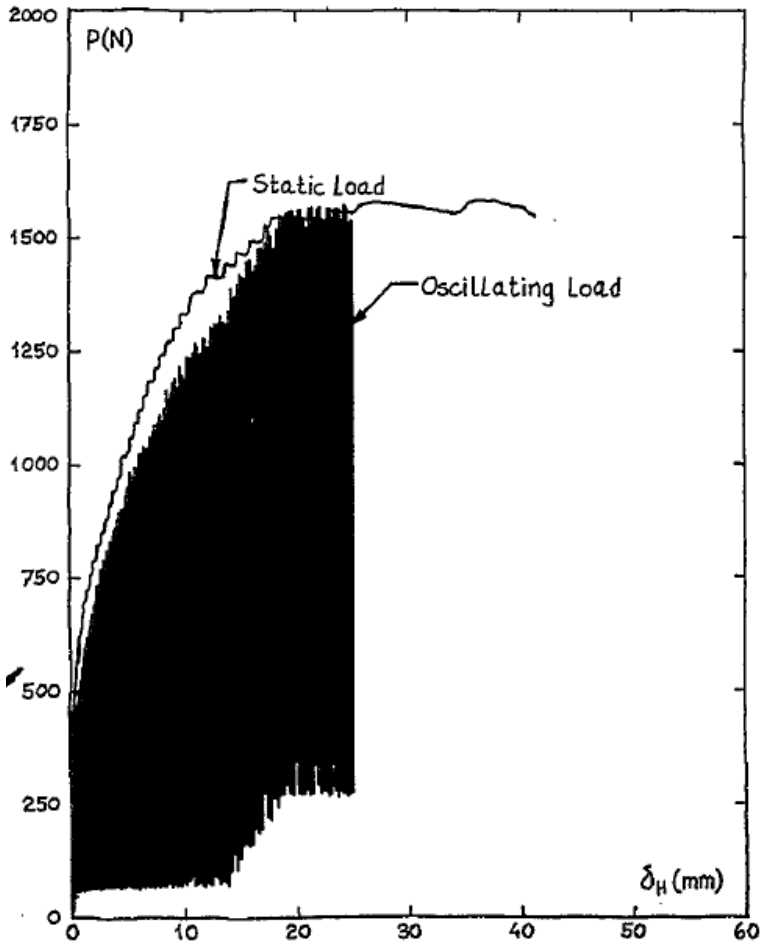

Figure 2.4 Static-and-oscillating load-displacement curves for model anchor (d=305 mm) (Larsen, 1989)

Rao et al. (1997) conducted pullout tests of suction anchors in clay. The model caisson was built on scale of 1:100 with diameter of 75 mm, thickness of 3 mm, and aspect ratio of 1, 1.5, and 2. The soil used was a typical marine clay from east coast of India. The suction anchor was pushed into the clay to the required position. Two days were allowed after the installation for consolidation. Short term pullout tests and sustained load tests were conducted. An ultimate uplift capacity, P_u, was obtained from the short term pullout test, and sustained load of 25%, 50%, and 75% of P_u were applied

in the sustained load tests. The authors found that a displacement of 16% of anchor diameter was needed to mobilize the ultimate pullout capacities. At this large deformation, skin friction, reverse end bearing, and the tensile strength of the soil at anchor base were all mobilized. In the sustained load tests, even at 75% P_u load, complete pullout failure was not observed within the test time frame.

El-Gharbawy and Olson (1998) conducted laboratory tests on model caissons to study the pullout behavior. The caisson models were built with a diameter of 125 mm with aspect ratio of 2, a diameter of 100 mm with aspect ratios of 4 and 6, and a diameter of 50 mm with aspect ratio of 12. All caissons had a wall thickness-to-diameter ratio of 0.03125. The soil used for experiments was a bleached kaolinite clay with a liquid limit of 57% and a plastic limit of 27%. After the clay was setup, shear strength was measured immediately. After consolidation, the caisson was installed under its own weight to create the sealing, and suction was applied after that to finish the penetration. Piping was not observed during suction installation. The authors found that the rate of pullout had a major impact on the capacity: undrained test with a rate of 25 mm/s to 50 mm/s resulted in a capacity approximately three time larger than the drained test. For undrained test, it was noted that the soil plug was retained inside the caisson during pullout.

El-Gharbawy and Olson (1999) conducted a series laboratory tests of suction caisson to study the cyclic pullout behavior. The test program was introduced in El-Gharbawy and Olson (1998). The authors found that when applied a peak cyclic load lower than the long-term capacity (LTC), no significant displacement was observed up to 10,000 cycles. When peak cyclic load exceeded LTC, the displacement rate was

proportional to the applied peak load. To reach the same displacement, greater number of cycles could be sustained at a lower oscillation frequency ratio (OFR), and smaller inclination.

Kim et al. (2001) conducted 8 centrifuge tests of suction piles in sand. The piles used had diameter of 10 cm and 6.1 cm, length of 11.7 cm and 17.4 cm, and thickness of 0.3 mm and 0.25 mm. The tests were performed under acceleration of 100g. The results indicated that the suction was very effective in penetrating the large-size suction piles. However, the suction pressure was limited to avoid a boiling condition.

Cao et al. (2002) conducted centrifuge tests of suction caissons in clay. Three caisson models were used, which all had the same length of 245 mm and diameters corresponded to prototype diameter of 5.17 m, 10.34 m, and 2.87 m, respectively. The tests were conducted at 100g condition. A 90% consolidation of clay was achieved at 100g, and penetration was started after 6 pre-determined time periods. The penetration was completed by self-weight penetration at first, and followed by the suction installation. The penetration resistance was shown in Figure 2.5, and the friction coefficient α was also plotted in Figure 2.6. The results showed that the penetration resistance increased linearly with depth for both self-weight and suction installation. The friction coefficient decreased from about 0.6 at surface to about 0.15 at the end of self-weight penetration. This indicated that the rate of resistance increase with depth was lower than the rate of soil strength increase. This may due to the disturbance of the surrounding soil.

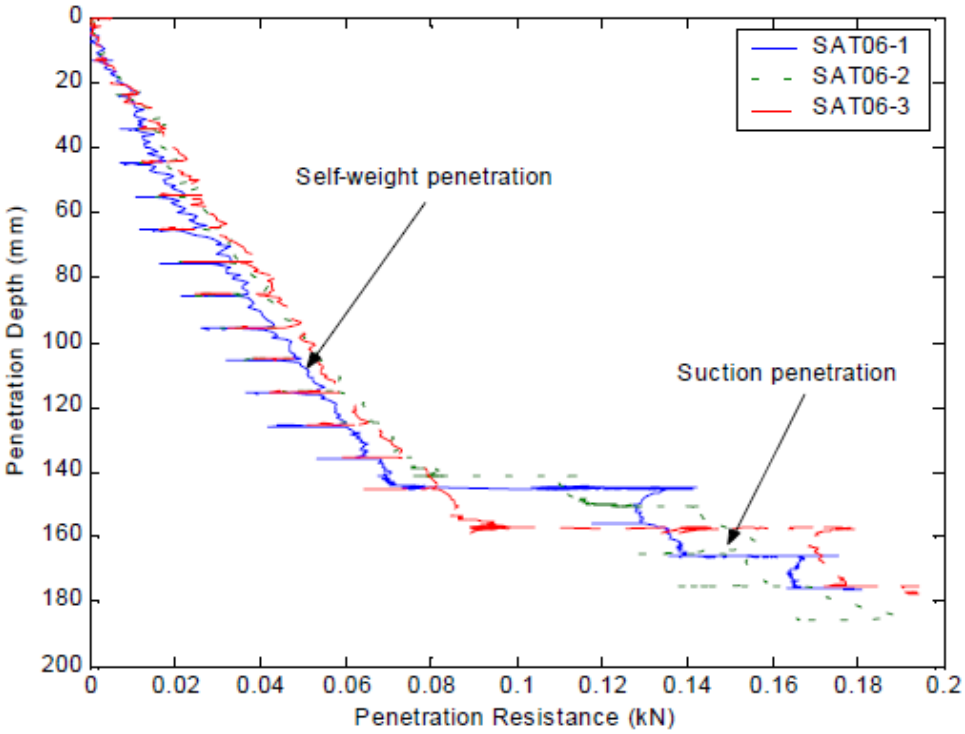

Figure 2.5 Penetration resistance with depth (Cao et al., 2002)

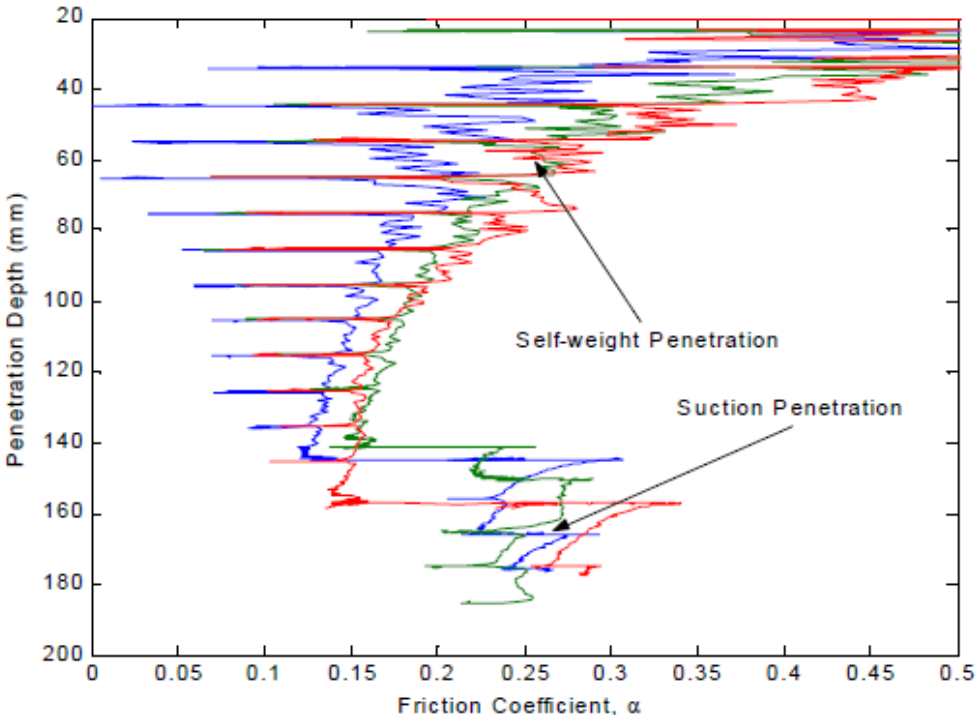

Figure 2.6 Friction coefficient with depth (Cao et al., 2002)

Cho et al. (2002) conducted a series of laboratory model tests to estimate the mobilized soil strength during installation. The tests were carried out with four model piles made from Plexiglas pipes. The tests were conducted in loose and medium dense sand, with friction angle of 30° and 36.5°. The author deduced that the density of sand would reduce at the tip and inside of the pile due to the upward flow of water, which would result in reduction of friction angle, and thus the friction resistance. The mobilized effective soil friction angle ratio, α, was introduced as follow:

$$\alpha = \frac{\tan \phi_m^{'}}{\tan \phi^{'}}$$

where,

φ_m'=mobilized effective soil friction angle necessary for the equilibrium between external force and the pile bearing capacity

φ'=fully available effective soil friction angle

The relationship between the calibrated values of α and the normalized equivalent external pressure was shown in Figure 2.7.

With evaluation of regression analysis, the relationship could be expressed as follow:

$$\alpha = 1 - \frac{1}{1 + 3.156X^{1.943}}$$

where,

$$X = \frac{p_s + F_b / A}{\gamma_b D_p} \frac{D}{D_{p-\max}}$$

where,

p_s=applied suction pressure

F_b=buoyant weight of the pile and the surcharge

γ_b=soil buoyant unit weight

A=area of soil plug inside the pile

D_p=penetration depth

$D_{p\text{-}max}$=the maximum penetration depth

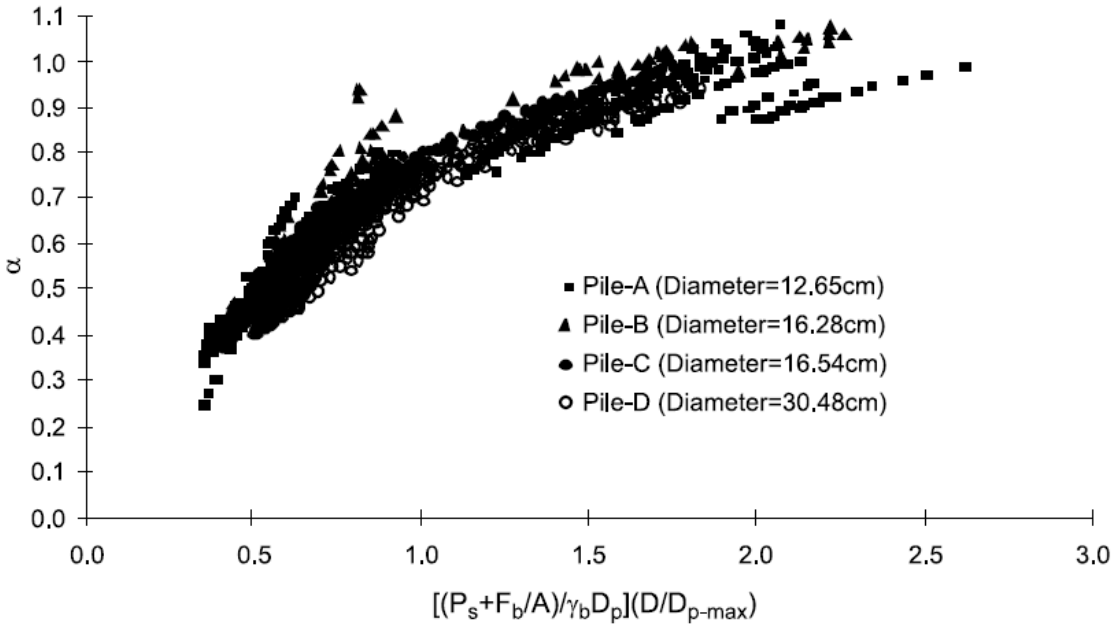

Figure 2.7 Mobilized effective soil friction angle ratio α versus normalized equivalent external pressure (Cho et al., 2002)

Coffman et al. (2004) conducted nine laboratory of suction caissons behavior under horizontal load below mudline. The caisson was made of aluminum tube with a diameter of 4 inch, length of 35.5 inch, and thickness of 0.032 inch, and was penetrated to a depth of 32 inch into normally consolidated kaolinite clay. The caissons were penetrated under self-weight to about 16 inch (halfway), and followed by suction installation. The suction was controlled to maintain a penetration rate of about 0.02 inch/s. The suction penetration was stopped at 32 inch embedment was reached. The caissons were allowed to setup for 48 hours before testing. The caisson was horizontally loaded at different points along the lower half of the caisson. The displacements of caisson padeye at failure were 3% to 12% of the caisson diameter. The maximum horizontal capacity was observed at loading points between two-thirds and three-fourths

of the caisson embedment depth. It was also observed that there was no gap formed between caisson and clay at back side of the caisson. This was due to low strength of the clay, which was insufficient to support a vertical face.

Andersen et al. (2005) conducted three centrifuge model test of suction anchors in Speswhite kaolin clay. The suction anchor model was built to represent a prototype caisson with a diameter of 2.175 m, a wall thickness of 37.5 mm, and a submerged weight of 250 kN. The tests were performed at 75g. The clay was prepared and achieved a 90% consolidation before testing. The Test P1 and P2 were installed by self-weight first, and followed by the underpressure. The Test P3 was installed by underpressure before self-weight penetration was completed. The authors found that the Test P1 and P2 penetrated to 5.5 m and 3.1 m, respectively, under self-weight. After a setup of 4.5 days and 0.8 days prototype time, the penetration resistance was noted to increase by 42% and 26%, respectively. When penetrated by underpressure, all the clay displaced moved into the anchor. The suction anchors could be penetrated by underpressure to a depth ranging from 12.4 to a little less than 14.5 times the anchor diameter, at which depth, large soil heave was observed inside the anchor.

Luke et al. (2005) conducted nine axial pullout tests on suction caisson installed in normally consolidated clay. The dimension of model caisson was detailed in El-Gharbawy and Olson (1998). The clay was prepared to consolidate under its own weight. Four tests were performed with top cap vented, two of which were installed with suction pressure. Four tests were performed with top cap sealed, one of which was installed with suction pressure. All these eight tests were rapid tests (undrained condition). Another

one slow test (drained condition) was also conducted with suction installation and loaded with vent open. In all cases, the peak pullout capacity was reached within about 13 mm (13% of the diameter). For vented tests, the test results indicated that the side resistance was about the same under drained and undrained conditions, and that the side resistance was smaller for suction installed caissons than for dead weight installed caissons. The pullout capacity was observed considerably larger for the sealed tests due to the large end bearing capacity and weight of soil attained inside the caisson during uplift.

Bang et al. (2006) conducted centrifuge tests to investigate the vertical pullout capacity of embedded suction anchor (ESA). The model ESA had the diameter of 3 cm, length of 5 cm, thickness of 1.5 cm, and made of stainless steel. For ESA with flanges, three flange were attached along the circumference at 120 degree apart. The flange had the same length as the ESA, 1 cm wide, and 1 mm thick. The centrifuge test was performed at 50 g, which corresponded to a prototype suction anchor with 1.5 m diameter and 2.5 m long. The ESA was installed during the construction of sand bed, instead of installation by suction pressure. The authors believed that the ESA would rotate and reached equilibrium during vertical loading, therefore the solution of deeply embedded plate anchors could be adopted. The authors developed an analytical solution based on the modification of Frydman and Shahan's solutions. The centrifuge test results had a good agreement with the analytical solution. Generally, the vertical pullout capacity increased with the loading point moving downward, and reach its maximum value at about 50% of anchor length. When the loading points were above the maximum loading point, the ESA experienced rotational as well as translational movement. When

the loading points were below the maximum loading point, the ESA experienced completely rotational movement. Purely translational movement occurred at maximum loading point.

Jiao et al. (2009) conducted experimental studies on horizontal and vertical capacities of suction caissons in sand. The model caissons had a length of 7.2 cm, a diameter of 4 cm, and a thickness of 0.2 cm. The test were tested on single caisson, and four caisson compartment. The caissons were installed by self-weight when not sealed, and by self-weight followed by suction pressure when sealed. The caisson were loaded under compression, uplift, and horizontally for both sealed and not sealed cases. For single caisson, it was noted that the capacities were almost the same for sealed and not sealed cases. Under drained condition, the capacity of four-caisson foundation was nearly 4 times the single caisson. Under undrained condition, the capacity increased with the increasing loading rate. For four-caisson foundation, the authors found that the capacity of loading along the direction of sidewall was almost the same as that of loading along the direction of diagonal. Also, the same capacities for sealed and not sealed tests were observed as in the single caisson tests.

Villalobos et al. (2010) conducted laboratory tests on suction caissons in clay subjected to vertical loadings. The caisson used was of diameter 150 mm, length 150 mm, and wall thickness 1 mm. The caissons were installed by vertical load and suction. The soil used was overconsolidated Speswhite kaolin clay. The caisson were subjected to compressive load and cyclic load. The results of installation showed that there was little different between pushing installation and suction installation. The authors found

that the ultimate tensile and compressive capacity was equivalent when converted to bearing capacity factor. Also, under the cyclic loading around a value equal to the maximum installation load, a permanent settlement was induced, while under the cyclic loading around zero, a permanent uplift was observed.

Gao et al. (2013) conducted a series of tests of suction caisson in sand. The caisson had a diameter of 101 mm, thickness of 2.0 mm, and lengths of 202 mm, 404 mm, and 606 mm. The sand used was a poorly graded sand with a dry density of 1.44 g/cm^3, a relative density of 0.49, and an effective internal friction angle of 36.8 degree. The tests were carried out at five loading points with Z/L=0, ½, ⅔, ¾, and 1, and five loading inclination (to the horizontal) of 0°, 15°, 30°, 60°, and 90°. The authors found that the capacity decreased with loading inclination increased, and the largest capacities were at 0°. When the loading inclination was relatively small, the maximum capacity loading point was at approximately between ⅔L to ¾L, and the minimum capacities was at the top of caisson. However, when the loading inclination became large, the effect of loading position was not significant. The aspect ratio had a direct influence on the capacity. The larger aspect ratio resulted in large capacities due to the increased shear strength with increasing depth. At the inclination angle of 60°, the maximum capacity occurred at loading at bottom of the caisson, and the translation occurred near the middle of the caisson.

Kim et al. (2013) conducted penetration tests on bucket foundation to access the penetration mechanism in sand. The model buckets had diameters of 50 mm, 100 mm, and 150 mm, and was made of acryl. The sand used was prepared to a relative density of

40%, and a friction angle of 30 degrees. The buckets were installed by suction pressure and human-power. The author found that the penetration load with human-power installation was 3.3 to 53.5 times larger than with suction method to reach the same penetration depth. Therefore, the suction installation method is more efficient than pushed installation method.

Kim et al. (2013) conducted a series of centrifuge tests of laterally loaded suction pile in sand. The model piles were 20-30 mm in diameter, 30-90 mm long, and 1.5 mm thick. The sand tested has a specific gravity of 2.62, friction angle of 37.8°, and was constructed to a relative density of 76% for testing. The tests were performed under acceleration of 50g. The results showed that the ultimate pullout capacity increased with increasing the diameter and length when the aspect ratio was high enough. For the lower aspect ratio, however, the normalized maximum resistance decreased despite of increasing diameter, but increased with increased pile length. Thus, it was concluded that increasing the length was more efficient in increasing the pullout resistance than increasing the diameter.

Li and Wang (2013) conducted model test of suction caisson in clay under 1g condition. The model caisson had a diameter of 76 mm, thickness of 2 mm, and aspect ratios of 4 and 6. The friction factor was calculated to be 0.077 and 0.27 after steel mesh was attached. The location of optimal attachment point was analyzed by finite element method, and was found to be in 0.69 times height of caisson. The authors found that the bearing capacity of suction caisson was related to friction factor and failure mode which was further changed with aspect ratio and loading direction. When loading angle was

35°, a lateral failure mode was expected for aspect ratio of 4, and a vertical failure mode was expected for aspect ratio of 6. However, for caisson with aspect ratio of 6, the lateral failure mode was observed when the loading angle reduced to 20°. The bearing capacity was also calculated based on Andersen (2005), and the maximum error was 7.63%, which verified the accuracy of the limiting equilibrium method.

Analytical Studies on Suction Caissons

Deng and Carter (2000) developed a simplified method for estimation of inclined uplift capacity of the suction caisson in dense sand under fully drained condition. The method was developed based on the numerical analysis using a finite element software package AFENA (A Finite Element Numerical Algorithm) developed at the University of Sydney. The semi-analytical approach was applied in the numerical analysis, make use of 20 node solid element. The caisson was assumed to be rigid, and installed without any soil disturbance. The caisson had a Young's modulus of 9×10^6 MPa and Poisson's ratio of 0.25. The soil had a Young's modulus of 50 MPa and Poisson's ratio of 0.25. Varies aspect ratio of caisson, lug depth, and load inclination angle were applied. Also, the soil dilatancy angle and initial stress state were included into consideration. The basic case expressions were firstly determined for the ultimate vertical and lateral loads for the associated plastic flow case by curve fitting the numerical results. Then, the effect of load inclination, soil dilatancy, and initial stress state were developed with the same technique. The authors found that the combined effect of dilatancy and stress state

had an approximately multiplicative relationship. Therefore, the the estimate of the uplift capacity for the most general case may be expressed as follow:

$$N_p = N_{p(\phi=\psi)} F_{K_0(\theta_a=90^\circ)} F_{\psi(\theta_a=90^\circ)}$$

$$N_h = N_{h(\phi=\psi)} F_{K_0(\theta_a=0^\circ)} F_{\psi(\theta_a=0^\circ)}$$

where,

N_p=uplift capacity

N_h=horizontal capacity

$$N_{p(\phi=\psi)} = 4.26\left(\frac{L}{d}\right)^{0.75}$$

$$F_{K_0(\theta_a=90^\circ)} = (0.6K_0 + 0.4)e^{(0.72-0.72K_0)\tan\psi/\tan\phi}$$

$$F_{\psi(\theta_a=90^\circ)} \cong 1.0$$

$$N_{h(\phi=\psi)} = \frac{\alpha}{\sqrt{\left(0.8-\frac{D}{L}\right)^2 + \left(\beta\frac{D}{L}\right)^2}}$$

$$F_{K_0(\theta_a=0^\circ)} = 0.1K_0 + 0.9$$

$$F_{\psi(\theta_a=0^\circ)} = \eta + \lambda\left(\frac{\sin\phi\cos\psi}{1-\sin\phi\sin\psi}\right)$$

The theoretical estimations and numerical results for different aspect ratio, lug depths, friction angles, dilation angles, and initial stress states were shown in Figure 2.8. The developed method showed a quite well agreement with the numerical results.

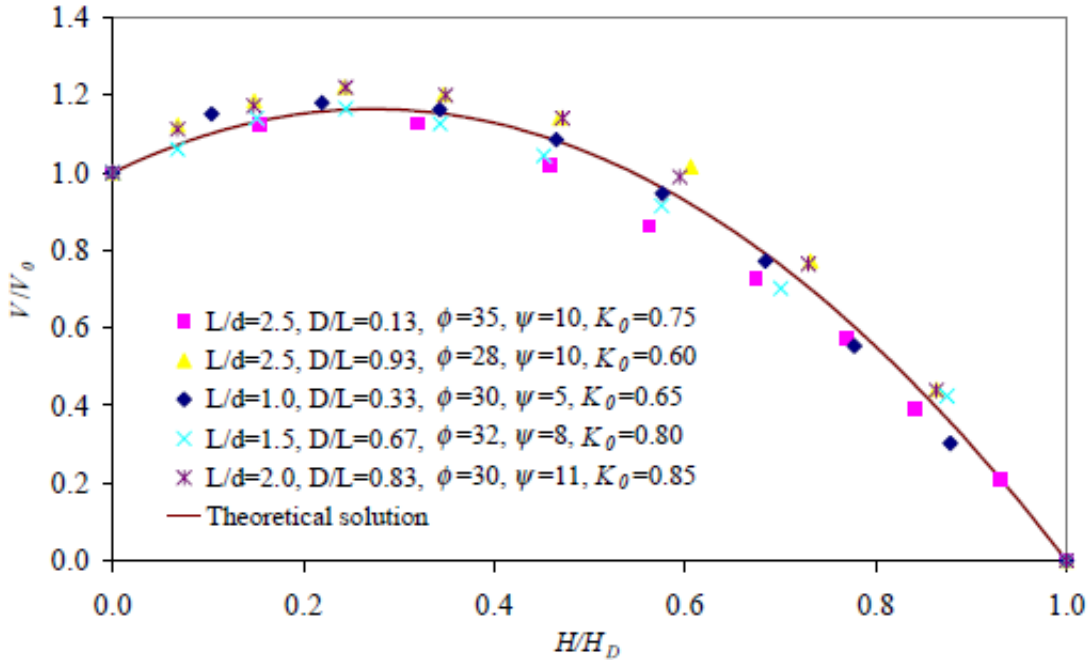

Figure 2.8 Theoretical estimation and numerical results for inclined load applied suction caisson in dense sand (Deng and Carter, 2000)

Cho and Bang (2002) developed an analytical solution to estimate the ultimate inclined loading capacity of suction piles based on the Bransby and Randolph's (1999) approach. The authors found that the ultimate inclined capacity directly correlated to the difference between the ultimate horizontal and vertical capacities. When the difference is large, the ultimate inclined capacity changed rapidly with load inclination angle to horizontal. The ultimate inclined capacity was controlled by the ultimate vertical capacity for clay, and by the ultimate horizontal capacity for sand, and was always slightly larger than either one. However, this difference is very small and almost negligible. Also, the aspect ratio of pile for clay and friction angle for sand had influenced greatly the ultimate inclined capacity.

Bang and Cho (2002) also developed an analytical solution to estimate the horizontal resistance of suction piles. Based on the force equilibrium, the horizontal force along the direction of loading was expressed as follow, and refer to the diagram in Figure 2.9:

$$F = 2\int_0^{\eta H}\left(\int_0^{\pi/2}\sigma_r \cos\theta dA + \int_0^{\pi/2}\tau_{r\theta}\sin\theta dA\right)dz$$

where,

η=pile rotation factor (defined as the distance to the pile rotation point divided by the pile length

H=pile length

σ_r=normal stress along the pile

$\tau_{r\theta}$=shear stress along the circumference

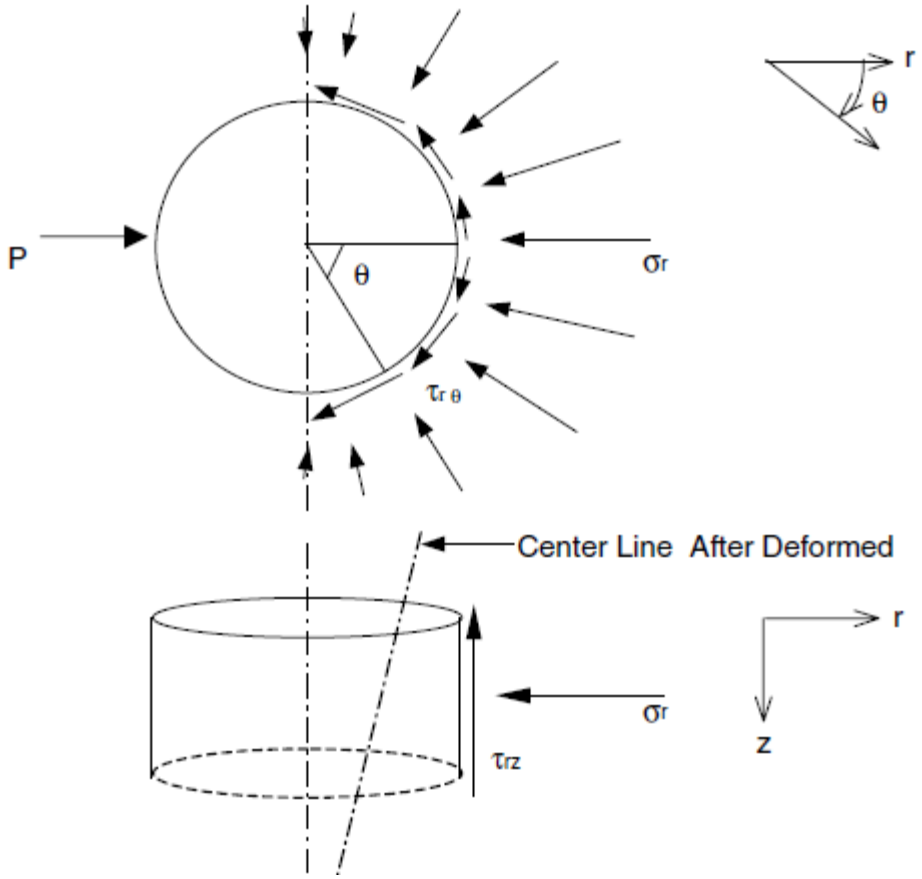

Figure 2.9 Stresses along pile circumference (Bang and Cho, 2002)

The analytical investigations was conducted for suction pile in clay and sand. In clay, the maximum ultimate horizontal loading capacity occurred at 0.55L, which associated with pure translation. In sand, however, the loading depth producing pure translation was approximately 0.675L, and the maximum ultimate horizontal loading capacity was approximately 0.8L, which meant higher capacity could be obtained by applying loading point even below the pure translation point. The analysis results are shown in Figure 2.10 and 2.11. By applying the centrifuge test results reported by

Allersma et al. (2000), the author found that the analytical prediction compared very well with the experimental data.

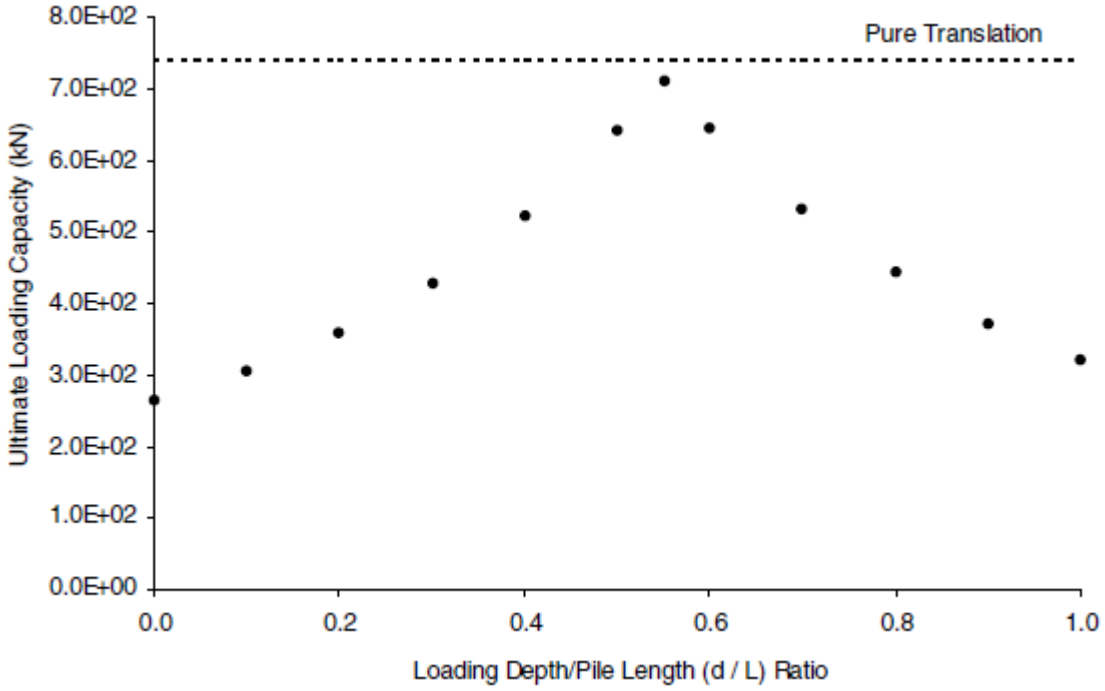

Figure 2.10 Ultimate horizontal loading capacity of pile in clay under various loading depths (Bang and Cho, 2002)

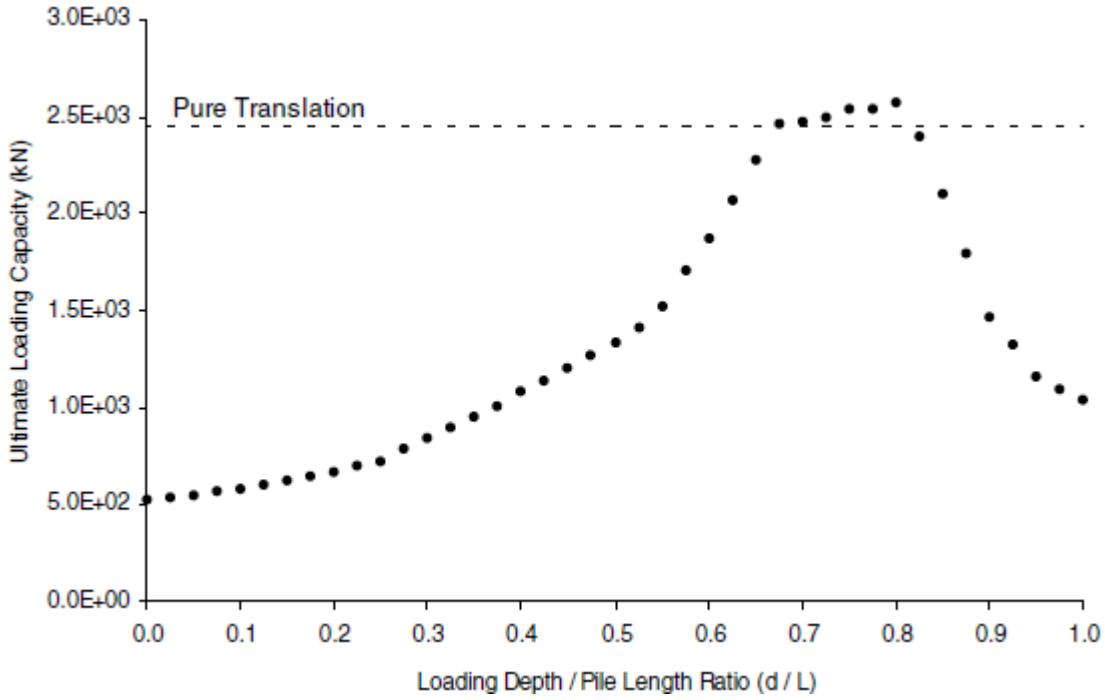

Figure 2.11 Ultimate horizontal loading capacity of pile in sand under various loading depths (Bang and Cho, 2002)

Deng and Carter (2002) further presented the theoretical investigation for vertically loaded suction caisson under undrained, partially drained, and fully drained conditions. Under undrained condition, a pullout capacity factor, N_p, was introduced, and was determined by finite element predictions as $N_p = 7.9\left(\frac{L}{d}\right)^{-0.18}$. The pullout capacity was expressed with this factor as follow:

$$p_u = 7.9\left(\frac{L}{d}\right)^{-0.18} \zeta_{cs}\zeta_{ce}S_{u(tip)}$$

where,

L=caisson length

d=caisson diameter

$\zeta_{cs} \approx 1.2$ for a circular foundation

$\zeta_{ce}=1+0.4(L/d)$, for $L/d<1$; $\zeta_{ce}=1+0.4\tan^{-1}(L/d)$, for $L/d \geq 1$

S_u=undrained shear strength at caisson tip

Under fully drained condition, a drained uplift factor, η, was introduced, and determined by finite element predictions as $\eta = 2.28\left(\frac{L}{d}\right)^{-0.46}$. The pullout capacity was expressed with this factor as follow:

$$p_u = 9.1\left(\frac{L}{d}\right)^{-0.46}\left(1-\sin\phi'\right)\left(OCR\right)^{\sin\phi'}\tan\phi'\sigma'_{v(bottom)}$$

where,

φ'=soil friction angle

OCR=over-consolidation ratio

$\sigma'_{v(bottom)}$=effective vertical stress at caisson bottom

Under partially drained condition, a bottom resistance factor, N_b, and a friction resistance factor were introduced, and determined by finite element predictions as $N_b = \left(-0.13-0.446\ln T_k\right)1.6^{\frac{L}{d}}$, $N_f = \left[0.632-0.091\ln\left(\frac{L}{d}\right)\right]\left[1+0.02\left(\frac{L}{d}\right)\right]^{T_k}$. The pullout capacity was expressed with this factor as follow:

$P_u=N_f p_{u(drained)}+N_b S_{u(tip)}$

Three different failure modes were suggested corresponding to these three loading conditions. Under undrained loading condition, the caisson was uplifted to fail by developing a reverse bearing capacity at the caisson bottom, and external wall friction was also contributed to pullout capacity. Under partially drained condition, a passive

suction in the caisson was generated, and hold the soil plug inside the caisson during pulling out. Under fully drained condition, the caisson was uplifted to fail by developing the external and internal wall friction. By comparing the theoretical solutions with some available experimental data, the authors concluded that the solution gave a reasonably well prediction.

Aubeny et al. (2003) proposed a simplified method for estimating the inclined load capacity of suction caissons. The proposed formulation expressed the ultimate unit axial and lateral resistance per unit projected area, P_a and P_l, as follow:

$$P_a=N_{as}(\psi)S_u$$

$$P_l=N_{ps}(\psi,z)S_u$$

where,

N_{as}=axial resistance factor

N_{ps}=lateral resistance factor

ψ=load inclination angle

S_u=undrained shear strength of soil

The resistance factors were easily defined for the limiting cases where ψ=0°and 90°. For 0°<ψ<90°, a series three dimensional FEM analysis was conducted using 8-node brick elements with a Prandtl-Reuss material model. The FEM predicted an N_{ps} of 13.2 for all depths versus the Randolph-Houlsby value of 11.94, and a N_{as} of 3.48 for all depths versus a theoretical value of 3.14. This indicated that the FEM predictions over estimated the value by about 10%. The FEM predictions of N_{as}-N_{ps} interaction was shown in Figure 2.12 below.

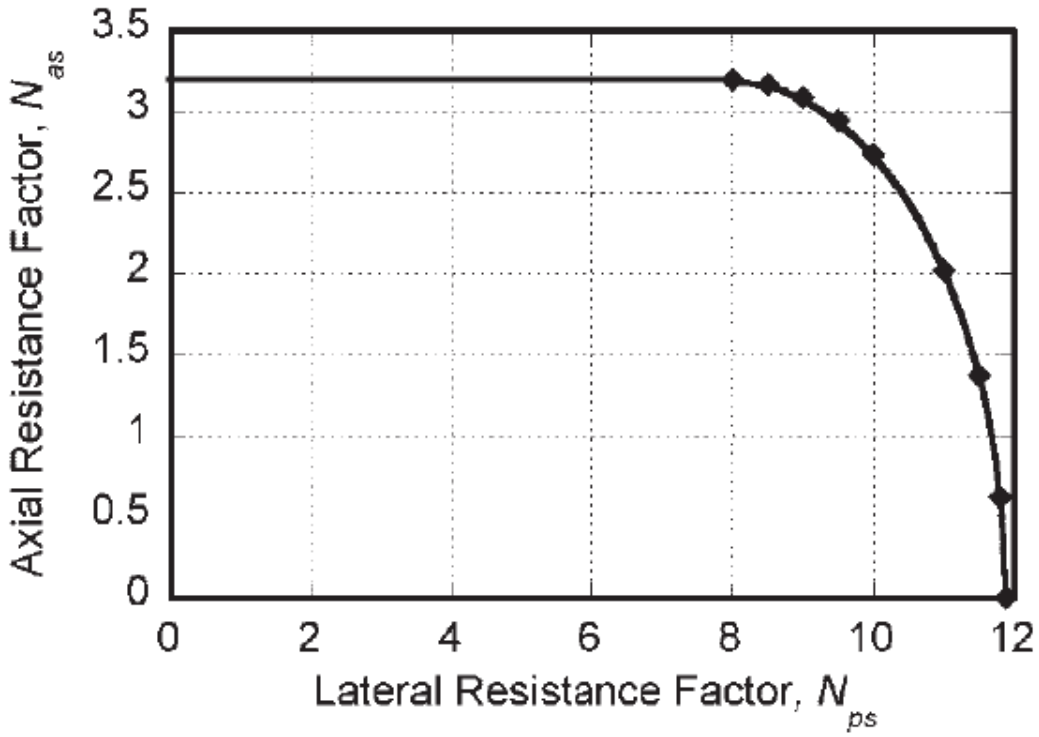

Figure 2.12 Axial and lateral resistance factors (Aubeny et al., 2003)

By equating the external work from load to the energy dissipation from side resistance and bottom resistance, the horizontal capacity was expressed as follow:

$$H = \frac{\int \left(F_{ls} \left| 1 - \left(z / L_0 \right) \right| + F_{as} \xi \right) dz + \left(M_b / L_0 \right) + V_b \xi}{\left(\xi \tan \psi + \left| 1 - L_i / L_0 \right| \right)}$$

where,

H=horizontally applied load

F_{ls}=lateral force per unit depth

F_{as}=axial force per unit depth

z=depth below mud line

L_i=load attachment depth

L_0=center of rotation of caisson

M_b=moment about the center of rotation

V_b=mobilized vertical resistance at bottom of caisson

ξ=optimization parameter controlling vertical velocity of caisson

ψ=load inclination angle from horizontal

The results by the developed method were compared to the FEM simulations. In general, the horizontal capacity was not significantly affected by the vertical load component when load inclination angle was less than 15°, and vise verse when load inclination angle was between 15° to 30°. The capacity is very sensitive to the load attachment depth when load inclination angle was less than 30°, and became less sensitive when the angle was larger than 45°. The optimal load attachment depth was at mid-depth for uniform soil strength profile, and was at three-quarter point for linearly increasing strength with depth soil profile. The author also found that the 10% reduction for the results from FEM analysis was appropriate for the pure translation, but this reduction may be excessive for the rotation movement.

Aubeny et al. (2003) refined the model with skin resistance coefficient α less than unity. The axial side resistance per unit depth F_{as} is reduced by coefficient α:

$$F_{as}=\alpha N_{as} S_u D$$

The lateral side resistance per unit depth F_{ls} is computed as:

$$F_{ls}=sR_f N_{ps} D S_u$$

Where scaling factor s was obtained by linear interpolation for an intermediate skin resistance factor, $0<\alpha<1$, as $s=0.2111\alpha+0.7889$. The reduction factor R_f was also modified to accommodate the skin resistance factor. The modified terms in R_f were expressed as follow:

$$(N_1-N_2)=4+1.62\alpha$$

$$N_2=sN_{ps}-4-1.62\alpha$$

For the case that a gap was formed on the back side of the caisson, N_1 and N_2 were divided by 2. The centrifuge test data by Clukey et al. (2003) showed the effect of reduced α on inclined capacity. The data showed that under purely vertical loading, a 30% reduction in α resulted in 20% reduction in uplift capacity. For purely lateral loading, a 30% reduction only resulted in 10% reduction in horizontal capacity.

Numerical Studies on Suction Caissons

Randolph and House (2002) conducted suction caisson capacity in clay using software AGSPANC. The soil strength based on the modified Von Mises yield criterion allowed the anisotropy soil property. The computed results were compared to the published three dimensional finite element solutions for caisson aspect ratio varying from 0.5 to 4. Rigorous upper bound capacities from AGSPANC were 1% to 10% higher than the FE results. However, when the flow region was introduced below conical wedge, the results lied 5% to 7% lower than the FE results. By assuming that the strength for shearing within the horizontal plan was equal to the triaxial extension strength, the author found that the anisotropy could result in a reduction of 30% as the capacity

defined in terms of triaxial extension strength to a reduction of 50% of the triaxial compression strength. For the capacity under combined loading, AGSPANC showed a reduction up to 16% due to interaction, and lied up to 20% outside the failure envelope from FE analysis.

Cao et al. (2003) conducted a finite element study using ABAQUS to study the passive suction simulation. The study used a modified Cam-Clay soil model, CAX8RP element for soil, and CAX8R element for caisson. Contact surface element was used to model the soil-caisson interaction. The passive suction was simulated by a very soft poro-elastic material. The centrifuge test data were used to validate the new method. The comparison showed a good agreement of pullout force from FEA and centrifuge tests. The passive suction generated from FEA was slightly different from that recorded in centrifuge tests. However, the maximum suction value were very close. Further researches were needed for improvement.

Supachawarote et al. (2004) performed a finite element study of pullout capacity of suction caissons in normally consolidated clay under inclined loading. The model used caisson diameter of 5 m, wall thickness of 50 mm, and aspect ratios of 1.5, 3, and 5. The analysis was carried out using ABAQUS. The soil was model with 8-node hybrid brick elements, applying an elastic perfectly plastic Von Mises failure criterion. A band of soil adjacent to caisson wall was remolded during installation, therefore suffered a strength reduction. This effect was simulated by a 50 mm thick soil band on the external caisson wall with a reduced shear strength of 65% of the remaining soil at that depth. This strength reduction was defined in terms of the friction coefficient α. The function of

caisson capacity under inclined loading was obtained by curve fitting the failure envelope from the finite element analysis, and shown as follow:

$$\left(\frac{H}{H_{ult}}\right)^{a}+\left(\frac{V}{V_{ult}}\right)^{b}=1$$

where,

H=horizontal loading

V=vertical loading

H_{ult}=ultimate horizontal loading

V_{ult}=ultimate vertical loading

a=0.5+L/D

b=4.5-L/3D

The results of a loading angle of 30° from horizontal showed that the optimal loading point was at approximately 0.7L irrespective of the caisson aspect ratio. For the shorter caisson, the capacity reduced as the loading angle became more horizontal. This was due to the shorter caisson exhibited a larger vertical pullout capacity than the lateral capacity. Conversely, for intermediate and long caissons, which mobilize a large lateral capacity than pullout capacity, the capacity reduced as the loading angle became more vertical.

Taiebat and Carter (2005) conducted a finite element study on suction caisson under axial, lateral, and torsion loads, and under combination of their load with each other. The aspect ratio of the caisson was 2. The simulation assumed a homogeneous elastoplastic soil deforms under undrained condition. A thin layer of elements was used

around and under the caisson to simulate the effect of shear close to the foundation. The pure axial uplift capacity from finite element analysis was slightly smaller than the theoretical solution by Deng and Carter (1999). Also, the inclination of axial load had a great effect in the capacity reduction at ground level and the tip of caisson. However, little of this effect occurred at optimal depth. The pure torsion capacity from FE analysis was in a good agreement with the theoretical value. The pure lateral capacity from FE analysis was smaller than those suggested by Deng and Carter (1999). And the maximum lateral capacity was found to be at about 0.6L. The failure locus for combination of these three loadings with each other were shown in Figure 2.13 to 2.15. The caissons were loaded to failure which was defined as 50% of the diameter for vertical displacement, 20% of the diameter for lateral displacement, and 0.4 radian of rotation. The authors found that torsion load had significant effect on axial capacity. When axial loads was lower than $0.6V_{max}$, torsional displacement control the failure mechanism. Interaction of torsional-lateral load showed that the maximum reduction of capacity occurred at load attachment depth at 0.6L, and the lateral capacity was a function of angle of misalignment and loading position.

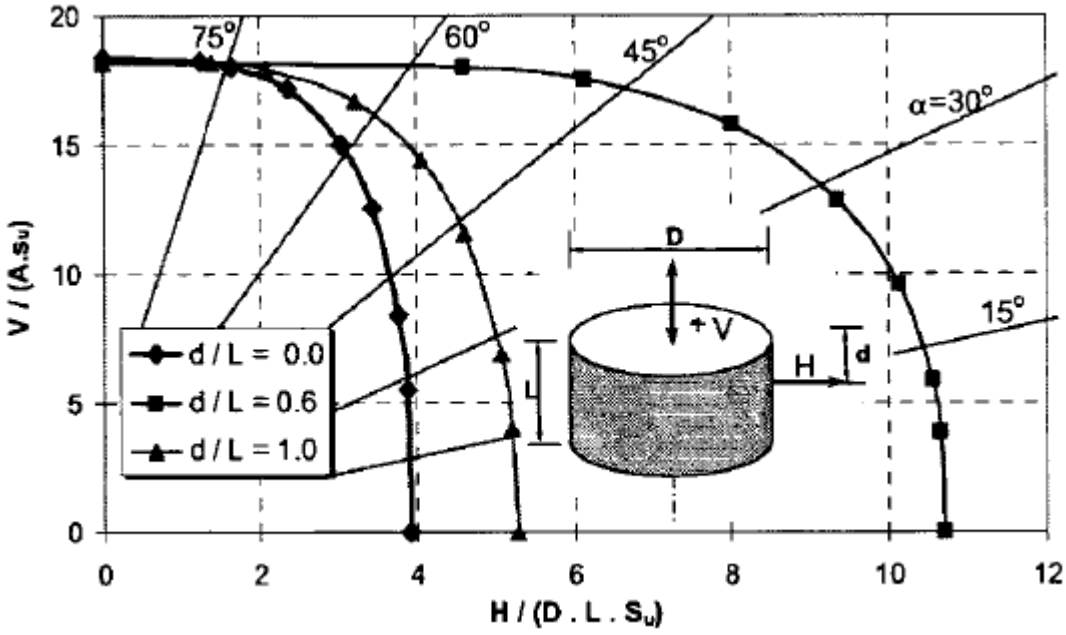

Figure 2.13 Failure locus in axial-lateral loading plane (Taiebat and Carter, 2005)

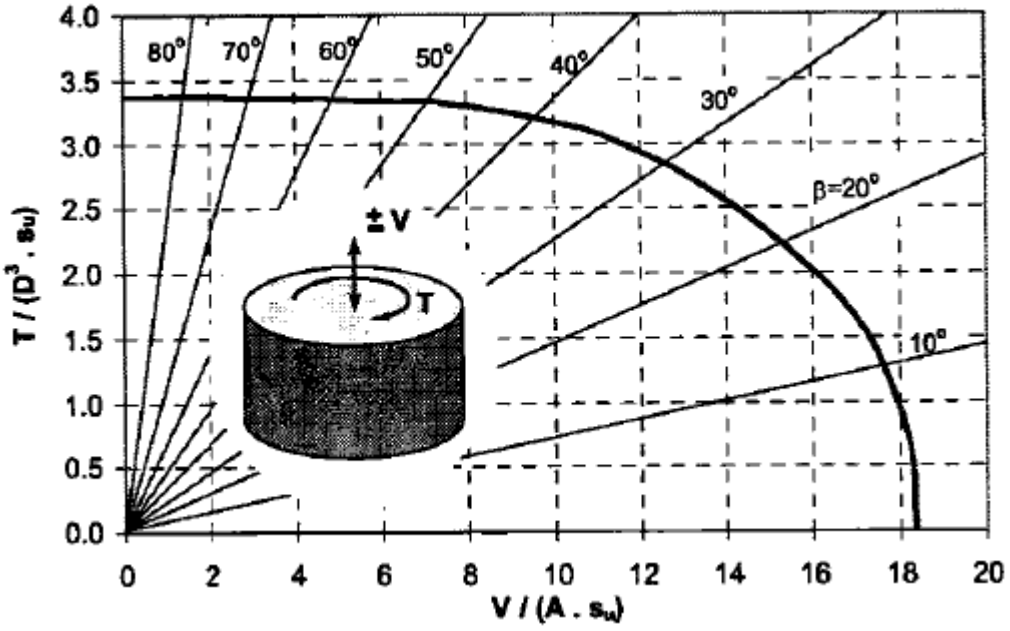

Figure 2.14 Failure locus in axial-torsional loading plane (Taiebat and Carter, 2005)

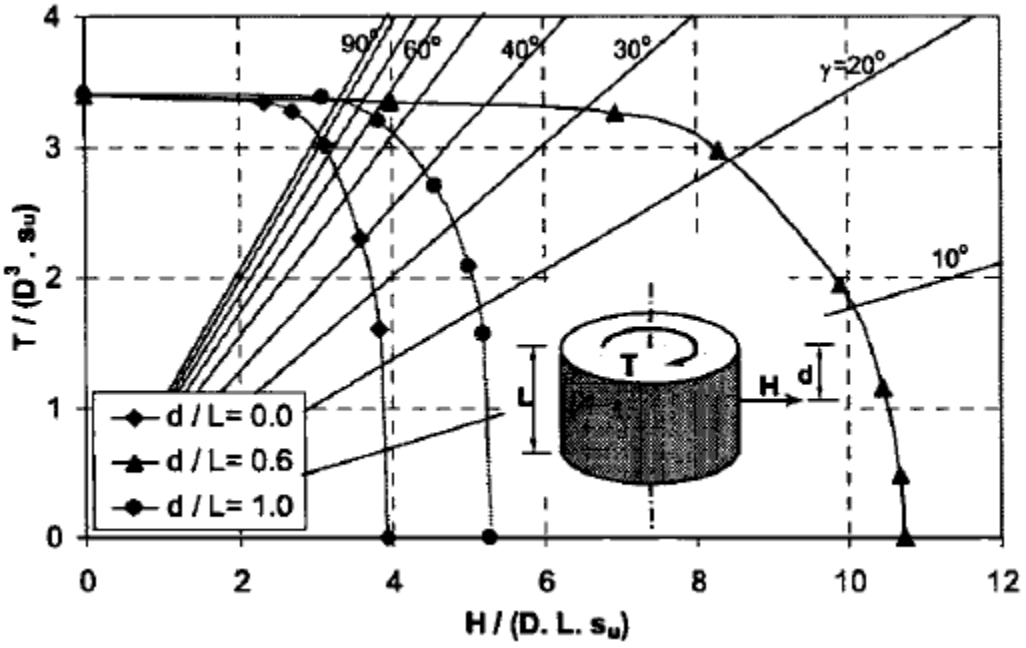

Figure 2.15 Failure locus in lateral-torsional loading plane (Taiebat and Carter, 2005)

Zhou and Randolph (2006) investigated the caisson installation using an axisymmetric large-deformation finite element approach. This numerical technique was called RITSS proposed by Hu and Randolph (1998). The approach was further implemented with the AFENA finite element analysis. The caisson had an internal caisson diameter of 4 m and wall thickness of 40 mm. The soil was modeled with six-node triangular axisymmetric elements with three Gauss points, and was considered elastic-perfectly plastic with Tresca failure criterion. The caisson-soil surface was simulated with elasto-plastic nodal joints. The caisson was simulated to be installed by self-weigh first, followed by either suction or jacking installation. The pattern of incremental displacements indicated that a higher proportion of soil is displaced by caisson tip flow inward the caisson for suction penetration than by jacking. This also

caused the lower total stresses outside the caisson for suction installation due to the smaller amount of soil moved outside the caisson during penetration. In general, higher amount of soil move inward the caisson and lower external radial stresses generated for suction installation compared to jacking installation, and suggested a long-term lower shaft friction for suction caissons.

El-Gharbawy (2007) conducted a finite element study to verify the limit equilibrium approach, in which the caisson were tested under drained and undrained conditions. The experimental results showed that the pullout under the drained condition was characterized by the caisson "slip" clean out of the soil. The pullout under undrained condition resulted in a general shear and reverse-bearing failure, and the holding capacities ranged from 1.9 to 3.5 times the drained capacity. The finite element analysis showed a good agreement with the limit equilibrium solution for a mid-range α value of 0.5. It was also noted that the finite element results were less sensitive to α than the limit equilibrium approach.

Fakharian and Iraji (2010) conducted a finite difference analysis using FLAC-2D to investigate the installation behavior of suction caisson in clay. The soil was modeled with elasto-perfectly plastic property with the Mohr-Coulomb failure criterion. The shear strength at soil-pile interface was modified by a reduction factor β' for the effective stress analysis as follow:

$$\tau_{max}=\beta'(c'+K\sigma_v'\tan\varphi')$$

The caisson was modeled by a linearly elastic property, with an outside diameter of 5.5 m, wall thickness of 20 mm, length of 12 m, and buoyant weight of 523 kN. The

reduction factor β' of 0.3 was used from back calculation of the Laminaria Case. One important finding was that a cylinder of about ⅔ of caisson diameter soil zone was generated during the suction installation. Inside this cylinder the effective stresses were lower than the hydrostatic pressure. Outside this cylinder and closer to the caisson wall were experiencing lower pore water pressure and thus higher effective stresses. The authors also found that the required suction decreased with increasing diameter at a diminishing rate. And the reverse end bearing factor increased with increasing embedment depth at a diminishing rate.

Vásquez et al. (2010) presented a finite element study of suction caisson installation by self-weight followed by suction. The authors introduced a simulation of clay based on Biot theory of porous media. The clay was described as a two-phase medium: a water-filled porous solid, which accounted for coupling between the deformation of the solid phase and the flow of the pore fluid. The interface between the soil and caisson wall was simulated based on a slide-line formulation allowing large relative displacement between the soil and caisson wall. The "stick" condition, or adhesion, was applied when the frictional force is lower than Coulomb force. The "slip" condition was the effective normal force multiplying the interface friction coefficient. A special remeshing scheme was used to track the caisson displacement path during installation. The results of simulation showed that suction comprised of about 40% capacity of total capacity for both cases. The external friction is the next most contribution of pullout capacity. The result had a generally good agreement with

experimental results. The differences were noted on soil resistance and pore-water pressure on the interior and exterior caisson wall.

Ahn et al. (2014) conducted a finite element analysis on holding capacity of suction caisson using ABAQUS. The soil was modeled by a 3-D continuum element with the Von Mises criterion. The caisson was modeled as a linear elastic material, and was considered rigid compared to the soil. The analysis found that the shape of normalized failure envelope appeared independent to soil profile but was affected by aspect ratio. This effect was found to diminish as aspect ratio became larger than 6. The normalized depth of optimal loading point was found independent to caisson dimensions but was affected by soil profile. When in uniform soil, the optimal depth was 0.55 of caisson length. While in linearly varying soil profile, the optimal depth was 0.65 of caisson length. The bearing capacity factor for reversed end bearing was found to be 9.4 for uniform soil profile and smaller for linearly increasing soil profile.

CHAPTER III

FUNDAMENTALS OF MECHANICS

In this Chapter, the basic geomechanics and shell mechanics will be demonstrated. The related application in Abaqus will also be debriefed. These fundamentals of mechanics including theory and terminology will be used in the following chapters and will not be further explained.

Geomechanics

Deformation

The displacement of a body has two components: a rigid-body displacement and a deformation. A rigid-body displacement consists of a simultaneous translation and rotation of the body without changing its shape or size. A deformation implies the change of shape and/or size of the body from an initial or undeformed configuration $K_0(B)$ to a current or deformed configuration $K_t(B)$ (Figure 3.1).

A change in the configuration of a continuum body can be described by a displacement field. A displacement field is a vector field of all displacement vectors for all particles in the body, which relates the deformed configuration with the undeformed configuration. Relative displacement between particles occurs if and only if deformation has occurred. If displacement occurs without deformation, then it is deemed a rigid-body displacement.

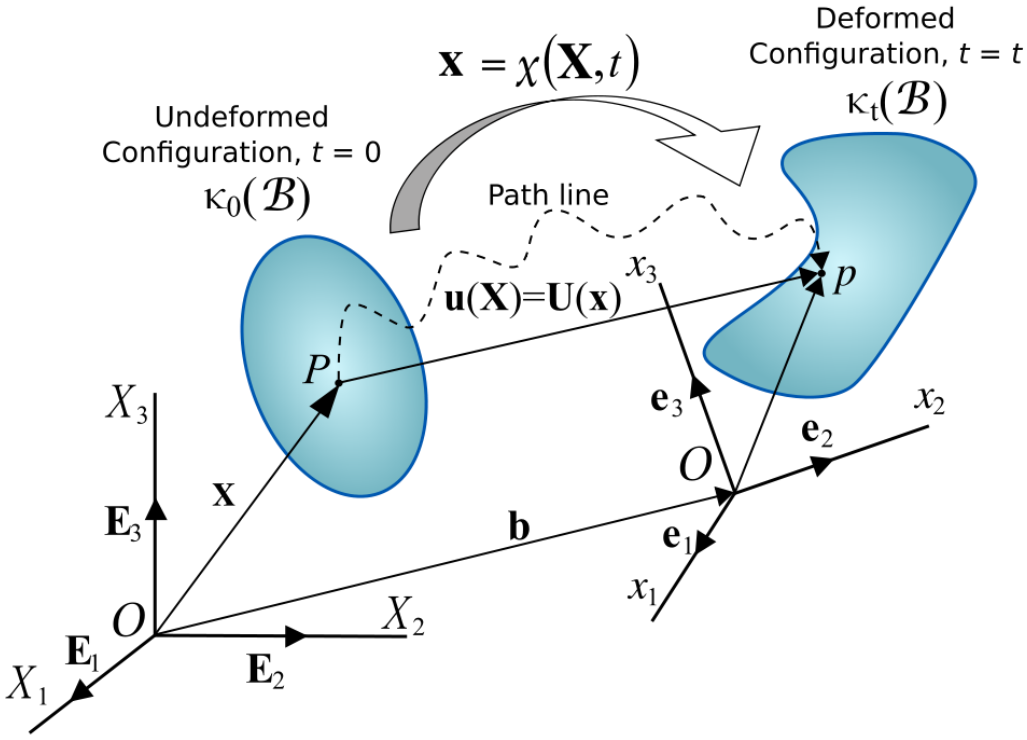

Figure 3.1 Motion of a continuum body (Wikipedia)

In any structural problem the analyst describes the initial configuration of the structure and is interested in its deformation throughout the history of loading. The material particle initially located at some position X in space will move to a new position x: since we assume material cannot appear or disappear, there will be a one-to-one correspondence between x and X, so we can always write the history of the location of a particle as:

x=x(X,t).....(3.1)

And this relationship can be inverted - we know X when we know x and t. Now consider two neighboring particles, located at X and at X+dX in the initial configuration. In the current configuration we must have the following using the "mapping" Equation 3.1:

$$dx = \frac{\partial x}{\partial X} dX \quad \text{.....(3.2)}$$

The matrix $F = \frac{\partial x}{\partial X}$ is called deformation gradient matrix, and equation 3.2 can be written as:

$$dx = F \cdot dX \text{.....(3.3)}$$

Material coordinates (Lagrangian description)

The displacement of particles indexed by variable i may be expressed as follows. The vector joining the positions of a particle in the undeformed configuration P_i and deformed configuration p_i is called the displacement vector. Using X in place of P_i and x in place of p_i, both of which are vectors from the origin of the coordinate system to each respective point, we have the Lagrangian description of the displacement vector:

$$u(X,t) = u_i e_i \text{.....(3.4)}$$

where e_i is the unit vector that defines the basis of the material (body-frame) coordinate system.

Expressed in terms of the material coordinates, the displacement field is:

$$u(X,t) = b(X,t) + x(X,t) - X \text{ or } u_i = \alpha_{iJ} b_J + x_i - \alpha_{iJ} X_J \text{.....(3.5)}$$

The partial derivative of the displacement vector with respect to the material coordinates yields the material displacement gradient tensor $\nabla_x u$. Thus we have,

$u(X,t)=x(X,t)-X$ or $u_i=x_i-\delta_{iJ}X_J=x_i-X_i$.....(3.6)

$$\nabla_x u = \nabla_x x - I = F - I \text{ or } \frac{\partial u_i}{\partial X_K} = \frac{\partial x_i}{\partial X_K} - \delta_{IK} = F_{iK} - \delta_{iK} \quad \text{.....(3.7)}$$

Spatial coordinates (Eulerian description)

In the Eulerian description, the vector joining the positions of a particle P in the undeformed configuration and deformed configuration is called the displacement vector:

$U(x,t)=U_iE_i$.....(3.8)

Where E_i is the unit vector that defines the basis of the spatial (lab-frame) coordinate system.

Expressed in terms of spatial coordinates, the displacement field is:

$U(x,t)=b(x,t)+x-X(x,t)$ or $U_J=b_J+\alpha_{Ji}-X_J$.....(3.9)

The partial derivative of the displacement vector with respect to the spatial coordinates yields the spatial displacement gradient tensor $\nabla_x U$. Thus we have,

$U(x,t)=x-X(x,t)$ or $U_J=\delta_{Ji}x_i-X_J=x_J-X_J$.....(3.10)

$$\nabla_x U = I - \nabla_x X = I - F^{-1} \text{ or } \frac{\partial U_J}{\partial x_k} = \delta_{Jk} - \frac{\partial X_J}{\partial x_k} = \delta_{Jk} - F^{-1}_{Jk} \quad \text{.....(3.11)}$$

Strain Measures

The strain usually refers to the local deformation in a material, i.e. deformation in the neighborhood of a particle, therefore is a description of deformation in terms of relative displacement of particles in the body that excludes rigid-body motions. A deformation field results from a stress field induced by a applied forces or is due to changes in temperature field inside the body. There are also other effects that may result in strain, such as changes in water content in wood and soil leads to swelling or shrinking. The three primary concepts of strain are: longitudinal strain ε, shear strain γ, and volumetric strain ε_v.

The longitudinal strain represents the change of length per unit length of undeformed line element in the direction e in particle r_0 as shown in Figure 3.2. The longitudinal strain is also called the normal strain, and is defined by:

$$\varepsilon = \lim_{s_0 \to 0} \frac{s - s_0}{s_0} = \frac{ds - ds_0}{ds_0} = \frac{ds}{ds_0} - 1 \quad \text{.....(3.12)}$$

The shear strain represents the change in the right angle between two material line elements.

The volumetric strain represents the change in volume per unit undeformed volume about particle r_0. The volumetric strain is defined by:

$$\varepsilon = \lim_{\Delta V_0 \to 0} \frac{\Delta V - \Delta V_0}{\Delta V_0} \quad \text{.....(3.13)}$$

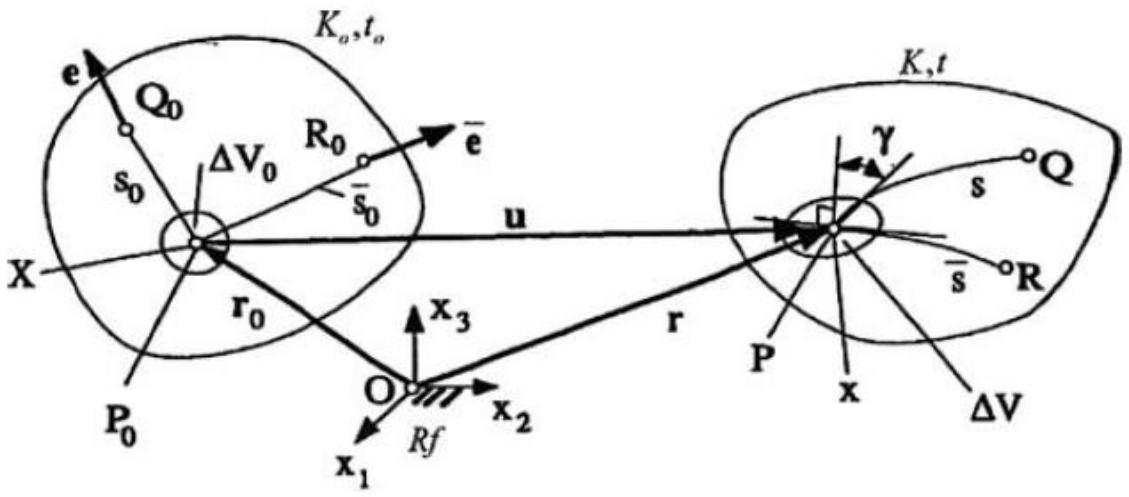

Figure 3.2 General deformation of a body (Irgens, 2008)

Finite Strain vs Small Strain

Finite strain, also called large strain, deals with deformation in which both rotations and strains are arbitrarily large. In this case, the undeformed and deformed configurations of the continuum are significantly different and a clear distinction has to be made between them. This is commonly the case with plastically-deforming materials.

Small stain, also called infinitesimal strain, deals with deformation of a solid body in which the displacements of the material particles are assumed to be much smaller than any relevant dimension of the body so that its geometry and the constitutive properties of the material (such as density and stiffness) at each point of space can be assumed to be unchanged by the deformation. This is commonly the case with stiff elastic material.

Cauchy Stress

The state of stress at a point in the body is then defined by all the stress vectors $T^{(n)}$ associated with all planes (infinite in number) that pass through that point. Cauchy's stress theorem states that there exists a second-order tensor field σ(x, t), called the Cauchy stress tensor, independent of n, such that T is a linear function of n:

$T^{(n)}=n\cdot\sigma$ or $T_j^{(n)}=\sigma_{ij}n_i$.....(3.14)

This equation implies that the stress vector $T^{(n)}$ at any point P in a continuum associated with a plane with normal unit vector n can be expressed as a function of the stress vectors on the planes perpendicular to the coordinate axes, i.e. in terms of the components σ_{ij} of the stress tensor σ.

Internal Virtual Work Rate

For these shell elements, the internal virtual work rate is assumed to be:

$$\delta W^I = \int_A \int_h \sigma^{\alpha\beta}\delta\varepsilon^f_{\alpha\beta} dz dA + \sum_r K_I^{(r)}\gamma_{3\alpha}^{(r)}\delta\gamma_{3\alpha}^{(r)} + \sum_{n^c} K_{II}^{(n)}\gamma_{SRC}^{(n)}\delta\gamma_{SRC}^{(n)} + \sum_{n^m} K_{III}^{(n)}\gamma_{SRM}^{(n)}\delta\gamma_{SRM}^{(n)}$$

where,

$K_I^{(r)}$, $K_{II}^{(n)}$, and $K_{III}^{(r)}$ are the transverse shear stiffness and the penalties and r indicates the integration points at which transverse shears are calculated, n^c indicates corner nodes at which six degrees of freedom are used, and n^m indicates midside nodes at which six degrees of freedom are used. Here, $\varepsilon^f_{\alpha\beta}$ and $\sigma^{\alpha\beta}$ are the strain and stress in the (dS^α, dS^β) material directions in a surface offset by a distance z from the reference surface.

Shell Mechanics

A shell structure is characterized by that one dimension is much smaller than the other two. The basic idea behind the shell analysis is that the stresses does not vary much across the thin dimension and hence the stress distribution across the thickness can be approximated by a Taylor series. In our analysis, shell is considered to be very thin. In this case, only the first term of the series will be important - this is the "membrane theory".

In our analysis, small strain shell elements are considered as a reasonable application since the design limit is below the material yielding point. The essential idea of these elements is that the position of a point in the shell reference surface, x, and the components of a vector n, which is approximately normal to the reference surface, are interpolated independently.

Shell Modeling Options

In Abaqus, the main category of shell element that can be used are conventional shell and continuum shell.

Conventional shell elements discretize a body by defining the geometry at a reference surface. In this case, the thickness is defined through the section property definition. These shell elements have displacement and rotational degrees of freedom.

In contrast, continuum shell elements discretize an entire three-dimensional body. The thickness is determined from the element nodal geometry. Continuum shell elements have only displacement degrees of freedom. From a modeling point of view,

continuum shell elements look like three-dimensional continuum solids, but their kinematic and constitutive behavior is similar to conventional shell elements. Figure 3.3 illustrates the difference between a conventional shell and a continuum shell element.

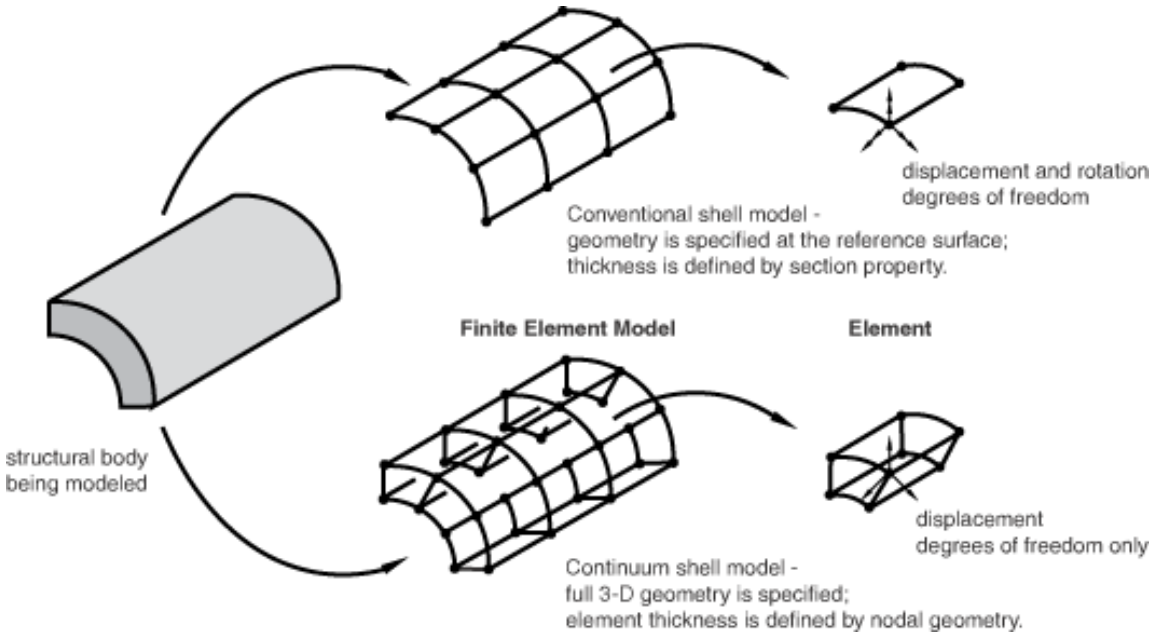

Figure 3.3 Conventional versus continuum shell element

Continuum shell elements are general-purpose shells that allow finite membrane deformation and large rotations and thus are suitable for nonlinear geometric analysis. Conventional shell elements can be used in static or dynamic procedures. Some elements include the effect of transverse shear deformation and thickness change, while others do not. Some elements allow large rotations and finite membrane deformation, while others allow large rotations but small strains.

Membrane Stresses in Cylinder Shell

There are two principal stresses in a cylinder shell element. One is parallel to the central axial, σ_1, and the other one is tangential to the shell curvature, σ_2, which is also called circumferential stress or hoop stress (Figure 3.4).

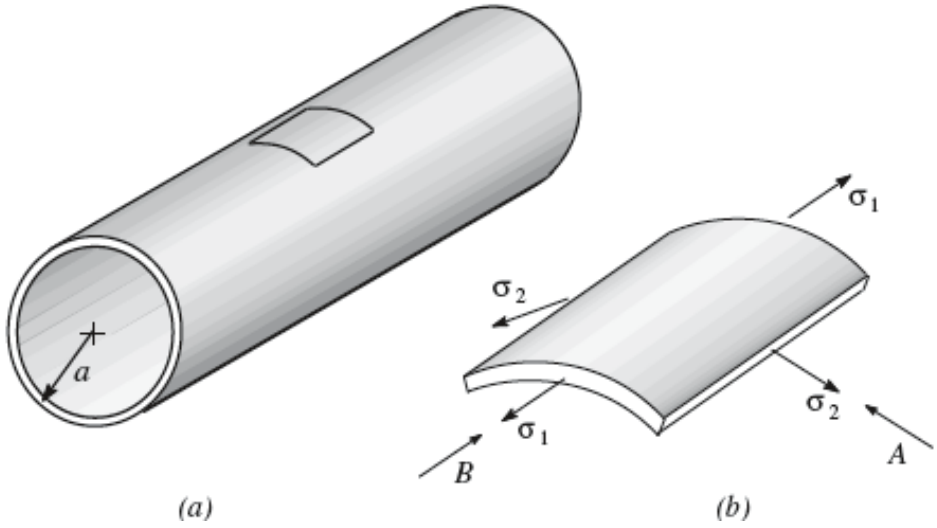

Figure 3.4 (a) A cylinder shell; (b) A rectangular shell element

Notation

A typical shell surface is shown in Figure 3.5.

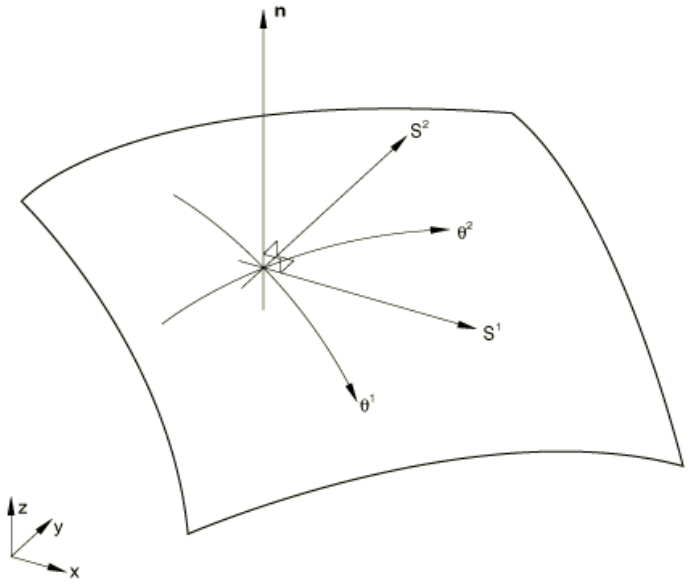

Figure 3.5 Shell reference surface

Let (θ^1, θ^2) be a set of Gaussian surface coordinates on the shell reference surface. Since these coordinates are only needed locally at an integration point, we use the element's isoparametric coordinates as these coordinates. Let $x(\theta^1, \theta^2)$ be the current position of a point on the interpolated reference surface, and $X(\theta^1, \theta^2)$ be the initial of the same point, then the unit vector is:

$$N = \frac{\frac{\partial X}{\partial \theta^1} \times \frac{\partial X}{\partial \theta^2}}{\sqrt{\frac{\partial X}{\partial \theta^1} \times \frac{\partial X}{\partial \theta^2}}} \quad \text{.....(3.15)}$$

This vector is the unit normal to the interpolated reference surface in the initial configuration. The vector gives a "sideness" to the surface - one side of the shell is the

"top" surface (in the positive direction along N from the shell's reference surface) and the other is the bottom surface.

Surface Measures

The metric of the deformed surface is defined as follow:

$$g_{\alpha\beta} = \frac{\partial x}{\partial S^{\alpha}} \cdot \frac{\partial x}{\partial S^{\beta}} \quad \text{.....(3.16)}$$

and an approximation to the curvature tensor (the second fundamental form) is:

$$b_{\alpha\beta} = -\frac{1}{2}\left(\frac{\partial n}{\partial S^{\alpha}} \cdot \frac{\partial x}{\partial S^{\beta}} + \frac{\partial n}{\partial S^{\beta}} \cdot \frac{\partial x}{\partial S^{\alpha}} \right) \quad \text{.....(3.17)}$$

The corresponding measures associated with original reference surface are the metric:

$$G_{\alpha\beta} = \frac{\partial X}{\partial S^{\alpha}} \cdot \frac{\partial X}{\partial S^{\beta}} \quad \text{.....(3.18)}$$

and the approximation to the curvature is:

$$B_{\alpha\beta} = -\frac{1}{2}\left(\frac{\partial N}{\partial S^{\alpha}} \cdot \frac{\partial X}{\partial S^{\beta}} + \frac{\partial N}{\partial S^{\beta}} \cdot \frac{\partial X}{\partial S^{\alpha}} \right) \quad \text{.....(3.19)}$$

The vectors $\frac{\partial N}{\partial S^{\alpha}}$ are defined from the derivatives of the interpolation functions and the "normals" at the nodes. These nodal normals are calculated as average values of the normals to the surfaces of all elements abutting the node.

Positive normal direction and is referred to as the positive (SPOS) face, and negative direction along the normal and is referred to as the negative (SNEG) are used to

designate top and bottom surfaces when specifying offsets of the reference surface from the shell's midsurface. The positive normal direction defines the convention for pressure load application and output of quantities that vary through the thickness of the shell. The positive normals for a three-dimensional conventional shell element is shown in Figure 3.6.

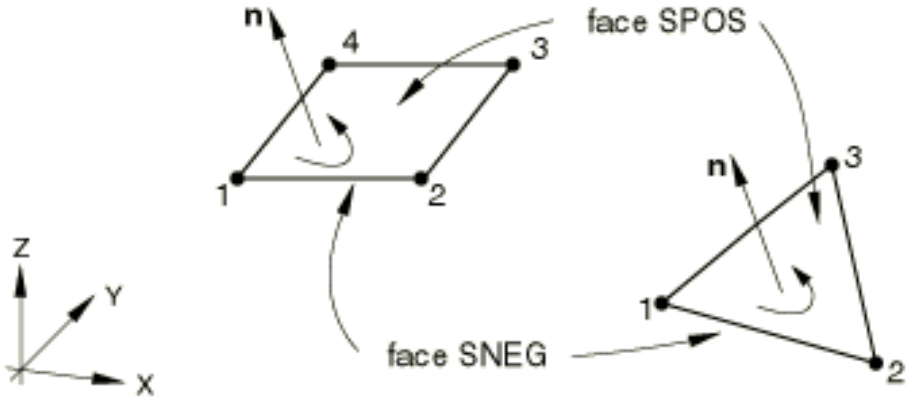

Figure 3.6 Positive normals for three-dimensional conventional shell elements

Strains

Therefore, the reference surface membrane strains is:

$$\varepsilon_{\alpha\beta} = \frac{1}{2}\left(g_{\alpha\beta} - G_{\alpha\beta}\right)$$

The curvature change is:

$$\kappa_{\alpha\beta} = B_{\alpha\beta} - b_{\alpha\beta} + \frac{1}{2}\left(B_{\alpha}^{\gamma}\varepsilon_{\gamma\beta} + B_{\beta}^{\gamma}\varepsilon_{\gamma\alpha}\right)$$

The transverse shears is:

$$\gamma_{3\alpha} = n \cdot t_{\alpha}$$

where,

$$t_\alpha = \frac{\frac{\partial x}{\partial S^\alpha}}{\sqrt{\frac{\partial x}{\partial S^\alpha} \cdot \frac{\partial x}{\partial S^\alpha}}}$$

t_α is a unit vector, tangent to the dS^α line in the current surface.

Spring Mechanics

In Abaqus, SPRING1 is between a node and ground, acting in a fixed direction, and can be linear or non-linear behavior. Spring element SPRING1 with non-linear behavior is used in our finite element analysis and is defined by giving pairs of force-displacement values in ascending order of relative displacement and should be over a sufficiently wide range of displacement values. Abaqus assumes that the force remains constant outside the range given. A conceptual non-linear spring force-displacement relationship is shown in Figure 3.7.

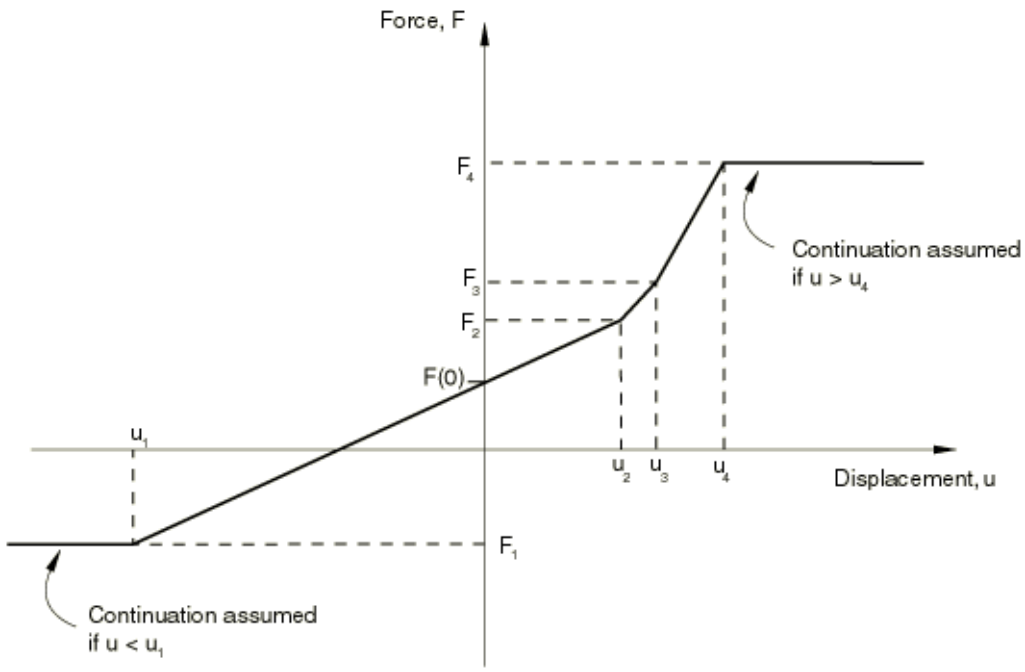

Figure 3.7 Nonlinear spring force-displacement relationship

For SPRING 1 type spring, the relative displacement across a spring element is the *i*th component of displacement of the spring's node:

$$\Delta u = u_i \,,$$

where *i* is defined as described as in Figure 3.7 and can be in a local direction

CHAPTER IV

DEVELOPMENT OF P-Y SPRINGS

General Scope

The ultimate objective of this study is to generate a 3-D model with caisson supported by springs which simulate the soil around the caisson in ABAQUS. In order to generate the spring properties for a 3-D finite element study, the following two procedures will be conducted:

1. A 2-D continuum finite element study is conducted with a steel circular shell surrounded by soil with the undrained shear strength equal to unity. The shell is then loaded horizontally by displacement control. For each soil element contacting the caisson (along caisson circumference), the relationship between the net soil reaction stresses and displacement is then obtained. The stresses are normalized by undrained shear strength, Su. These 2-D stress-displacement spring properties are then used to generate the 3-D spring properties for 3-D finite element analysis. It is noted that these stresses correspond to each soil element. However, ABAQUS input for spring property is based on force at each node. Therefore, the stresses of elements are then converted to nodal forces. The forces are based on the area of discretization. The study includes the investigation for two cases: a flexible caisson considering both external and internal soil resistance and a rigid caisson considering only external soil resistance.

2. The 2-D normalized spring stresses generated are used to generate springs for the 3-D analysis. For 3-D analysis, a specific nodal area based on discretization is

obtained corresponding to one node. This nodal area is then multiplied by the stresses generated in 2-D analysis to obtain the nodal force of the spring. For the case that the undrained shear strength is not unity, the corresponding undrained shear strength at a certain depth will be assessed first and then multiplied by the above mentioned spring force to get the spring force at that depth. In addition, close to free surface, where free surface effect becomes prominent, the stresses are scaled down by a factor, $N_p(z)/N_p(\infty)$, where $N_p(z)$ is the lateral bearing resistance factor at a finite depth and $N_p(\infty)$ is the Randolph-Houlsby bearing factor for infinite depth. Therefore, spring properties can be generated to couple with a 3-D caisson model with any soil strength profile and bearing resistance utilizing this method. Then, a 3-D finite element study will then be conducted with a 3-D steel caisson surrounded by springs with properties generated by the above mentioned method.

Finite element analyses are carried out using ABAQUS 6.9 computer program. Taking advantage of the symmetry about the plane in which the load is applied, only one-half of the caisson (180 degrees) is simulated in all the analyses.

2D Finite Element Model

Model Description

Considering the caisson is a thin shell structure, 2-node linear beam element B21 is used to simulate the caisson shell. Soil inside the caisson is not considered in our analysis. The thickness of shell of 4 cm is selected for the 2-D study. Soil is simulated

using 4-node bilinear continuum element with reduced integration - CPE4R. The soil is modeled as undrained, elastic-plastic property, and a von Mises yield criterion is used.

In order to generate a base model, the undrained shear strength of soil, S_u, is set to be one. ABAQUS characterizes the von Mises surface in terms of yield strength Y, which is related to the undrained shear strength used in the study (Figure 4.1):

$$Y = \sqrt{3}S_u \quad \text{.....(4.1)}$$

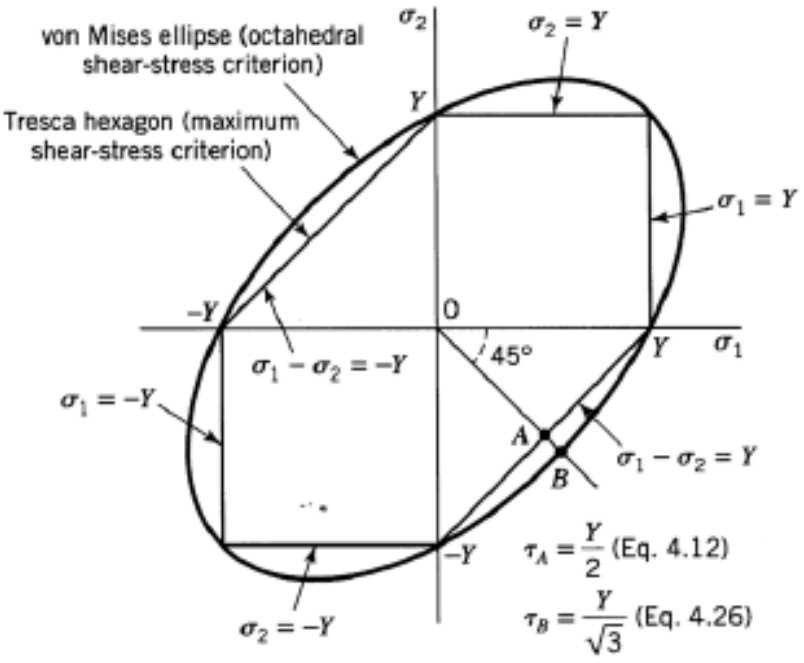

Figure 4.1 Von Mises and Tresca yield surface under biaxial loading (Boresi and Schmidt, 2002)

The displacement for both x and y directions at the outer boundary of the mesh are constrained. The nodes at the plane of symmetry is constrained in normal direction

(y-direction). The caisson had a diameter of 5 m. The properties of soil and caisson are summarized in the following Table 4.1. A general mesh of this 2-D problem is illustrated in Figure 4.2.

The caisson is sub-divided into 50 segments around the circumference to obtain the fine enough mesh for analysis. The detailed 2-D mesh discretization is discussed in the next chapter.

Table 4.1 Soil and Caisson Properties

<table>
<tr><th colspan="2">Soil</th><th colspan="3">Caisson</th></tr>
<tr><th>Soil Rigidity Index (RI) kPa</th><th>Poisson's Ratio</th><th>Elastic Modulus, kPa</th><th>Poisson's Ratio</th><th>D/t *</th></tr>
<tr><td>300</td><td rowspan="3">0.49</td><td rowspan="3">$2*10^8$ Rigid</td><td rowspan="3">0.3</td><td>80</td></tr>
<tr><td>200</td><td>125</td></tr>
<tr><td>100</td><td>160</td></tr>
</table>

* D=caisson diameter; t=caisson shell thickness

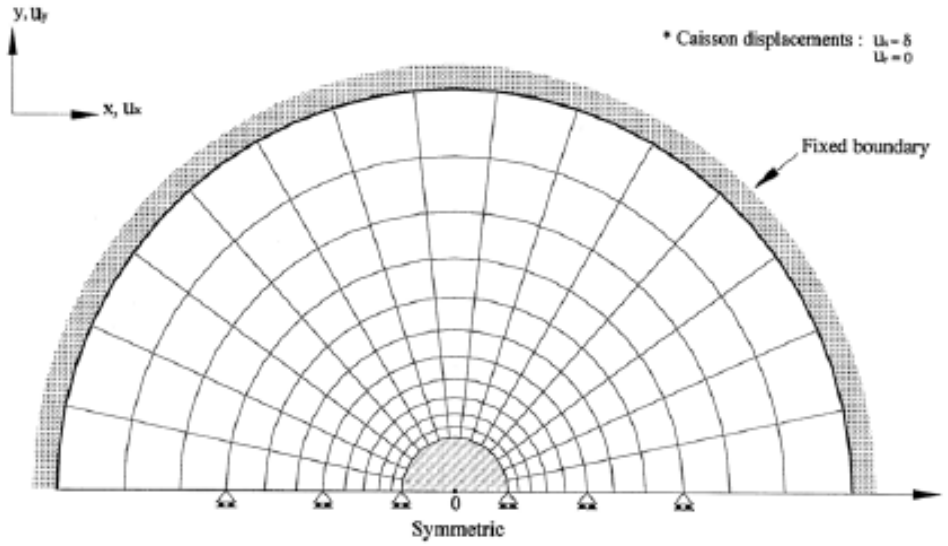

Figure 4.2 2-D mesh (Moon, 2000)

Finite Element Analysis Program

The caisson was loaded horizontally in the soil by the displacement-controlled loading. The shell is considered as a rigid body. The horizontal displacement input is 0.01 m, 0.05 m, 0.1 m, 0.2 m, 0.3 m, 0.4 m, 0.5 m, 0.6 m, 0.8 m, 1.0 m, 1.4 m, 2.0 m, and 2.8 m. At each loading stage, the corresponding external and internal reaction stresses for each soil element contacting the caisson is obtained from the stresses output from the finite element analysis. The net stresses are then obtained by subtracting the internal soil stresses from the external soil stresses. The net stresses in global x and y directions will need to be converted to forces in radial and tangential directions for spring generation purpose. A typical soil stress diagram is shown in Figure 4.3.

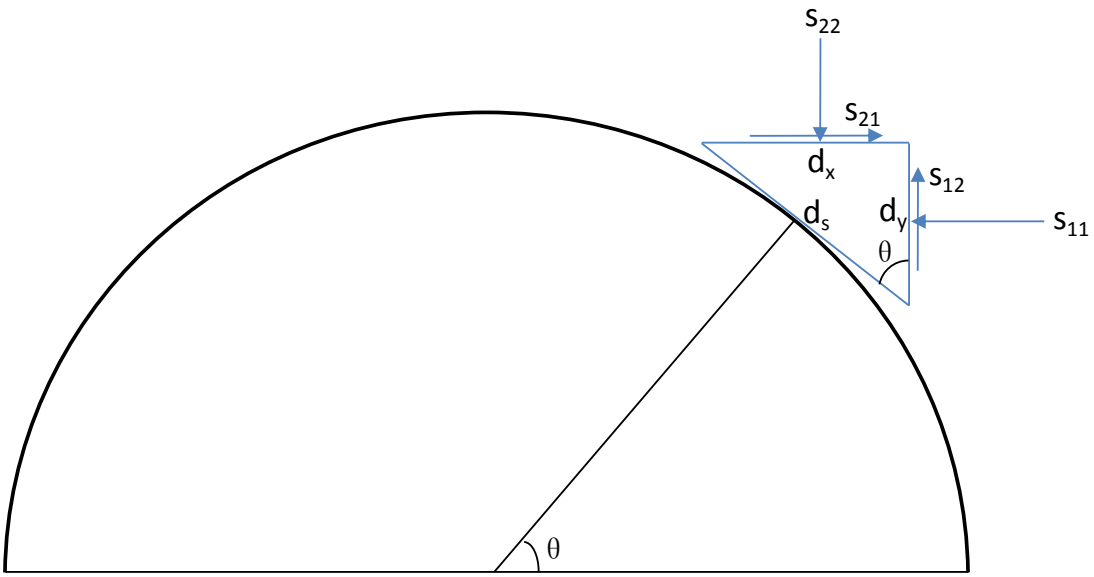

Figure 4.3 Stress diagram of soil element around caisson

The forces in global x and y directions are expressed as follow:

$f_x = s_{11}\cos\theta + s_{12}\sin\theta$.....(4.2)

$f_y = s_{22}\sin\theta + s_{12}\cos\theta$.....(4.3)

Where,

s_{11}=stress in x direction

s_{22}=stress in y direction

s_{12}=shear stress

As the caisson is displaced, the soil reaction stress can also be expressed in radial and tangential components as illustrated in Figure 4.4.

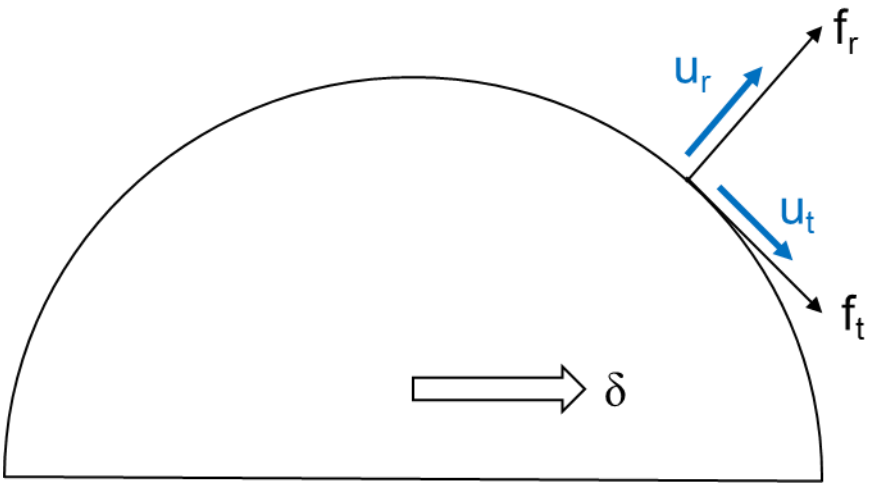

Figure 4.4 Radial and tangential soil stress due to caisson lateral displacement

The soil reaction forces in radial and tangential directions are related to the components in x and y directions, and can be expressed as follow:

$f_r=f_x\cos\theta+f_y\sin\theta$.....(4.4)

$f_t=f_x\sin\theta+f_y\cos\theta$.....(4.5)

In order to perform parametric study, the different caisson shell thickness (t), soil rigidity index ($RI=G/S_u$), and flexibility of caisson are utilized for generating the spring properties. Three caisson shell thickness, D/t=160 (t=3.125 cm), D/t=125 (t=4 cm), and D/t=80 (t=6.25 cm), three rigidity index RI=100, RI=200, and RI=300, and caisson stiffness with regular steel modulus and fully rigid caisson are used for the spring properties generating.

Analysis Results

The results of normal stress in x-direction, s_{11}, in y-direction, s_{22}, and shear stress, s_{12}/s_{21} for all the soil elements contacting caisson internally and externally are obtained from 2-D analyses for the cases with different caisson shell thickness, soil rigidity index, and caisson stiffness. As discussed in the previous section, the net soil stresses are then converted to radial and tangential stresses. It is noted that the above stresses are soil element stresses. While for spring property input for ABAQUS program, nodal property will be needed instead of element property since each spring will be connected to each node. Therefore, a simple step will be conducted to obtain the nodal stresses. It is considered that each nodal stress will be the average stresses of the adjacent two elements. For the node at 0 and 180 degree, the extrapolation will be used to obtain approximate nodal stress. The results of radial nodal stress for the different cases are shown in Figure 4.5 to 4.10.

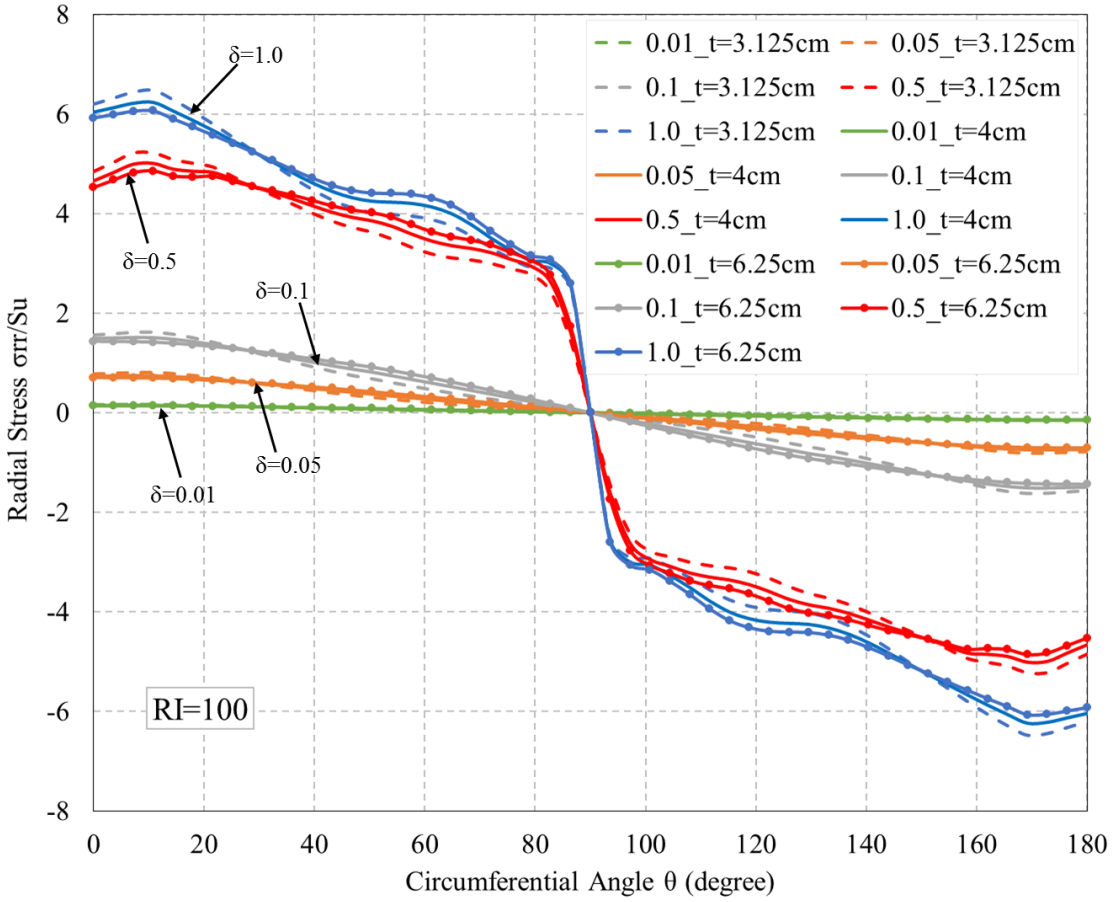

Figure 4.5 Radial net soil stress for flexible caisson with RI=100 for different caisson shell thickness

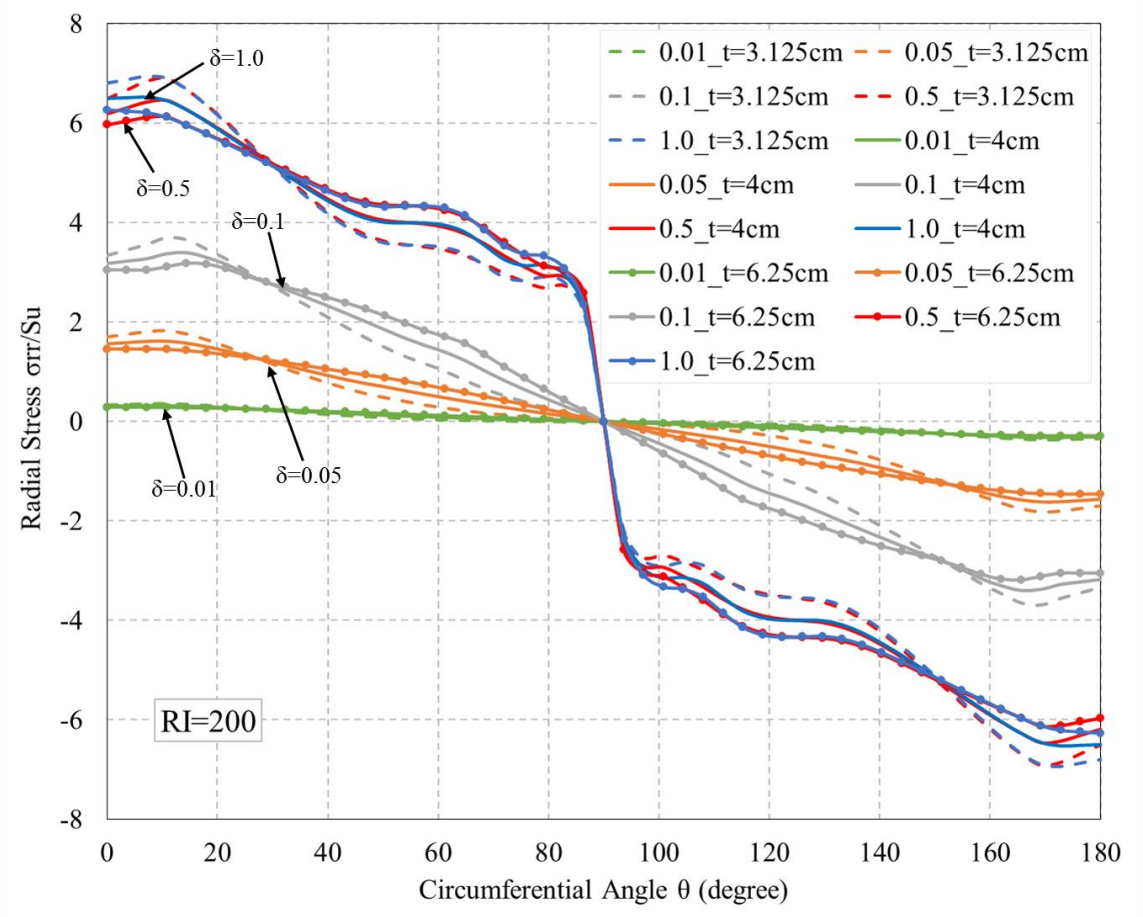

Figure 4.6 Radial net soil stress for flexible caisson with RI=200 for different caisson shell thickness

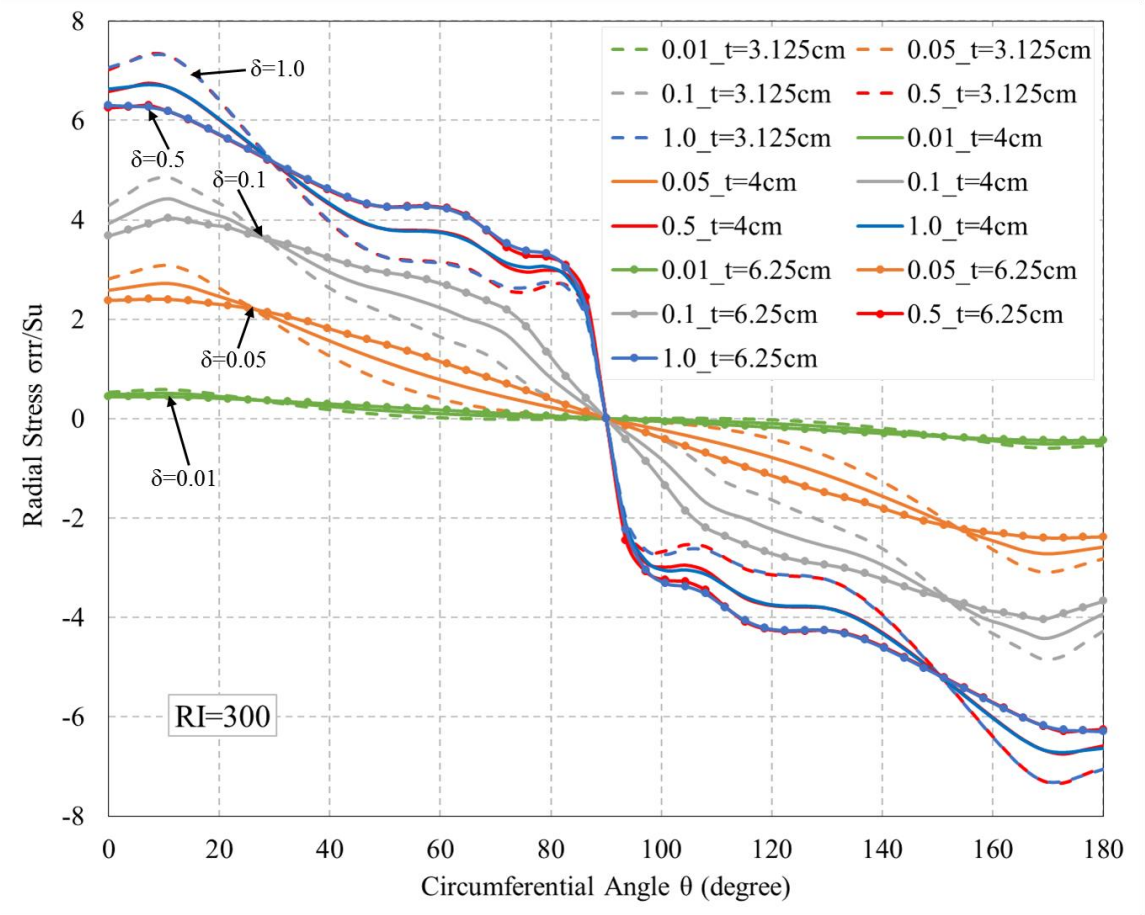

Figure 4.7 Radial net soil stress for flexible caisson with RI=300 for different caisson shell thickness

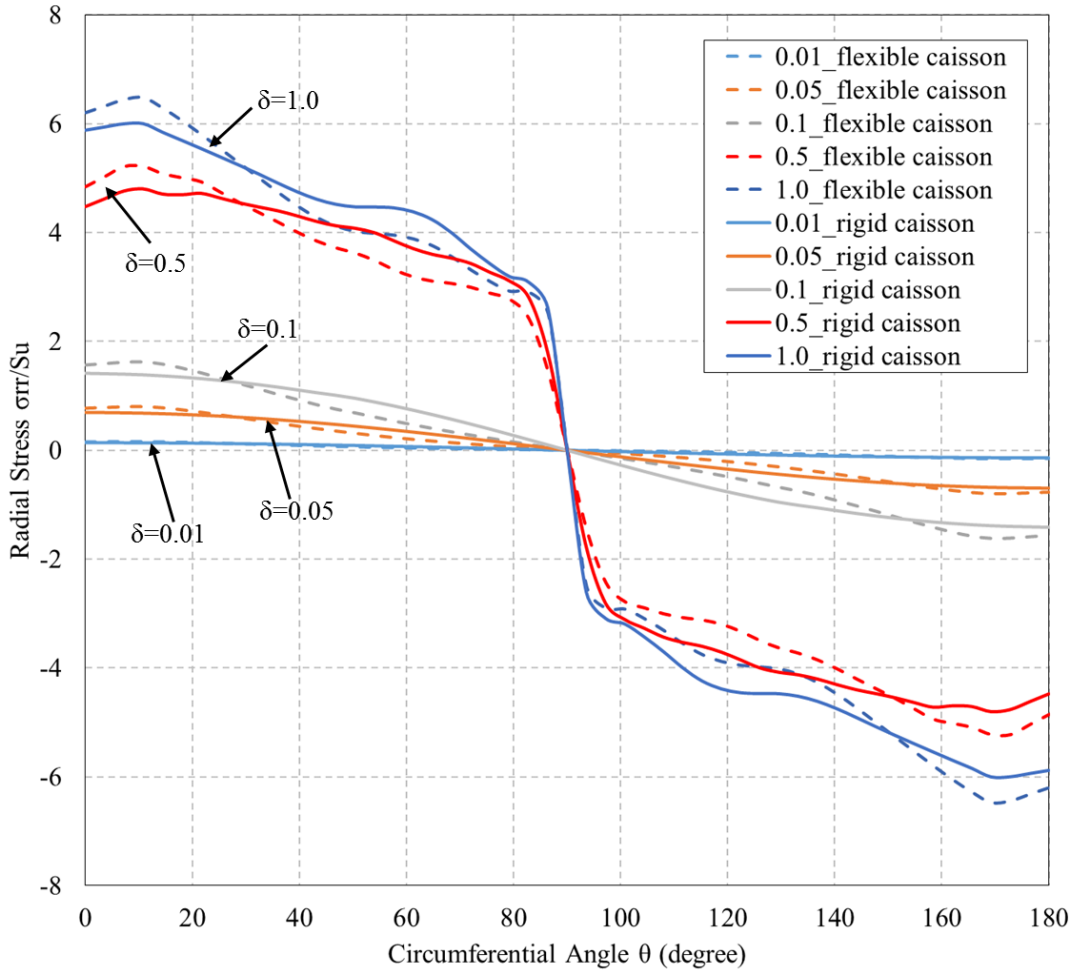

Figure 4.8 Radial net soil stress flexible caisson (t=3.125cm) and rigid caisson with RI=100

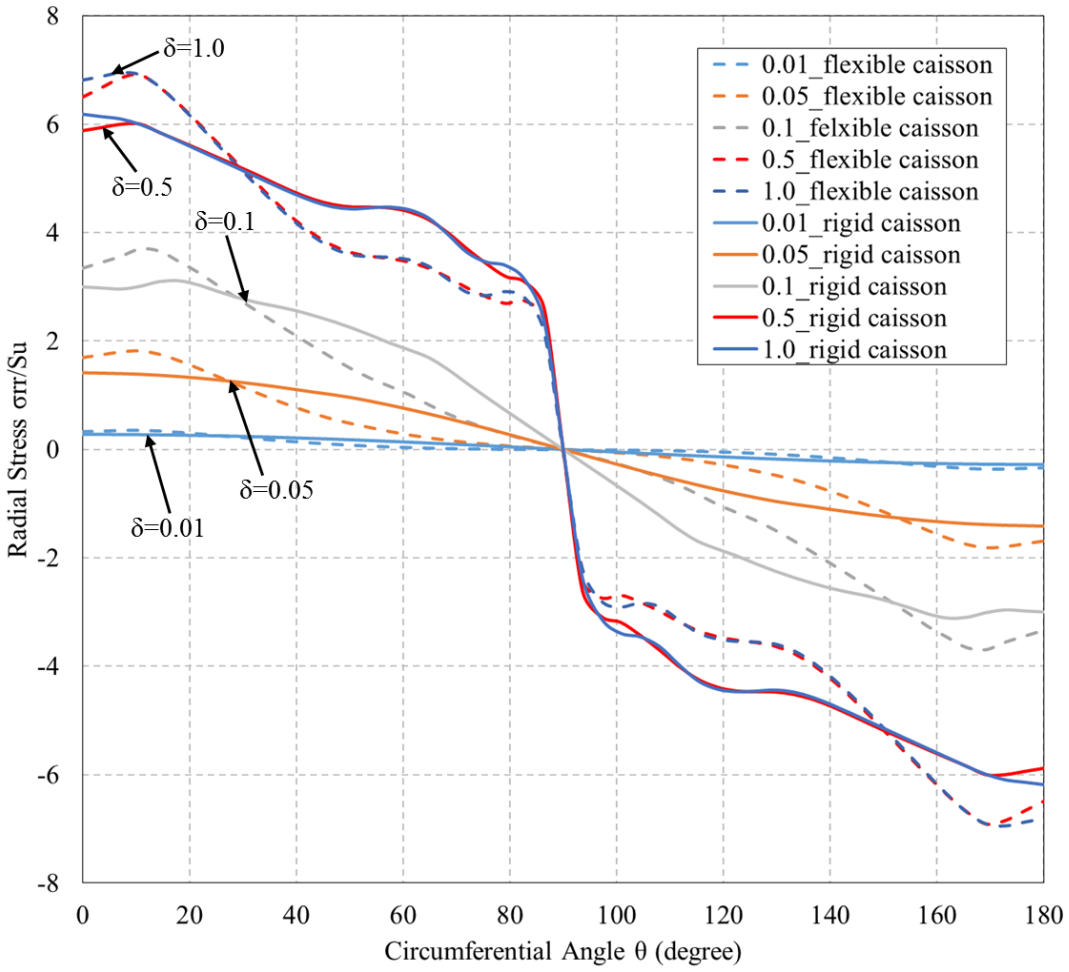

Figure 4.9 Radial net soil stress flexible caisson (t=3.125cm) and rigid caisson with RI=200

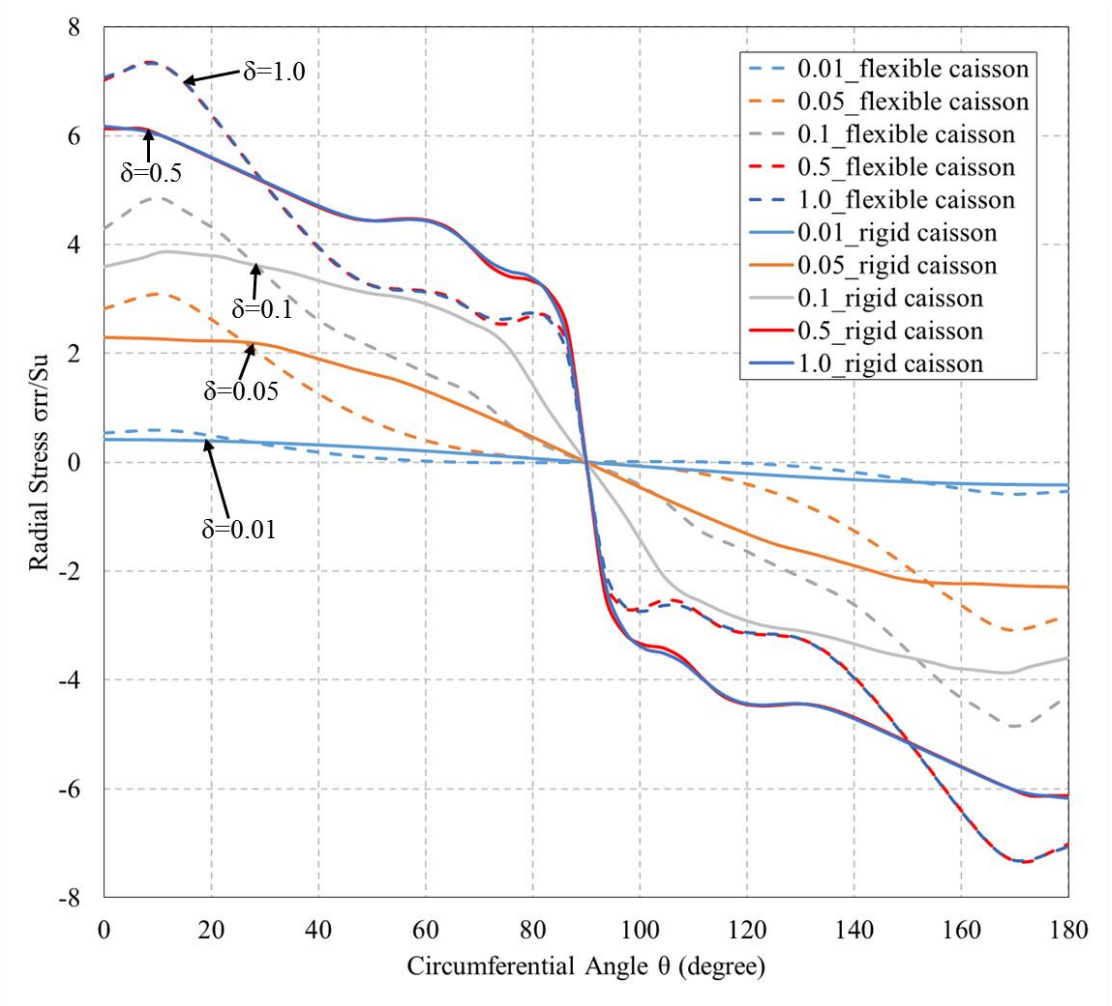

Figure 4.10 Radial net soil stress flexible caisson (t=3.125cm) and rigid caisson with RI=300

The results showed that the radial stresses with thicker caisson shell were lower than with the thinner shell at front and back side of the caisson, approximately from 0 to 30 degrees and 150 to 180 degrees, but turned higher than the lower RI from 30 to 150 degrees. Generally, the difference between the thick and thin shells was greater with larger soil RI. The radial stresses with rigid caisson had the same tendency that they were lower than the flexible caisson at front and back side of the caisson, but were

higher from 30 to 150 degrees, and that difference between the rigid and flexible caisson was great with larger soil RI.

The results of tangential nodal stress for the different cases are also shown in Figure 4.11 to 4.16.

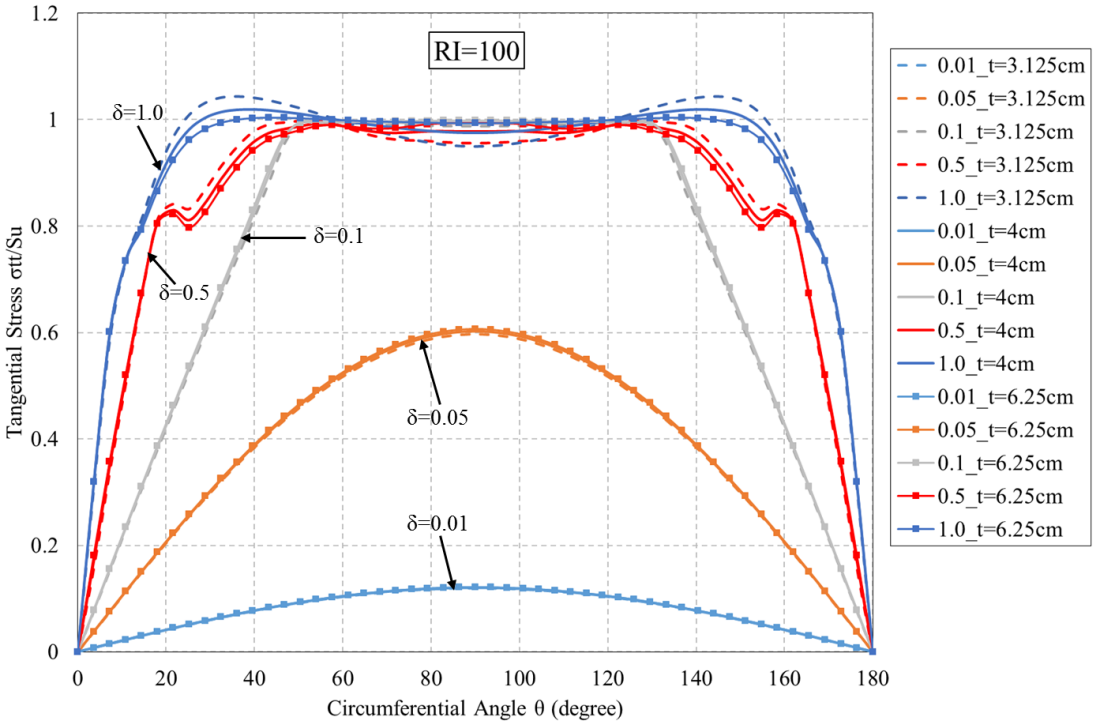

Figure 4.11 Tangential net soil stress with RI=100 for different caisson shell thickness

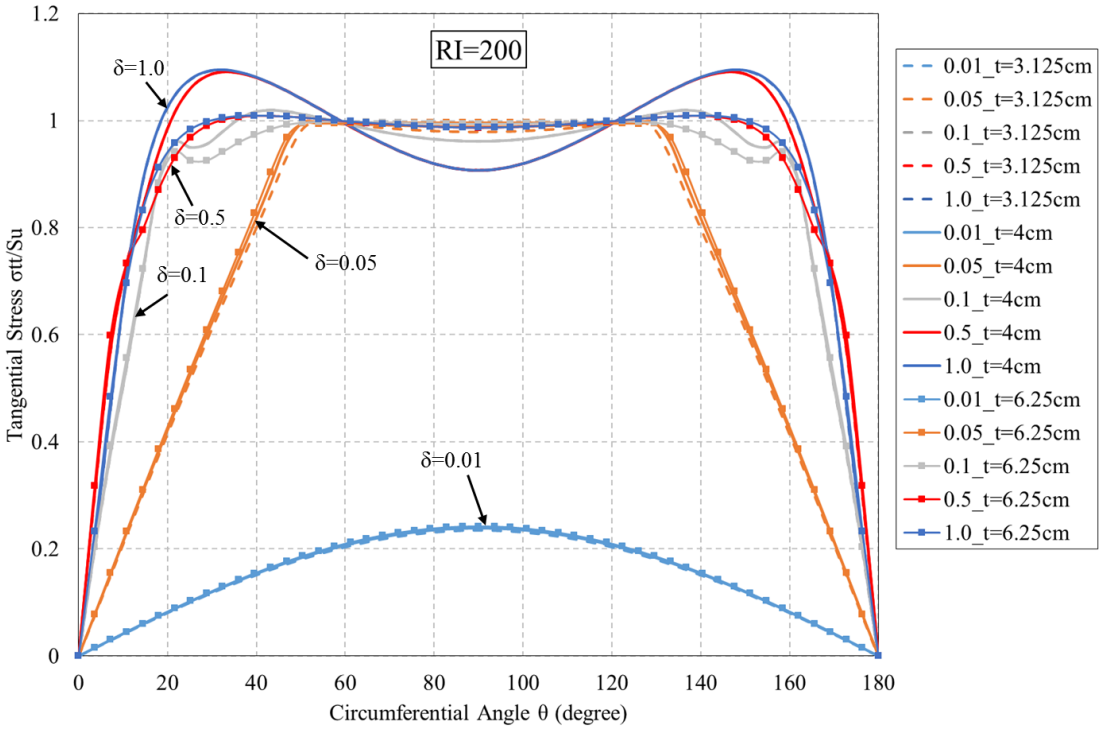

Figure 4.12 Tangential net soil stress with RI=200 for different caisson shell thickness

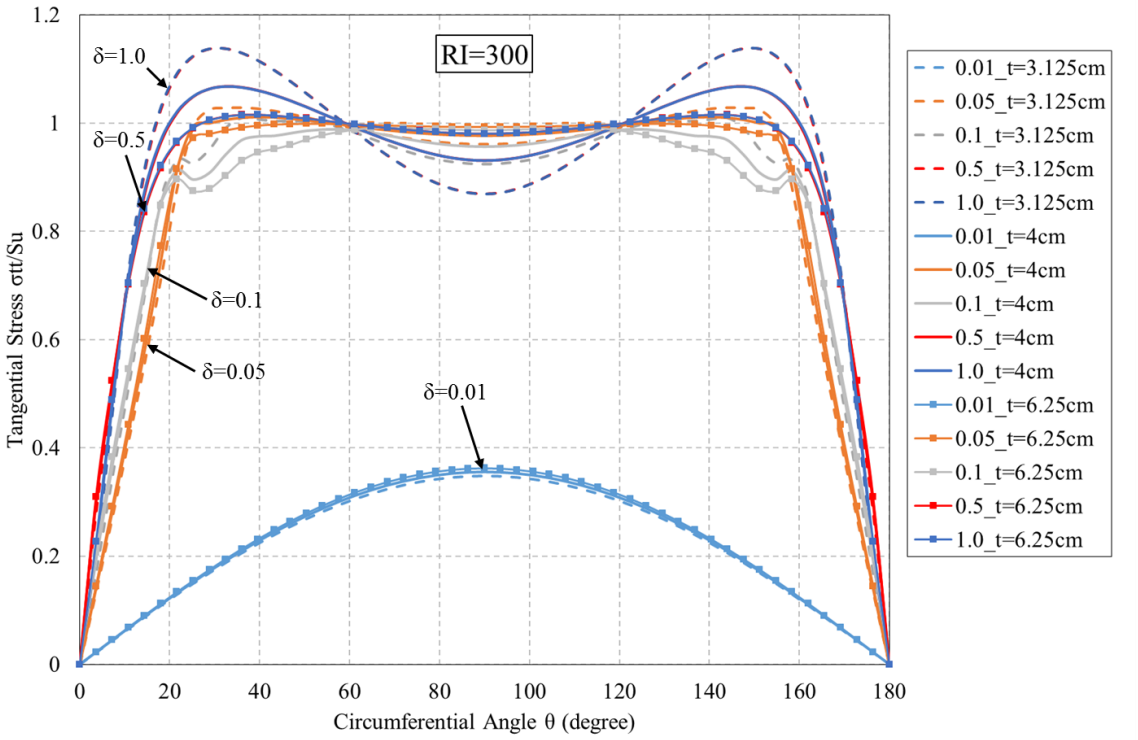

Figure 4.13 Tangential net soil stress with RI=300 for different caisson shell thickness

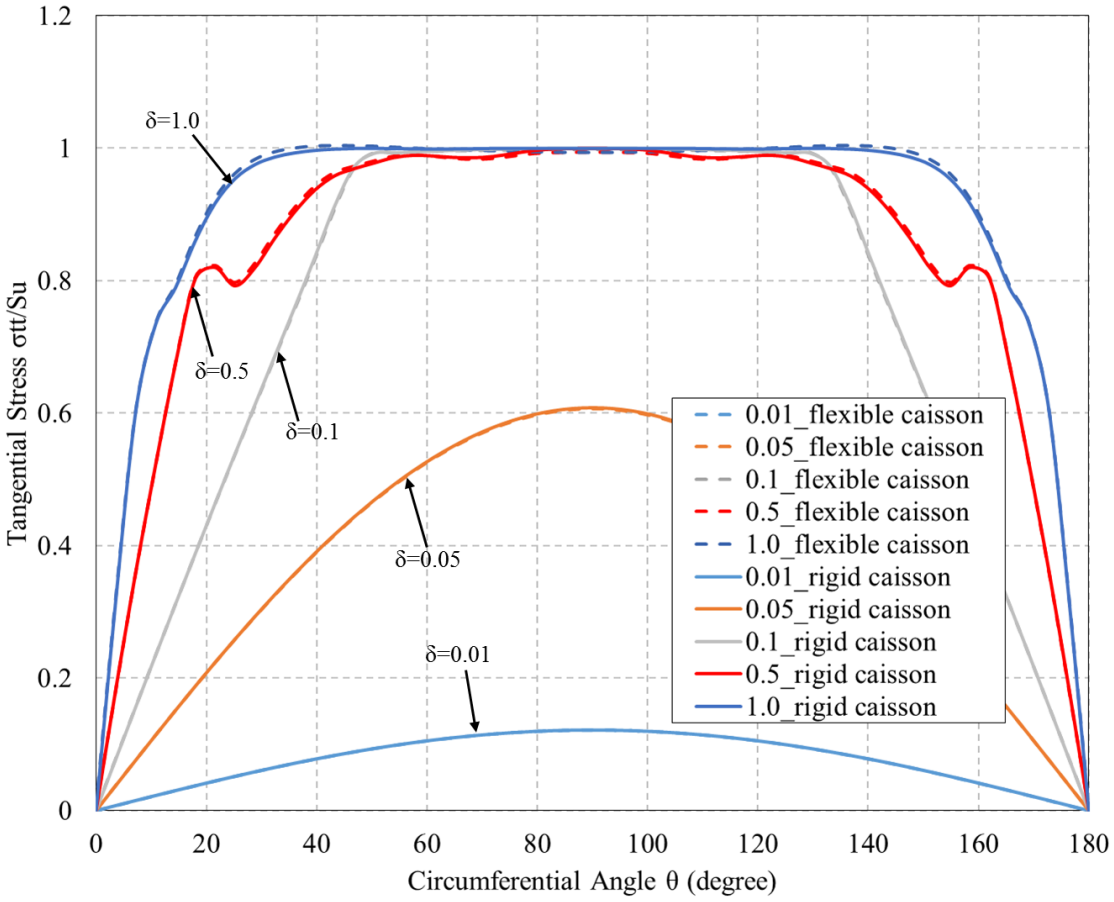

Figure 4.14 Radial net soil stress flexible caisson (t=6.25cm) and rigid caisson with RI=100

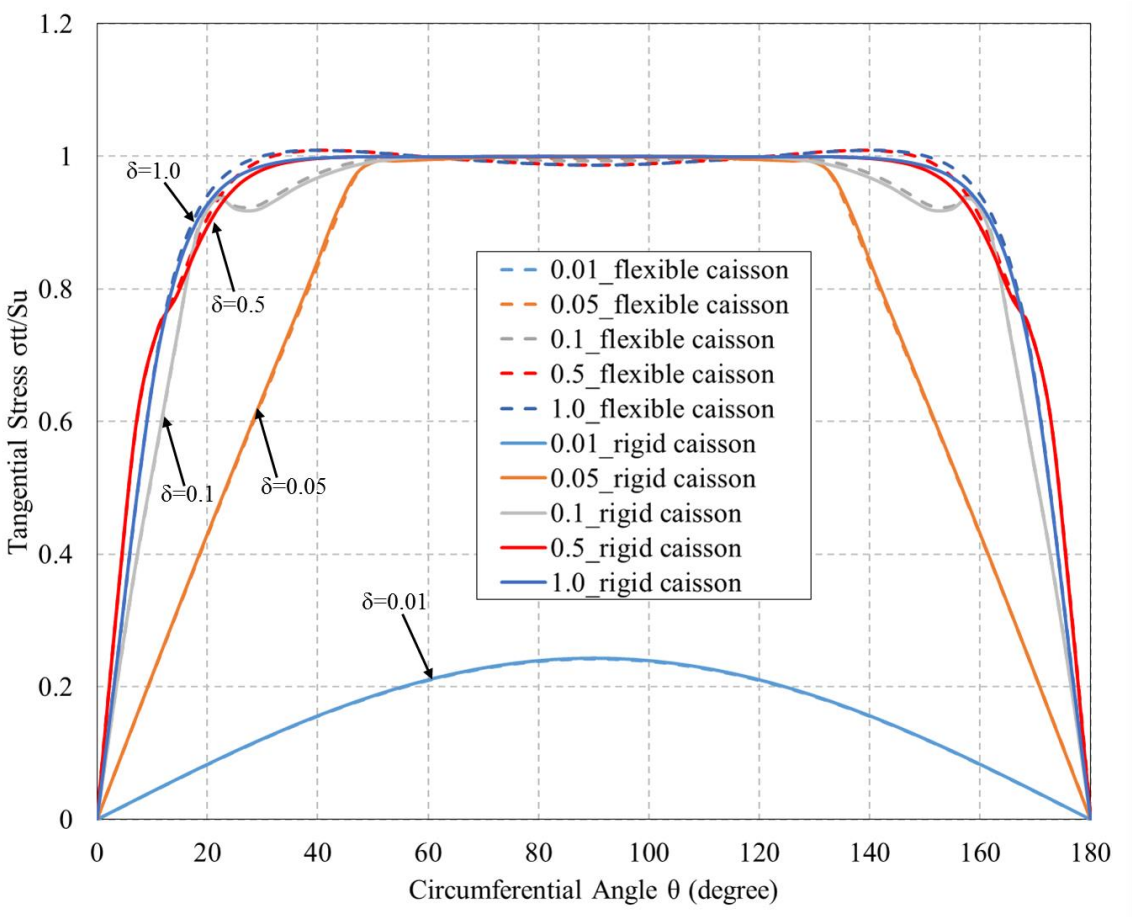

Figure 4.15 Radial net soil stress flexible caisson (t=6.25cm) and rigid caisson with RI=200

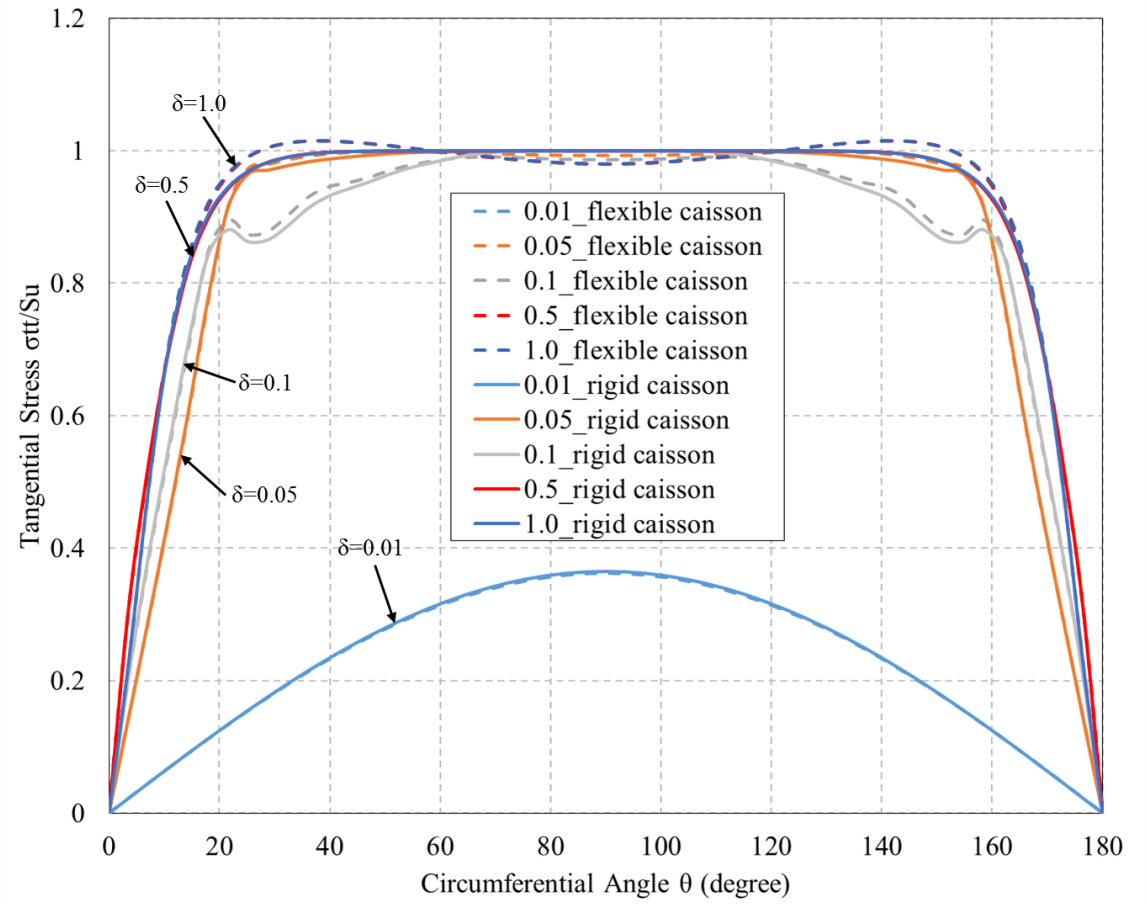

Figure 4.16 Radial net soil stress flexible caisson (t=6.25cm) and rigid caisson with RI=300

The results showed that generally the tangential stresses were greater with larger RI and maximized at around 1 kPa which was the undrained shear strength of the soil. The tangential stresses curves for flexible caisson were characterized with two humps at about 30 and 150 degrees, and dipped at about 90 degree. This 'up-and-down' effect decreased with decreasing RI. The tangential stresses for rigid caisson were almost identical to flexible caisson with shell thickness of 6.25 cm for all RIs.

In Abaqus, the spring property are input as pairs of radial force and radial displacement, or tangential force and tangential displacement. Therefore, the radial and tangential normalized radial soil force and displacement are shown in tabular forms needed to generate 3-D spring property in Table 4.2, 4.3, and 4.4, and tangential soil nodal forces and displacement are shown in Table 4.5, 4.6, and 4.7. The corresponding p-y curves of spring forces and displacement in radial direction are shown in Figure 4.17 to 4.19, and tangential direction in 4.20 to 4.22.

Table 4.2 Radial soil nodal forces for RI of 100

θ	u_x	0.01	0.05	0.1	0.2	0.3	0.4	0.5	0.6	0.8	1	1.4	2	2.8
3.6	u_r	0.00998027	0.049901336	0.099802673	0.199605346	0.299408019	0.399210691	0.499013364	0.598816037	0.798421383	0.998026728	1.39723742	1.996053457	2.79447484
	σ_r	0.1384138	0.692268751	1.406837194	2.978812318	3.674296116	4.15014365	4.619778715	4.951754286	5.605056741	5.939440402	6.120484599	6.139125068	6.135258292
18	u_r	0.00951057	0.047552826	0.095105652	0.190211303	0.285316955	0.380422607	0.475528258	0.57063391	0.760845213	0.951056516	1.331479123	1.902113033	2.662958246
	σ_r	0.13190532	0.659656766	1.344937101	3.111168641	3.809899216	4.316947765	4.694491391	5.011699173	5.644853658	5.695386985	5.68404707	5.685932684	5.692189509
32.4	u_r	0.00844328	0.042216396	0.084432793	0.168865585	0.253298378	0.33773117	0.422163963	0.506596755	0.67546234	0.844327926	1.182059096	1.688655851	2.364118191
	σ_r	0.11709804	0.585570779	1.205590865	2.716043389	3.537944584	4.038642943	4.469631583	4.77901601	5.21932268	5.075311777	5.029843773	5.035264033	5.044244182
46.8	u_r	0.00684547	0.034227355	0.068454711	0.136909421	0.205364132	0.273818842	0.342273553	0.410728264	0.547637685	0.684547106	0.958365948	1.369094212	1.916731897
	σ_r	0.09494738	0.474693042	1.010268142	2.363884318	3.158960615	3.749242555	4.125919724	4.415567671	4.726774075	4.519465046	4.468394511	4.476308187	4.482283234
61.2	u_r	0.00481754	0.024087684	0.048175367	0.096350735	0.144526102	0.19270147	0.240876837	0.289052204	0.385402939	0.481753674	0.674455144	0.963507348	1.348910287
	σ_r	0.0668139	0.33405467	0.737945936	1.834097839	2.879290355	3.37418179	3.707623268	3.984741141	4.16174913	4.383499354	4.431277299	4.420157689	4.412608399
75.6	u_r	0.0024869	0.012434494	0.024868989	0.049737977	0.074606966	0.099475955	0.124344944	0.149213932	0.19895191	0.248689887	0.348165842	0.497379774	0.696331684
	σ_r	0.03448698	0.172435264	0.388673348	0.963610265	2.088355117	2.899205523	3.269314018	3.457447473	3.473032073	3.427441778	3.401382749	3.455886696	3.500393134
90	u_r	2.833E-18	1.41651E-17	2.83302E-17	5.66604E-17	8.49906E-17	1.13321E-16	1.41651E-16	1.69981E-16	2.26642E-16	2.83302E-16	3.96623E-16	5.66604E-16	7.93246E-16
	σ_r	1.223E-16	6.12357E-16	1.00614E-15	1.02002E-15	1.01308E-15	1.02696E-15	9.99201E-16	1.11022E-15	1.11022E-15	1.33227E-15	1.11022E-15	1.11022E-15	9.99201E-16
104.4	u_r	-0.0024869	-0.012434494	-0.024868989	-0.049737977	-0.074606966	-0.099475955	-0.124344944	-0.149213932	-0.19895191	-0.248689887	-0.348165842	-0.497379774	-0.696331684
	σ_r	-0.034487	-0.172435264	-0.388673348	-0.963610265	-2.088355117	-2.899205523	-3.269314018	-3.457447473	-3.473032073	-3.427441778	-3.401382749	-3.455886696	-3.500393134
118.8	u_r	-0.0048175	-0.024087684	-0.048175367	-0.096350735	-0.144526102	-0.19270147	-0.240876837	-0.289052204	-0.385402939	-0.481753674	-0.674455144	-0.963507348	-1.348910287
	σ_r	-0.0668139	-0.33405467	-0.737945936	-1.834097839	-2.879290355	-3.37418179	-3.707623268	-3.984741141	-4.16174913	-4.383499354	-4.431277299	-4.420157689	-4.412608399
133.2	u_r	-0.0068455	-0.034227355	-0.068454711	-0.136909421	-0.205364132	-0.273818842	-0.342273553	-0.410728264	-0.547637685	-0.684547106	-0.958365948	-1.369094212	-1.916731897
	σ_r	-0.0949474	-0.474693042	-1.010268142	-2.363884318	-3.158960615	-3.749242555	-4.125919724	-4.415567671	-4.726774075	-4.519465046	-4.468394511	-4.476308187	-4.482283234
147.6	u_r	-0.0084433	-0.042216396	-0.084432793	-0.168865585	-0.253298378	-0.33773117	-0.422163963	-0.506596755	-0.67546234	-0.844327926	-1.182059096	-1.688655851	-2.364118191
	σ_r	-0.117098	-0.585570779	-1.205590865	-2.716043389	-3.537944584	-4.038642943	-4.469631583	-4.77901601	-5.21932268	-5.075311777	-5.029843773	-5.035264033	-5.044244182
162	u_r	-0.0095106	-0.047552826	-0.095105652	-0.190211303	-0.285316955	-0.380422607	-0.475528258	-0.57063391	-0.760845213	-0.951056516	-1.331479123	-1.902113033	-2.662958246
	σ_r	-0.1319053	-0.659656766	-1.344937101	-3.111168641	-3.809899216	-4.316947765	-4.694491391	-5.011699173	-5.644853658	-5.695386985	-5.68404707	-5.685932684	-5.692189509
176.4	u_r	-0.0099803	-0.049901336	-0.099802673	-0.199605346	-0.299408019	-0.399210691	-0.499013364	-0.598816037	-0.798421383	-0.998026728	-1.39723742	-1.996053457	-2.79447484
	σ_r	-0.1384138	-0.692268751	-1.406837194	-2.978812318	-3.674296116	-4.15014365	-4.619778715	-4.951754286	-5.605056741	-5.939440402	-6.120484599	-6.139125068	-6.135258292

Table 4.3 Radial soil nodal forces for RI of 200

θ	u_x	0.01	0.05	0.1	0.2	0.3	0.4	0.5	0.6	0.8	1	1.4	2	2.8
3.6	u_r	0.009980267	0.049901336	0.099802673	0.199605346	0.299408019	0.399210691	0.499013364	0.598816037	0.798421383	0.998026728	1.39723742	1.996053457	2.79447484
	σ_r	0.276939419	1.406896108	2.978918078	4.153150412	4.948578635	5.604326145	5.939635602	6.098979663	6.132394785	6.138841511	6.134954716	6.130560725	6.125400624
18	u_r	0.009510565	0.047552826	0.095105652	0.190211303	0.285316955	0.380422607	0.475528258	0.57063391	0.760845213	0.951056516	1.331479123	1.902113033	2.662958246
	σ_r	0.263914983	1.34545221	3.11126594	4.314890243	5.014734771	5.646290018	5.695981264	5.686766725	5.68369265	5.68608526	5.691854376	5.701445723	5.712632777
32.4	u_r	0.008443279	0.042216396	0.084432793	0.168865585	0.253298378	0.33773117	0.422163963	0.506596755	0.67546234	0.844327926	1.182059096	1.688655851	2.364118191
	σ_r	0.234234591	1.205577365	2.71602033	4.039558084	4.780547826	5.219469034	5.075027277	5.030214812	5.03099107	5.034857599	5.043708141	5.058491641	5.078114312
46.8	u_r	0.006845471	0.034227355	0.068454711	0.136909421	0.205364132	0.273818842	0.342273553	0.410728264	0.547637685	0.684547106	0.958365948	1.369094212	1.916731897
	σ_r	0.189853378	1.010168221	2.363773332	3.741679204	4.420517713	4.727016702	4.51950651	4.464804182	4.472233686	4.475852646	4.481857845	4.494659297	4.519519172
61.2	u_r	0.004817537	0.024087684	0.048175367	0.096350735	0.144526102	0.19270147	0.240876837	0.289052204	0.385402939	0.481753674	0.674455144	0.963507348	1.348910287
	σ_r	0.133611071	0.737797436	1.833854071	3.380486469	3.993820693	4.163454223	4.384330866	4.438628971	4.424325014	4.419800718	4.412310442	4.396699859	4.357332209
75.6	u_r	0.002486899	0.012434494	0.024868989	0.049737977	0.074606966	0.099475955	0.124344944	0.149213932	0.19895191	0.248689887	0.348165842	0.497379774	0.696331684
	σ_r	0.068961615	0.38855239	0.963432454	2.90180193	3.449922793	3.468399503	3.426296978	3.37579596	3.426220861	3.456215179	3.50072143	3.545751914	3.569470622
90	u_r	2.83302E-18	1.41651E-17	2.83302E-17	5.66604E-17	8.49906E-17	1.13321E-16	1.41651E-16	1.69981E-16	2.26642E-16	2.83302E-16	3.96623E-16	5.66604E-16	7.93246E-16
	σ_r	2.46331E-16	1.01308E-15	1.01308E-15	9.99201E-16	9.99201E-16	1.11022E-15	1.33227E-15	1.11022E-15	9.99201E-16	9.99201E-16	1.11022E-15	9.99201E-16	1.11022E-15
104.4	u_r	-0.002486899	-0.012434494	-0.024868989	-0.049737977	-0.074606966	-0.099475955	-0.124344944	-0.149213932	-0.19895191	-0.248689887	-0.348165842	-0.497379774	-0.696331684
	σ_r	-0.068961615	-0.38855239	-0.963432454	-2.90180193	-3.449922793	-3.468399503	-3.426296978	-3.37579596	-3.426220861	-3.456215179	-3.50072143	-3.545751914	-3.569470622
118.8	u_r	-0.004817537	-0.024087684	-0.048175367	-0.096350735	-0.144526102	-0.19270147	-0.240876837	-0.289052204	-0.385402939	-0.481753674	-0.674455144	-0.963507348	-1.348910287
	σ_r	-0.133611071	-0.737797436	-1.833854071	-3.380486469	-3.993820693	-4.163454223	-4.384330866	-4.438628971	-4.424325014	-4.419800718	-4.412310442	-4.396699859	-4.357332209
133.2	u_r	-0.006845471	-0.034227355	-0.068454711	-0.136909421	-0.205364132	-0.273818842	-0.342273553	-0.410728264	-0.547637685	-0.684547106	-0.958365948	-1.369094212	-1.916731897
	σ_r	-0.189853378	-1.010168221	-2.363773332	-3.741679204	-4.420517713	-4.727016702	-4.51950651	-4.464804182	-4.472233686	-4.475852646	-4.481857845	-4.494659297	-4.519519172
147.6	u_r	-0.008443279	-0.042216396	-0.084432793	-0.168865585	-0.253298378	-0.33773117	-0.422163963	-0.506596755	-0.67546234	-0.844327926	-1.182059096	-1.688655851	-2.364118191
	σ_r	-0.234234591	-1.205577365	-2.71602033	-4.039558084	-4.780547826	-5.219469034	-5.075027277	-5.030214812	-5.03099107	-5.034857599	-5.043708141	-5.058491641	-5.078114312
162	u_r	-0.009510565	-0.047552826	-0.095105652	-0.190211303	-0.285316955	-0.380422607	-0.475528258	-0.57063391	-0.760845213	-0.951056516	-1.331479123	-1.902113033	-2.662958246
	σ_r	-0.263914983	-1.34545221	-3.11126594	-4.314890243	-5.014734771	-5.646290018	-5.695981264	-5.686766725	-5.68369265	-5.68608526	-5.691854376	-5.701445723	-5.712632777
176.4	u_r	-0.009980267	-0.049901336	-0.099802673	-0.199605346	-0.299408019	-0.399210691	-0.499013364	-0.598816037	-0.798421383	-0.998026728	-1.39723742	-1.996053457	-2.79447484
	σ_r	-0.276939419	-1.406896108	-2.978918078	-4.153150412	-4.948578635	-5.604326145	-5.939635602	-6.098979663	-6.132394785	-6.138841511	-6.134954716	-6.130560725	-6.125400624

Table 4.4 Radial soil nodal forces for RI of 300

θ	u_x	0.01	0.05	0.1	0.2	0.3	0.4	0.5	0.6	0.8	1	1.4	2	2.8
3.6	u_r	0.009980267	0.049901336	0.099802673	0.199605346	0.299408019	0.399210691	0.499013364	0.598816037	0.798421383	0.998026728	1.39723742	1.996053457	2.79447484
	σ_r	0.41537738	2.28626186	3.6742819	4.946957062	5.833245375	6.095543007	6.12744111	6.139991218	6.13722019	6.134631445	6.12970259	6.124412163	6.120053449
18	u_r	0.009510565	0.047552826	0.095105652	0.190211303	0.285316955	0.380422607	0.475528258	0.57063391	0.760845213	0.951056516	1.331479123	1.902113033	2.662958246
	σ_r	0.395845554	2.230591459	3.811300132	5.016765473	5.700206078	5.687943145	5.683552884	5.684504129	5.689092156	5.693934553	5.703143407	5.715944386	5.731490401
32.4	u_r	0.008443279	0.042216396	0.084432793	0.168865585	0.253298378	0.33773117	0.422163963	0.506596755	0.67546234	0.844327926	1.182059096	1.688655851	2.364118191
	σ_r	0.351328042	2.116211947	3.537868925	4.777500789	5.143419123	5.031407796	5.030318309	5.033138345	5.039210739	5.045945654	5.06093085	5.082578676	5.110144023
46.8	u_r	0.006845471	0.034227355	0.068454711	0.136909421	0.205364132	0.273818842	0.342273553	0.410728264	0.547637685	0.684547106	0.958365948	1.369094212	1.916731897
	σ_r	0.284762	1.707411524	3.161560919	4.420197383	4.614726482	4.466214726	4.470703521	4.474328392	4.478727398	4.483184534	4.498122481	4.525215767	4.554991431
61.2	u_r	0.004817537	0.024087684	0.048175367	0.096350735	0.144526102	0.19270147	0.240876837	0.289052204	0.385402939	0.481753674	0.674455144	0.963507348	1.348910287
	σ_r	0.20031134	1.267692247	2.874469921	3.993145173	4.263668257	4.438149768	4.426244747	4.421594188	4.415647643	4.410056164	4.390842814	4.347563979	4.297631862
75.6	u_r	0.002486899	0.012434494	0.024868989	0.049737977	0.074606966	0.099475955	0.124344944	0.149213932	0.19895191	0.248689887	0.348165842	0.497379774	0.696331684
	σ_r	0.103388663	0.660200274	2.089524311	3.455754137	3.51704534	3.376127219	3.414025295	3.440573117	3.479576799	3.508522822	3.54965478	3.572351908	3.595493363
90	u_r	2.83302E-18	1.41651E-17	2.83302E-17	5.66604E-17	8.49906E-17	1.13321E-16	1.41651E-16	1.69981E-16	2.26642E-16	2.83302E-16	3.96623E-16	5.66604E-16	7.93246E-16
	σ_r	3.67761E-16	1.00614E-15	9.99201E-16	9.99201E-16	8.88178E-16	1.11022E-15	9.99201E-16	1.11022E-15	9.99201E-16	9.99201E-16	9.99201E-16	1.11022E-15	9.99201E-16
104.4	u_r	-0.002486899	-0.012434494	-0.024868989	-0.049737977	-0.074606966	-0.099475955	-0.124344944	-0.149213932	-0.19895191	-0.248689887	-0.348165842	-0.497379774	-0.696331684
	σ_r	-0.103388663	-0.660200274	-2.089524311	-3.455754137	-3.51704534	-3.376127219	-3.414025295	-3.440573117	-3.479576799	-3.508522822	-3.54965478	-3.572351908	-3.595493363
118.8	u_r	-0.004817537	-0.024087684	-0.048175367	-0.096350735	-0.144526102	-0.19270147	-0.240876837	-0.289052204	-0.385402939	-0.481753674	-0.674455144	-0.963507348	-1.348910287
	σ_r	-0.20031134	-1.267692247	-2.874469921	-3.993145173	-4.263668257	-4.438149768	-4.426244747	-4.421594188	-4.415647643	-4.410056164	-4.390842814	-4.347563979	-4.297631862
133.2	u_r	-0.006845471	-0.034227355	-0.068454711	-0.136909421	-0.205364132	-0.273818842	-0.342273553	-0.410728264	-0.547637685	-0.684547106	-0.958365948	-1.369094212	-1.916731897
	σ_r	-0.284762	-1.707411524	-3.161560919	-4.420197383	-4.614726482	-4.466214726	-4.470703521	-4.474328392	-4.478727398	-4.483184534	-4.498122481	-4.525215767	-4.554991431
147.6	u_r	-0.008443279	-0.042216396	-0.084432793	-0.168865585	-0.253298378	-0.33773117	-0.422163963	-0.506596755	-0.67546234	-0.844327926	-1.182059096	-1.688655851	-2.364118191
	σ_r	-0.351328042	-2.116211947	-3.537868925	-4.777500789	-5.143419123	-5.031407796	-5.030318309	-5.033138345	-5.039210739	-5.045945654	-5.06093085	-5.082578676	-5.110144023
162	u_r	-0.009510565	-0.047552826	-0.095105652	-0.190211303	-0.285316955	-0.380422607	-0.475528258	-0.57063391	-0.760845213	-0.951056516	-1.331479123	-1.902113033	-2.662958246
	σ_r	-0.395845554	-2.230591459	-3.811300132	-5.016765473	-5.700206078	-5.687943145	-5.683552884	-5.684504129	-5.689092156	-5.693934553	-5.703143407	-5.715944386	-5.731490401
176.4	u_r	-0.009980267	-0.049901336	-0.099802673	-0.199605346	-0.299408019	-0.399210691	-0.499013364	-0.598816037	-0.798421383	-0.998026728	-1.39723742	-1.996053457	-2.79447484
	σ_r	-0.41537738	-2.28626186	-3.6742819	-4.946957062	-5.833245375	-6.095543007	-6.12744111	-6.139991218	-6.13722019	-6.134631445	-6.12970259	-6.124412163	-6.120053449

Table 4.5 Tangential soil nodal forces for RI of 100

θ	u_x	0.01	0.05	0.1	0.2	0.3	0.4	0.5	0.6	0.8	1	1.4	2	2.8
3.6	u_r	0.000627905	0.003139526	0.006279052	0.012558104	0.018837156	0.025116208	0.03139526	0.037674312	0.050232416	0.06279052	0.087906727	0.125581039	0.175813455
	σ_r	0.007638707	0.03820006	0.078476004	0.204173121	0.210466245	0.189790253	0.184479364	0.151119033	0.157888709	0.320164675	0.338123926	0.236382604	0.230921834
18	u_r	0.00309017	0.01545085	0.030901699	0.061803399	0.092705098	0.123606798	0.154508497	0.185410197	0.247213595	0.309016994	0.432623792	0.618033989	0.865247584
	σ_r	0.037588235	0.187993525	0.388360995	0.879644986	0.844197189	0.821185918	0.803166658	0.784123357	0.785673166	0.860431925	0.898548289	0.900255879	0.902646522
32.4	u_r	0.005358268	0.02679134	0.053582679	0.107165359	0.160748038	0.214330718	0.267913397	0.321496077	0.428661436	0.535826795	0.750157513	1.07165359	1.500315026
	σ_r	0.06518392	0.325959261	0.686041711	0.933946248	0.888886871	0.885635558	0.864159788	0.881365544	0.903496113	0.986735082	0.990549341	0.990530523	0.990251704
46.8	u_r	0.007289686	0.036448431	0.072896863	0.145793725	0.218690588	0.291587451	0.364484314	0.437381176	0.583174902	0.728968627	1.020556078	1.457937255	2.041112157
	σ_r	0.088699332	0.443446929	0.971748388	0.986596653	0.951243724	0.966900674	0.969138882	0.974743383	0.982755383	0.999634958	0.999431445	0.999552492	0.999434105
61.2	u_r	0.008763067	0.043815334	0.087630668	0.175261336	0.262892004	0.350522672	0.43815334	0.525784008	0.701045344	0.87630668	1.226829352	1.75261336	2.453658704
	σ_r	0.106625811	0.533093873	0.995652278	0.998910766	0.986717505	0.976050716	0.988297358	0.99037293	0.998203071	0.998812308	0.999499482	0.999586602	0.999714635
75.6	u_r	0.009685832	0.048429158	0.096858316	0.193716632	0.290574948	0.387433264	0.484291581	0.581149897	0.774866529	0.968583161	1.356016426	1.937166322	2.712032851
	σ_r	0.117851507	0.589250643	0.998990469	0.999984633	0.999386218	0.996437574	0.992040196	0.990565075	0.99713305	0.999877735	1.000016381	0.999847456	0.999942203
90	u_r	0.01	0.05	0.1	0.2	0.3	0.4	0.5	0.6	0.8	1	1.4	2	2.8
	σ_r	0.121619084	0.608295027	0.999933822	1.000003875	0.999921959	0.999921687	0.999845044	0.999704208	0.999645888	0.999868961	0.999883549	0.999940695	0.999972066
104.4	u_r	0.009685832	0.048429158	0.096858316	0.193716632	0.290574948	0.387433264	0.484291581	0.581149897	0.774866529	0.968583161	1.356016426	1.937166322	2.712032851
	σ_r	0.117851507	0.589250643	0.998990469	0.999984633	0.999386218	0.996437574	0.992040196	0.990565075	0.99713305	0.999877735	1.000016381	0.999847456	0.999942203
118.8	u_r	0.008763067	0.043815334	0.087630668	0.175261336	0.262892004	0.350522672	0.43815334	0.525784008	0.701045344	0.87630668	1.226829352	1.75261336	2.453658704
	σ_r	0.106625811	0.533093873	0.995652278	0.998910766	0.986717505	0.976050716	0.988297358	0.99037293	0.998203071	0.998812308	0.999499482	0.999586602	0.999714635
133.2	u_r	0.007289686	0.036448431	0.072896863	0.145793725	0.218690588	0.291587451	0.364484314	0.437381176	0.583174902	0.728968627	1.020556078	1.457937255	2.041112157
	σ_r	0.088699332	0.443446929	0.971748388	0.986596653	0.951243724	0.966900674	0.969138882	0.974743383	0.982755383	0.999634958	0.999431445	0.999552492	0.999434105
147.6	u_r	0.005358268	0.02679134	0.053582679	0.107165359	0.160748038	0.214330718	0.267913397	0.321496077	0.428661436	0.535826795	0.750157513	1.07165359	1.500315026
	σ_r	0.06518392	0.325959261	0.686041711	0.933946248	0.888886871	0.885635558	0.864159788	0.881365544	0.903496113	0.986735082	0.990549341	0.990530523	0.990251704
162	u_r	0.00309017	0.01545085	0.030901699	0.061803399	0.092705098	0.123606798	0.154508497	0.185410197	0.247213595	0.309016994	0.432623792	0.618033989	0.865247584
	σ_r	0.037588235	0.187993525	0.388360995	0.879644986	0.844197189	0.821185918	0.803166658	0.784123357	0.785673166	0.860431925	0.898548289	0.900255879	0.902646522
176.4	u_r	0.000627905	0.003139526	0.006279052	0.012558104	0.018837156	0.025116208	0.03139526	0.037674312	0.050232416	0.06279052	0.087906727	0.125581039	0.175813455
	σ_r	0.007638707	0.03820006	0.078476004	0.204173121	0.210466245	0.189790253	0.184479364	0.151119033	0.157888709	0.320164675	0.338123926	0.236382604	0.230921834

Table 4.6 Tangential soil nodal forces for RI of 200

θ	u_x	0.01	0.05	0.1	0.2	0.3	0.4	0.5	0.6	0.8	1	1.4	2	2.8
3.6	u_t	0.000627905	0.003139526	0.006279052	0.012558104	0.018837156	0.025116208	0.03139526	0.037674312	0.050232416	0.06279052	0.087906727	0.125581039	0.175813455
	σ_r	0.015280157	0.078474778	0.204170527	0.190926138	0.15029645	0.157462169	0.320272213	0.390019527	0.287216935	0.236085063	0.230845562	0.230706981	0.232994679
18	u_t	0.00309017	0.01545085	0.030901699	0.061803399	0.092705098	0.123606798	0.154508497	0.185410197	0.247213595	0.309016994	0.432623792	0.618033989	0.865247584
	σ_r	0.075200346	0.388502145	0.879657823	0.820659934	0.785215153	0.78624874	0.860574321	0.896461455	0.899173579	0.900317468	0.902616394	0.905724963	0.909186238
32.4	u_t	0.005358268	0.02679134	0.053582679	0.107165359	0.160748038	0.214330718	0.267913397	0.321496077	0.428661436	0.535826795	0.750157513	1.07165359	1.500315026
	σ_r	0.130385346	0.686050097	0.933961155	0.885542121	0.882883814	0.903548348	0.987038435	0.990614465	0.990498384	0.990339798	0.990280081	0.990185136	0.989547571
46.8	u_t	0.007289686	0.036448431	0.072896863	0.145793725	0.218690588	0.291587451	0.364484314	0.437381176	0.583174902	0.728968627	1.020556078	1.457937255	2.041112157
	σ_r	0.177379761	0.971787408	0.986604372	0.965972286	0.972763107	0.982514901	0.999400799	0.999546858	0.999249384	0.999318333	0.999201927	0.99916699	0.998969772
61.2	u_t	0.008763067	0.043815334	0.087630668	0.175261336	0.262892004	0.350522672	0.43815334	0.525784008	0.701045344	0.87630668	1.226829352	1.75261336	2.453658704
	σ_r	0.21324703	0.995693249	0.99897282	0.976584059	0.991441638	0.998171027	0.999004732	0.999474155	0.999378471	0.99938181	0.999688012	0.999574573	0.999656439
75.6	u_t	0.009685832	0.048429158	0.096858316	0.193716632	0.290574948	0.387433264	0.484291581	0.581149897	0.774866529	0.968583161	1.356016426	1.937166322	2.712032851
	σ_r	0.235700496	0.9989795	0.999999034	0.996709095	0.990279395	0.99724825	0.999901207	0.99994649	1.000028208	0.999828741	0.99992347	0.999796738	0.999986293
90	u_t	0.01	0.05	0.1	0.2	0.3	0.4	0.5	0.6	0.8	1	1.4	2	2.8
	σ_r	0.243336597	0.999927108	0.999991798	0.999894563	0.999716745	0.999620266	0.999843328	0.999900621	0.999920717	0.99988368	0.999946423	0.999977752	0.999877872
104.4	u_t	0.009685832	0.048429158	0.096858316	0.193716632	0.290574948	0.387433264	0.484291581	0.581149897	0.774866529	0.968583161	1.356016426	1.937166322	2.712032851
	σ_r	0.235700496	0.9989795	0.999999034	0.996709095	0.990279395	0.99724825	0.999901207	0.99994649	1.000028208	0.999828741	0.99992347	0.999796738	0.999986293
118.8	u_t	0.008763067	0.043815334	0.087630668	0.175261336	0.262892004	0.350522672	0.43815334	0.525784008	0.701045344	0.87630668	1.226829352	1.75261336	2.453658704
	σ_r	0.21324703	0.995693249	0.99897282	0.976584059	0.991441638	0.998171027	0.999004732	0.999474155	0.999378471	0.99938181	0.999688012	0.999574573	0.999656439
133.2	u_t	0.007289686	0.036448431	0.072896863	0.145793725	0.218690588	0.291587451	0.364484314	0.437381176	0.583174902	0.728968627	1.020556078	1.457937255	2.041112157
	σ_r	0.177379761	0.971787408	0.986604372	0.965972286	0.972763107	0.982514901	0.999400799	0.999546858	0.999249384	0.999318333	0.999201927	0.99916699	0.998969772
147.6	u_t	0.005358268	0.02679134	0.053582679	0.107165359	0.160748038	0.214330718	0.267913397	0.321496077	0.428661436	0.535826795	0.750157513	1.07165359	1.500315026
	σ_r	0.130385346	0.686050097	0.933961155	0.885542121	0.882883814	0.903548348	0.987038435	0.990614465	0.990498384	0.990339798	0.990280081	0.990185136	0.989547571
162	u_t	0.00309017	0.01545085	0.030901699	0.061803399	0.092705098	0.123606798	0.154508497	0.185410197	0.247213595	0.309016994	0.432623792	0.618033989	0.865247584
	σ_r	0.075200346	0.388502145	0.879657823	0.820659934	0.785215153	0.78624874	0.860574321	0.896461455	0.899173579	0.900317468	0.902616394	0.905724963	0.909186238
176.4	u_t	0.000627905	0.003139526	0.006279052	0.012558104	0.018837156	0.025116208	0.03139526	0.037674312	0.050232416	0.06279052	0.087906727	0.125581039	0.175813455
	σ_r	0.015280157	0.078474778	0.204170527	0.190926138	0.15029645	0.157462169	0.320272213	0.390019527	0.287216935	0.236085063	0.230845562	0.230706981	0.232994679

Table 4.7 Tangential soil nodal forces for RI of 300

θ	u_x	0.01	0.05	0.1	0.2	0.3	0.4	0.5	0.6	0.8	1	1.4	2	2.8
3.6	u_r	0.000627905	0.003139526	0.006279052	0.012558104	0.018837156	0.025116208	0.03139526	0.037674312	0.050232416	0.06279052	0.087906727	0.125581039	0.175813455
	σ_r	0.022913974	0.14640365	0.209022225	0.148697543	0.21333683	0.390897794	0.313867143	0.243149108	0.232107513	0.230469813	0.230781319	0.233848714	0.241231408
18	u_r	0.00309017	0.01545085	0.030901699	0.061803399	0.092705098	0.123606798	0.154508497	0.185410197	0.247213595	0.309016994	0.432623792	0.618033989	0.865247584
	σ_r	0.11278542	0.779776565	0.843965288	0.785748628	0.805056057	0.894934725	0.898954393	0.899549272	0.901618464	0.903417901	0.906365013	0.910208057	0.914656122
32.4	u_r	0.005358268	0.02679134	0.053582679	0.107165359	0.160748038	0.214330718	0.267913397	0.321496077	0.428661436	0.535826795	0.750157513	1.07165359	1.500315026
	σ_r	0.195572628	0.977474383	0.88667414	0.881476236	0.967763066	0.990686213	0.990587605	0.990447436	0.990357032	0.990186675	0.989835227	0.989350849	0.988841964
46.8	u_r	0.007289686	0.036448431	0.072896863	0.145793725	0.218690588	0.291587451	0.364484314	0.437381176	0.583174902	0.728968627	1.020556078	1.457937255	2.041112157
	σ_r	0.26609093	0.992999479	0.951911262	0.972355414	0.9978764	0.99976684	0.999246404	0.999550854	0.999396855	0.999249116	0.999226717	0.998806543	0.998417706
61.2	u_r	0.008763067	0.043815334	0.087630668	0.175261336	0.262892004	0.350522672	0.43815334	0.525784008	0.701045344	0.87630668	1.226829352	1.75261336	2.453658704
	σ_r	0.319830781	0.998563197	0.987188565	0.991256338	0.998876498	0.999512653	0.999619094	0.999398058	0.999728345	0.999685473	0.999632646	0.9999042	0.999671681
75.6	u_r	0.009685832	0.048429158	0.096858316	0.193716632	0.290574948	0.387433264	0.484291581	0.581149897	0.774866529	0.968583161	1.356016426	1.937166322	2.712032851
	σ_r	0.353496658	0.999808337	0.999387503	0.990353401	0.999513057	0.999988996	1.0000285	0.999913463	0.99994698	0.999862506	0.999907652	1.000051951	0.999925173
90	u_r	0.01	0.05	0.1	0.2	0.3	0.4	0.5	0.6	0.8	1	1.4	2	2.8
	σ_r	0.364952902	0.999983566	0.999887119	0.999692232	0.999765952	0.999906431	0.999863731	0.999858078	0.999889421	0.999920764	0.999952063	0.999852129	0.999851982
104.4	u_r	0.009685832	0.048429158	0.096858316	0.193716632	0.290574948	0.387433264	0.484291581	0.581149897	0.774866529	0.968583161	1.356016426	1.937166322	2.712032851
	σ_r	0.353496658	0.999808337	0.999387503	0.990353401	0.999513057	0.999988996	1.0000285	0.999913463	0.99994698	0.999862506	0.999907652	1.000051951	0.999925173
118.8	u_r	0.008763067	0.043815334	0.087630668	0.175261336	0.262892004	0.350522672	0.43815334	0.525784008	0.701045344	0.87630668	1.226829352	1.75261336	2.453658704
	σ_r	0.319830781	0.998563197	0.987188565	0.991256338	0.998876498	0.999512653	0.999619094	0.999398058	0.999728345	0.999685473	0.999632646	0.9999042	0.999671681
133.2	u_r	0.007289686	0.036448431	0.072896863	0.145793725	0.218690588	0.291587451	0.364484314	0.437381176	0.583174902	0.728968627	1.020556078	1.457937255	2.041112157
	σ_r	0.26609093	0.992999479	0.951911262	0.972355414	0.9978764	0.99976684	0.999246404	0.999550854	0.999396855	0.999249116	0.999226717	0.998806543	0.998417706
147.6	u_r	0.005358268	0.02679134	0.053582679	0.107165359	0.160748038	0.214330718	0.267913397	0.321496077	0.428661436	0.535826795	0.750157513	1.07165359	1.500315026
	σ_r	0.195572628	0.977474383	0.88667414	0.881476236	0.967763066	0.990686213	0.990587605	0.990447436	0.990357032	0.990186675	0.989835227	0.989350849	0.988841964
162	u_r	0.00309017	0.01545085	0.030901699	0.061803399	0.092705098	0.123606798	0.154508497	0.185410197	0.247213595	0.309016994	0.432623792	0.618033989	0.865247584
	σ_r	0.11278542	0.779776565	0.843965288	0.785748628	0.805056057	0.894934725	0.898954393	0.899549272	0.901618464	0.903417901	0.906365013	0.910208057	0.914656122
176.4	u_r	0.000627905	0.003139526	0.006279052	0.012558104	0.018837156	0.025116208	0.03139526	0.037674312	0.050232416	0.06279052	0.087906727	0.125581039	0.175813455
	σ_r	0.022913974	0.14640365	0.209022225	0.148697543	0.21333683	0.390897794	0.313867143	0.243149108	0.232107513	0.230469813	0.230781319	0.233848714	0.241231408

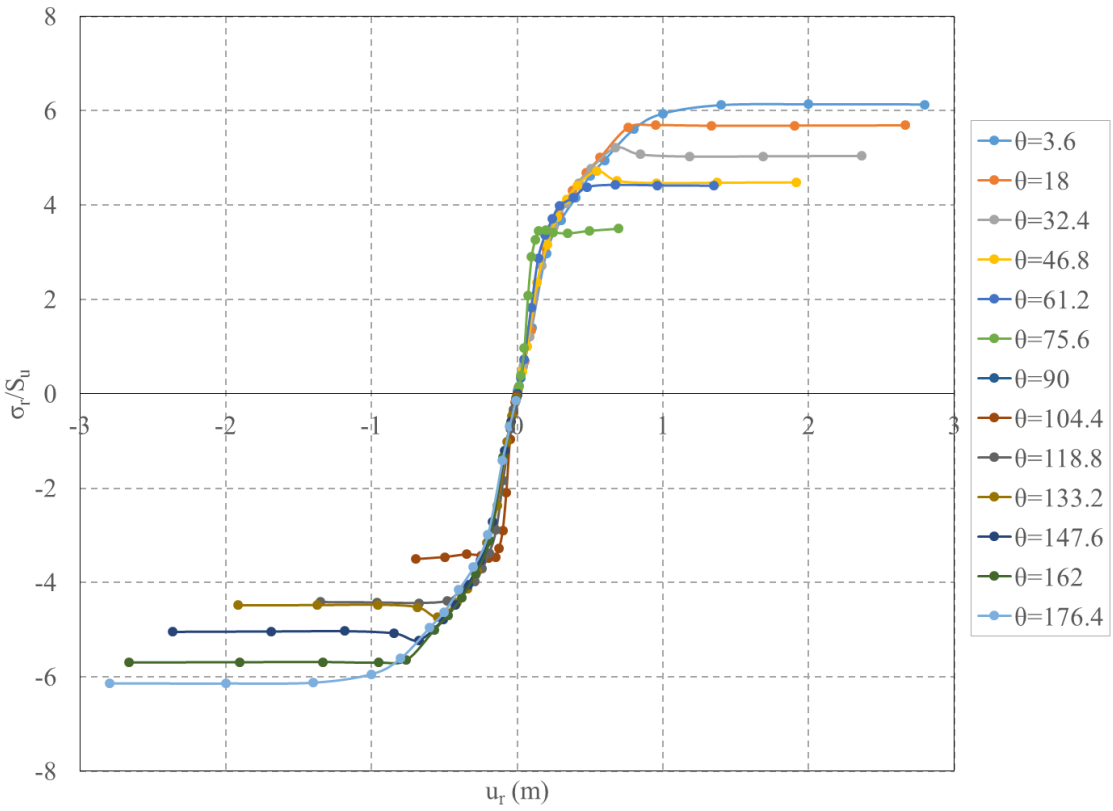

Figure 4.17 Radial soil p-y curves for RI of 100

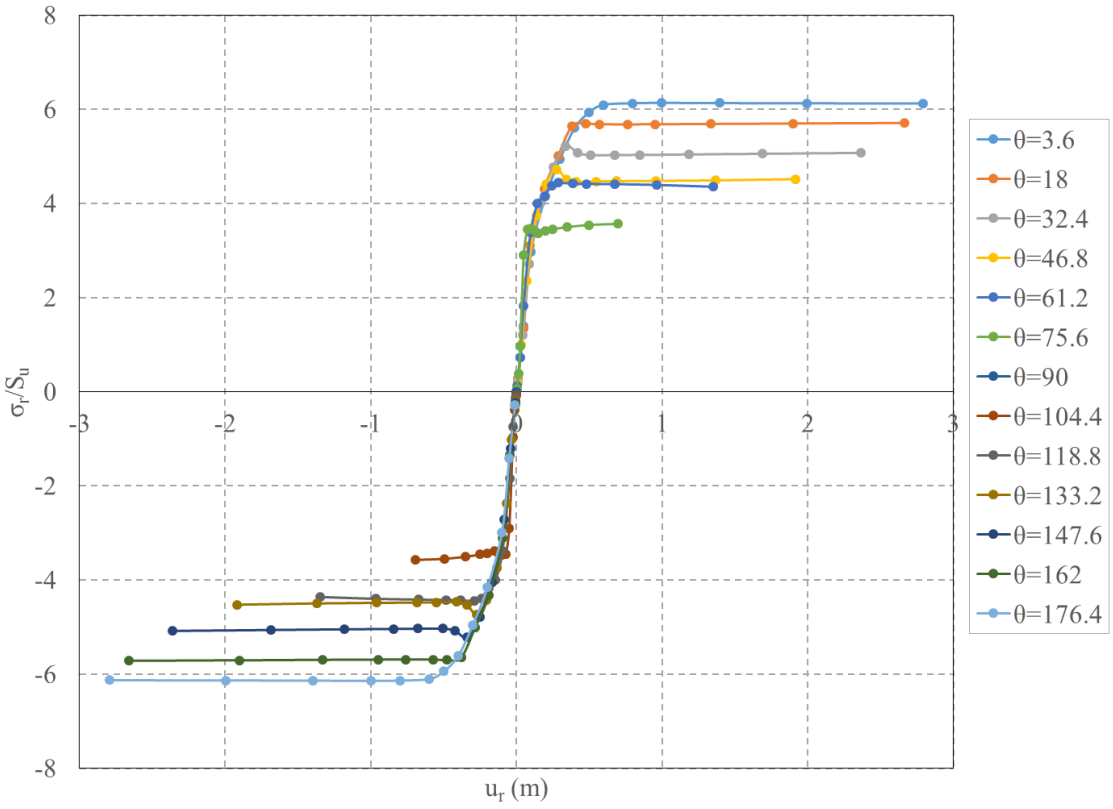

Figure 4.18 Radial soil p-y curves for RI of 200

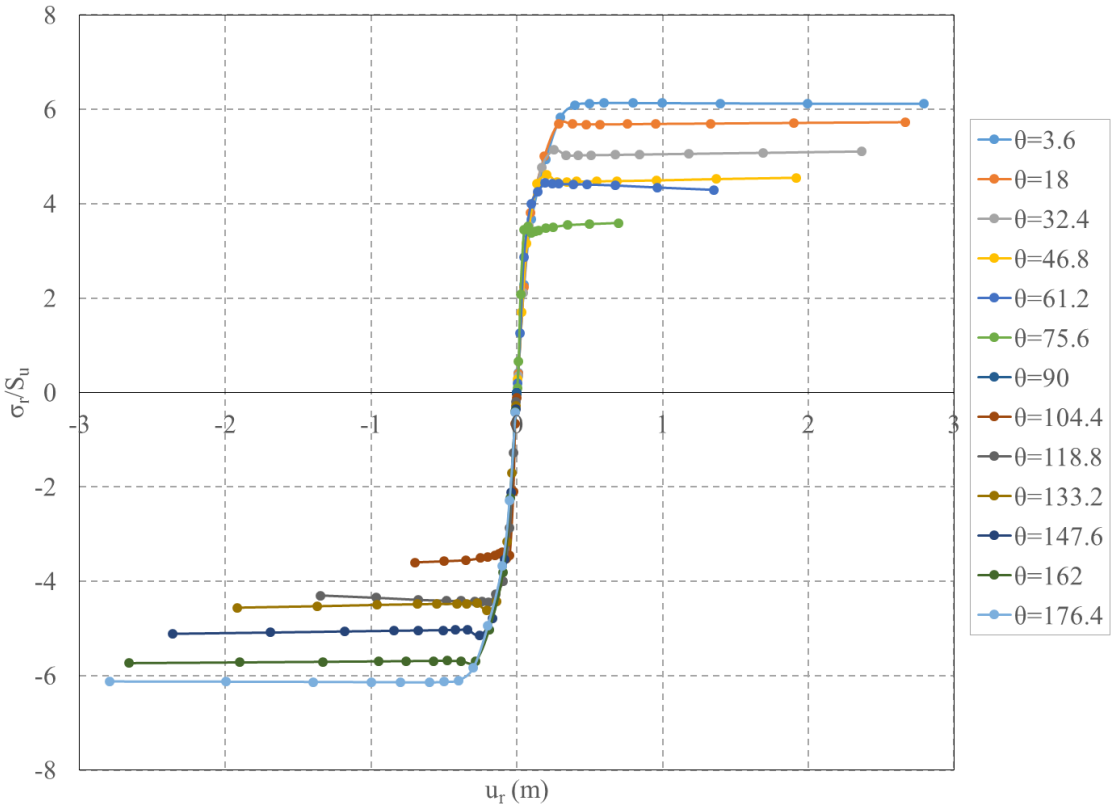

Figure 4.19 Radial soil p-y curves for RI of 300

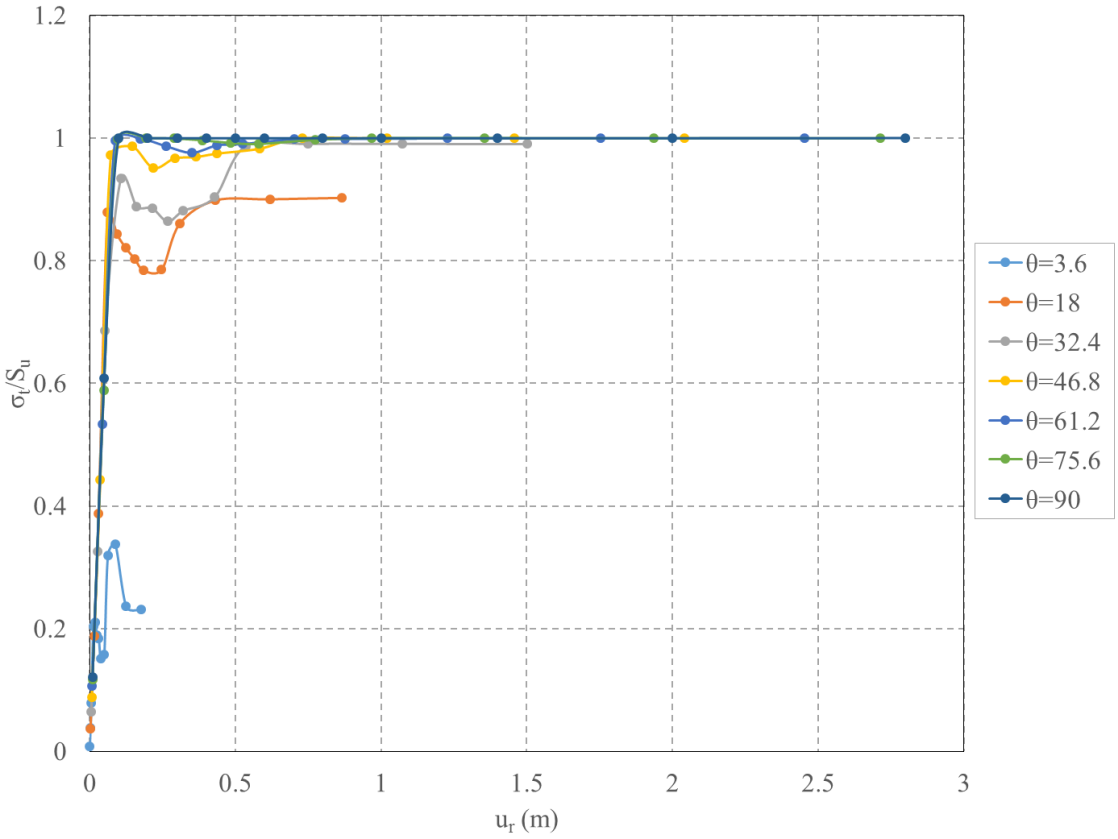

Figure 4.20 Tangential soil p-y curves for RI of 100

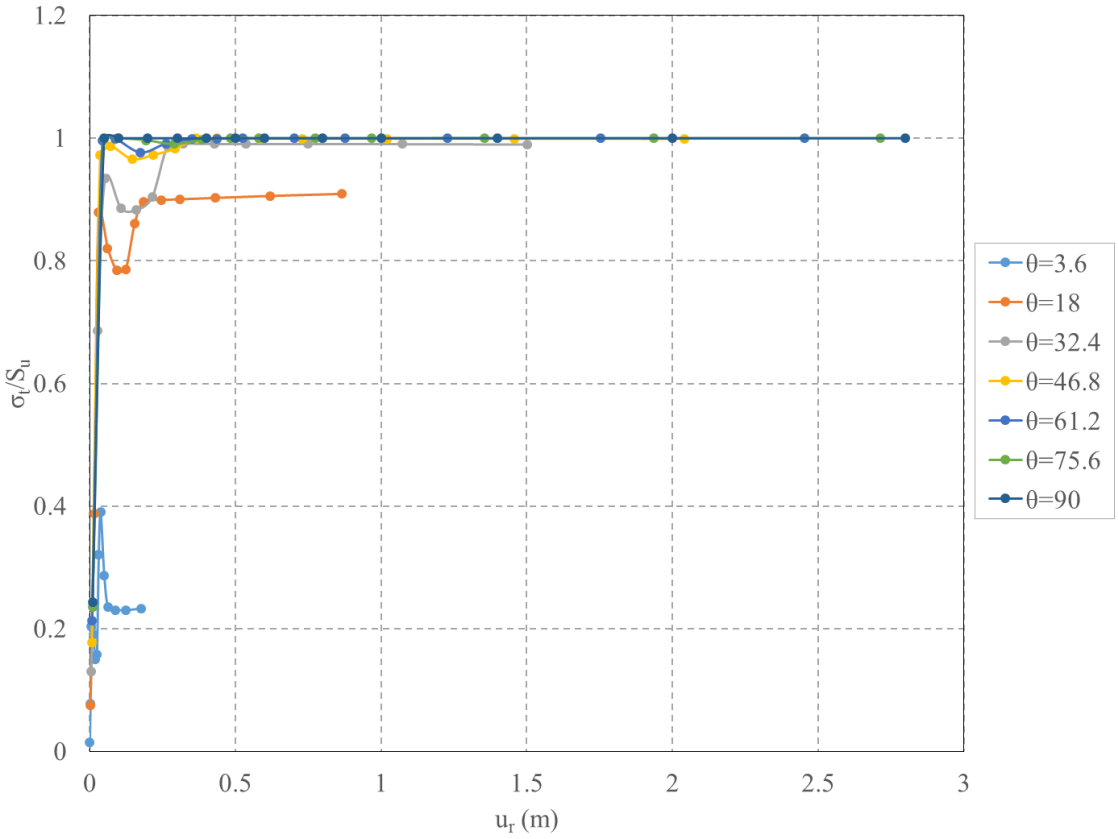

Figure 4.21 Tangential soil p-y curves for RI of 200

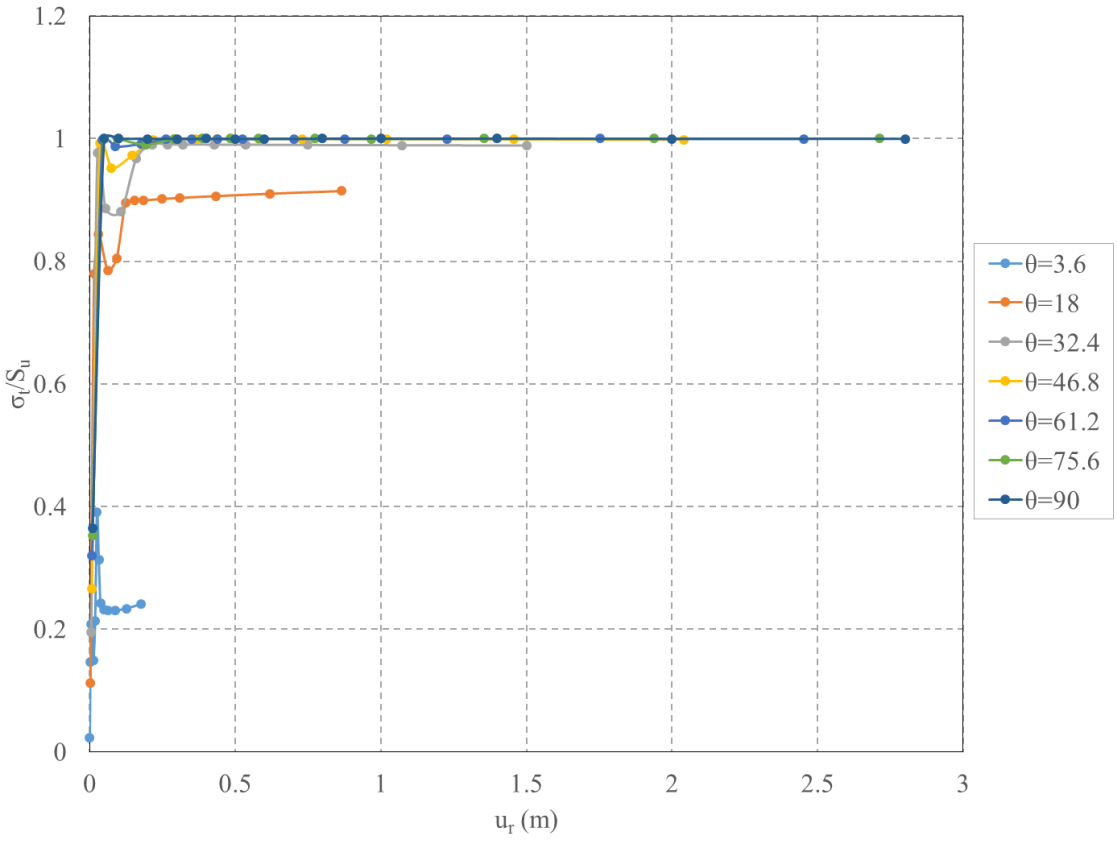

Figure 4.22 Tangential soil p-y curves for RI of 300

Model Validation

The accuracy of the 2-D model is validated by calculating the bearing capacity factor, N_p, and compare the calculated N_p value with the solution from plasticity theory presented by Randolph and Houlsby (1984) (N_p=11.94).

The bearing capacity factor is calculated as follow:

$$N_p = \frac{\Delta F}{S_u D \Delta L} \quad \text{..... (4.6)}$$

where,

Np=bearing capacity factor

ΔF=increase in lateral capacity

S_u=undrained shearing strength

D=caisson diameter

ΔL=incremental length

The summation of lateral capacity is calculated by adding up all the lateral component of the soil stress around the caisson. The calculated N_p values for rigid caisson with soil rigidity of 100, 200, and 300 are shown in Table 4.8, and percent error is also shown in the Table 4.8.

Table 4.8 Bearing Capacity Factors and Percent Error

RI	N_p	N_p (Randolph and Houlsby)	Percent Error
100	12.17118	11.94	1.9%
200	12.19396	11.94	2.1%
300	12.20541	11.94	2.2%

Randolph and Houlsby (1984) presented solutions from plasticity theory to give N_p=11.94. It is noted that our numerical analysis comes out an N_p value using the spring forces larger than the Randolph-Houlsby solution for only about 2% for all RIs. The larger N_p value resulted from numerical analysis is also observed by other researchers (Aubeny et al., 2001). Aubeny et al. (2001) conducted a 3-D numerical analysis and

obtained N_p=13.19, or 10% greater than Randolph-Houlsby solution. Generally, the spring properties resulted in the reasonably good results. The detailed analyses and discussions of the results are presented in the next chapter.

Spring Property in 3-D Model

As discussed previously, for 3-D analysis, the spring forces are obtained by multiplying the stresses generated from 2-D analysis to a nodal area. This area will be equal to the finite element area created for a certain size of caisson.

Model Description

Considering the model structure of caisson in which the thickness is significantly smaller than the other dimensions, shell element is selected to simulate the caisson for 3-D analysis. The conventional shell element S4R5, which is a 4-node thin shell element, with reduced integration, and five degrees of freedom per node, is selected for caisson simulation. The caisson diameter is still 5 m with different aspect ratio. Shell stress at section point 1 is selected for analysis purposes.

The soil around the caisson is simulated by spring element, SPRING1. Based on soil element responses from 2-D model, the spring properties was generated to couple with a 3-D model as described in Chapter 4.

Similar to the 2-D model, the n_{row} of 50 is used in the 3-D model. In the vertical direction, the caisson is divided into certain layers (nlayerp) that makes each element a best square. Each node on caisson is connected to one end of the spring element. The

other end of the spring element is grounded (constrained) which services as the boundary condition in the model. The stress and displacement in the spring element is measured to simulate the soil reaction around the caisson. A typical mesh of caisson with spring elements is shown in Figure 4.17.

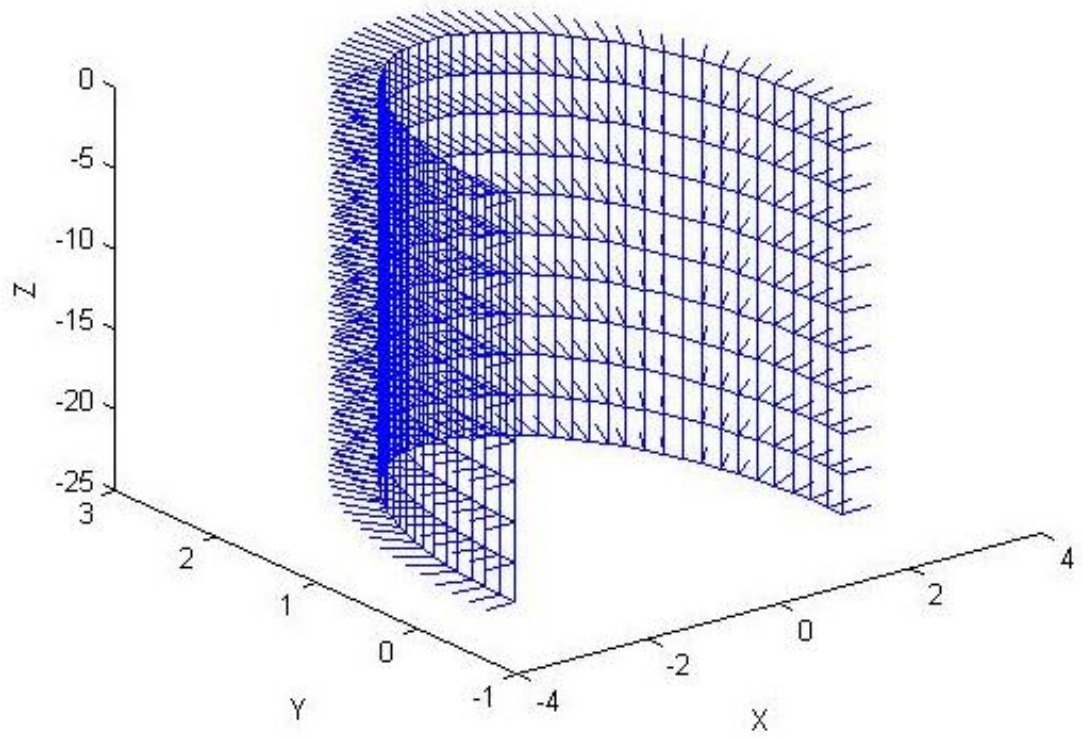

Figure 4.23 3-D mesh of caisson with spring elements

Spring Properties

In ABAQUS program, the spring property is input as forces instead of stresses. Therefore, each nodal stress will be multiplied by an area to obtain the corresponding nodal force which will be the spring force connected to that node.

For a 3-D analysis, this area will be:

$dA=dl*dz$.....(4.7)

where,

$dz=L/nlayerp$ (L is caisson length)

$dl=\frac{\pi D}{2*50}$ (D is caisson diameter; caisson is divided to 50 segments as finite element)

For 3-D analysis, free surface condition should be considered for generating the spring properties since the lateral resistance factor decreases from at mudline to bottom of caisson. The reduction factor R_f can be expressed as proposed by Murff and Hamilton (1993) as follow:

$$R_f=\frac{N_1-N_2\exp(-\eta z/D)}{N_1} \quad \text{..... (4.8)}$$

where,

$N_1=9.42+2.52\alpha$ (α is assumed to be 1 for fully rough caisson)

$N_2=7.42+1.7\alpha$

$\eta=0.25+0.05\rho$ for $\rho<6$

$\eta=0.55$ for $\rho>6$

$\rho=S_{u0}/S_{u1}D$ (S_{u0} is soil strength at mudline and S_{u1} is vertical strength gradient)

Therefore, the spring forces at radial and tangential directions can be obtained as follow:

$dF_r=f_r*dA*R_f*Su$.....(4.9)

$$dF_t = f_t * dA * R_f * Su \quad \text{.....(4.10)}$$

Finally, as the spring properties are calculated, these springs are coupled with the caisson which is modeled by shell elements to make the coupled caisson-springs 3-D model for the analysis. The results and discussions are presented in the following chapter.

CHAPTER V

FINITE ELEMENT STUDY RESULTS AND DISCUSSIONS

General Scope

Finite element analyses are carried out using ABAQUS 6.9 computer program. A 3-D caisson and springs coupled model is generated for the finite element analysis. Spring properties discussed in the previous chapter are utilized for 3-D analysis. The caisson is loaded laterally at different location on caisson surrounded by the springs, and the results of caisson capacity, shell radial stress, shell moment, and spring radial forces at interesting locations are investigated. Taking advantage of the symmetry about the plane in which the load is applied, only one-half of the caisson (180 degrees) is simulated in all the analyses.

Description of Study

The analyses were performed for the caisson with dimeter of 5 m, two aspect ratios of 5 (L/D=5) and 3 (L/D=3), two modulus of regular steel modulus and fully rigid, and three shell thickness of D/t=80 (base case), D/t=125 (medium case), and D/t=160 (ring stiffened case). Two undrained shear strength profiles were included in the analyses: linearly increasing (S_u=2+1.6z) and uniform strength based on the averaged value of the linear profile (S_{uavg}). Three soil rigidity index, RI=100, RI=200, and RI=300 were included in the analyses. In order to simulate the real world application, a ring stiffener was put at the level of load attachment location. The load attachment point was

located at $L_i/L=0$, $L_i/L=1/3$, $L_i/L=1/2$, and $L_i/L=2/3$ for L/D=5 caisson, and $L_i/L=0$, $L_i/L=1/3$, and $L_i/L=2/3$ for L/D=3 caisson. All the loading were in the lateral direction.

Analysis Matrix

Based on the parameters included in the description of the study, the matrix of the analyses are summarized in the Table 5.1 and Table 5.2. It is noted that for the analysis of rigid caisson, only one caisson shell thickness of 4 cm was used since it made no difference with different shell thickness when the caisson was fully rigid. A thickness was still input just for analysis purpose.

Table 5.1 Analysis Matrix for Flexible Caisson

Flexible Caisson																	
RI	D/L	Soil Profile	D/t	t,cm	Li/L	RI	D/L	Soil Profile	D/t	t,cm	Li/L	RI	D/L	Soil Profile	D/t	t,cm	Li/L
100	5	Uniform	80	6.250	0	200	5	Uniform	80	6.250	0	300	5	Uniform	80	6.250	0
					1/3						1/3						1/3
					1/2						1/2						1/2
					2/3						2/3						2/3
			125	4.000	0				125	4.000	0				125	4.000	0
					1/3						1/3						1/3
					1/2						1/2						1/2
					2/3						2/3						2/3
			160	3.125	0				160	3.125	0				160	3.125	0
					1/3						1/3						1/3
					1/2						1/2						1/2
					2/3						2/3						2/3
		Su=2+1.6z	80	6.250	0			Su=2+1.6z	80	6.250	0			Su=2+1.6z	80	6.250	0
					1/3						1/3						1/3
					1/2						1/2						1/2
					2/3						2/3						2/3
			125	4.000	0				125	4.000	0				125	4.000	0
					1/3						1/3						1/3
					1/2						1/2						1/2
					2/3						2/3						2/3
			160	3.125	0				160	3.125	0				160	3.125	0
					1/3						1/3						1/3
					1/2						1/2						1/2
					2/3						2/3						2/3

Table 5.2 Analysis Matrix for Rigid Caisson

Rigid Caisson											
RI	D/L	Soil Profile	Li/L	RI	D/L	Soil Profile	Li/L	RI	D/L	Soil Profile	Li/L
100	3	Uniform	0	200	3	Uniform	0	300	3	Uniform	0
			1/3				1/3				1/3
			2/3				2/3				2/3
			0				0				0
			1/3				1/3				1/3
			2/3				2/3				2/3
			0				0				0
			1/3				1/3				1/3
			1/2				1/2				1/2
			2/3				2/3				2/3
		Su=2+1.6z	0			Su=2+1.6z	0			Su=2+1.6z	0
			1/3				1/3				1/3
			2/3				2/3				2/3
			0				0				0
			1/3				1/3				1/3
			2/3				2/3				2/3
			0				0				0
			1/3				1/3				1/3
			1/2				1/2				1/2
			2/3				2/3				2/3

Soil Data

As mentioned previously, two undrained soil strength profiles were utilized in the parametric study: linearly increasing (S_u=2+1.6z) and uniform strength based on the averaged value of the linear profile. Therefore, since there were two caisson length used in the study (L=25 m and L=15 m), the uniform undrained shear strength for L=25 m caisson is S_u=41 kPa and the uniform undrained shear strength for L=15 m caisson is S_u=14 kPa.

Mesh Discretization

The nodal density for the 3-D analysis was based on the 2-D model mesh and then size matched for the 3-D mesh to obtain the enough fineness.

In order to achieve the enough fineness of the 2-D mesh, the bending theory of curved beams (Housner and Vreeland, 1991) is introduced. The governing differential equation for bending moment of a circular bar is given by following equation:

$$M = EI'_{\chi_0} = EI'\left(\frac{\partial^2 u_0}{r_0^2 \partial\theta^2} + \frac{u_0}{r_0^2}\right) \quad \text{.....(5.1)}$$

where,

M=bending moment

E=young's modulus

I=moment inertia

u=radial displacement

r_0=initial radius

θ=rotation

In a 2-D mesh, this governing equation can be developed, and applied for a slender circular beam loaded by diametrically opposed forces as shown in Figure 5.1. The relative displacement of the two opposed forces P is then given in a close form solution:

$$u = -0.149\frac{Pr^3}{EI} \quad \text{.....(5.2)}$$

where,

u=displacement

P=loading force

r=radius

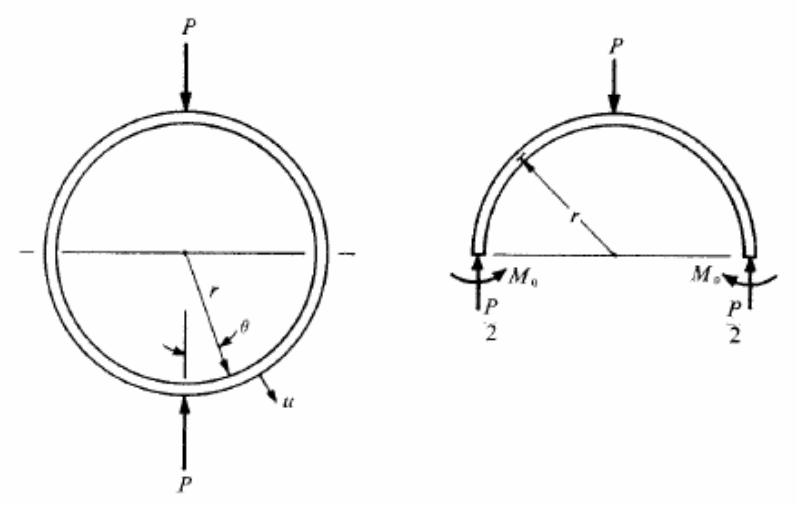

Figure 5.1 Bending of slender circular beam

With a testing finite element analysis using a shell structure with thickness t=0.04 m, r=2.5 m, P=100 N, and E=3*10^{10} Pa, the half of the caisson length is then divided by 10, 30, 50, and 100 (n_{row}) to represent cases for different element size. The loading is applied at one end of the half caisson using a load-control, and the corresponded displacement at the other end was measured. The results of numerical solutions are compared to the result from analytical solution for n_{row} of 50 and is shown in Table 5.3. The results shows that as n_{row} of 50, the results from analytical and numerical are close enough. Therefore, n_{row} of 50 is fine enough to for the 2-D mesh.

Table 5.3 Nodal Density Analysis for a 2-D Mesh

nrow	P, kN	δ_{abaqus}	E	t	I	r	$\delta_{close\ form}$	Difference
50	0.1	0.6966	2.000E+08	0.04	3.333E-09	2.5	0.6984	0.0018

For a 3-D mesh, the discretization in z-direction is based on the best matched element size in z-direction to make the shell element size a close-square. Based on this philosophy, the caisson length is divided into 160 elements for an L/D=5 caisson and 95 elements for an L/D=3 caisson.

Analysis Results

Some important features are observed in the analysis and examples of results are presented and discussed below.

Elastic Behavior of Caisson

Effect of Load Attachment Point and Caisson Shell Thickness (Ring Stiffener)

The results of caisson capacity versus displacement (p-y curve) for the rigid caisson with aspect ratio of 5, linearly increasing soil strength, and RI of 300 are shown in Figure 5.2.

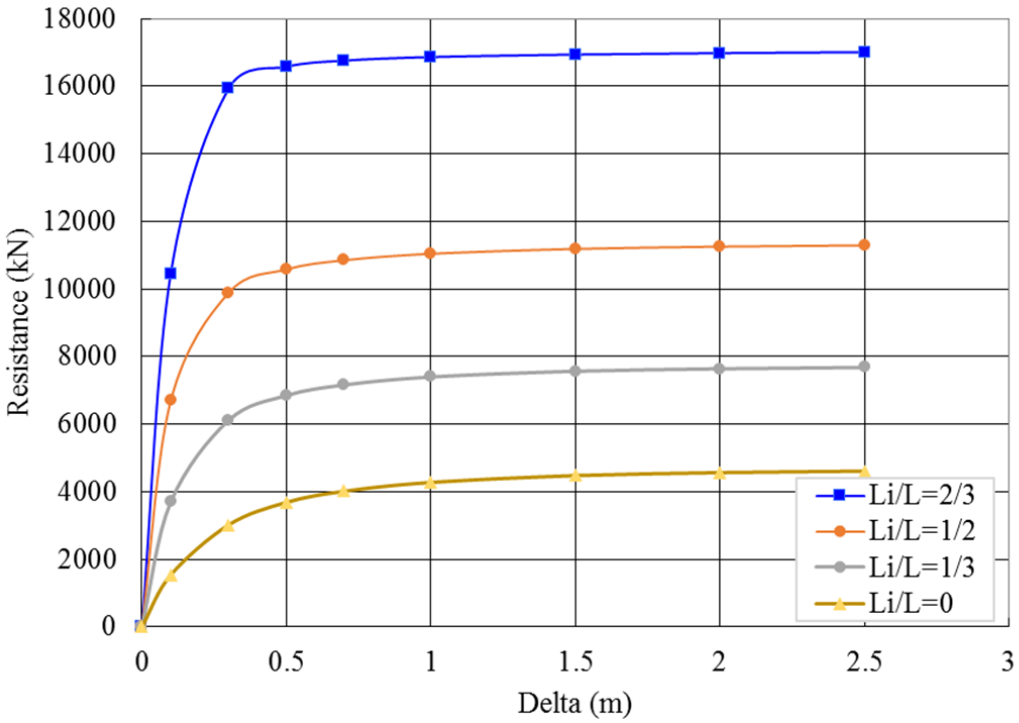

Figure 5.2 P-y curve of the rigid caisson, aspect ratio of 5, linearly increasing soil strength, and RI=300

The results of p-y curves of flexible caisson with different caisson shell thickness are added to the Figure 5.2 and is shown in Figure 5.3.

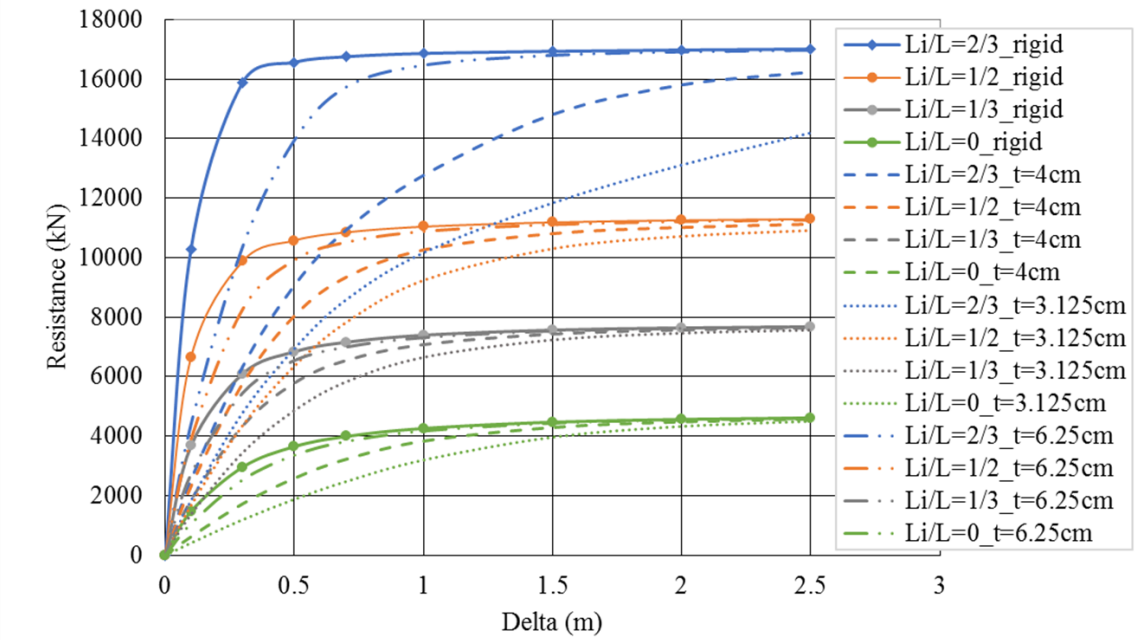

Figure 5.3 P-y curves of the rigid caisson and flexible caisson with different shell thickness, aspect ratio of 5, linearly increasing soil strength, and RI=300

The results of caisson capacity versus displacement (p-y curve) for the rigid caisson with aspect ratio of 5, linearly increasing soil strength, and RI of 300 are shown in Figure 5.4.

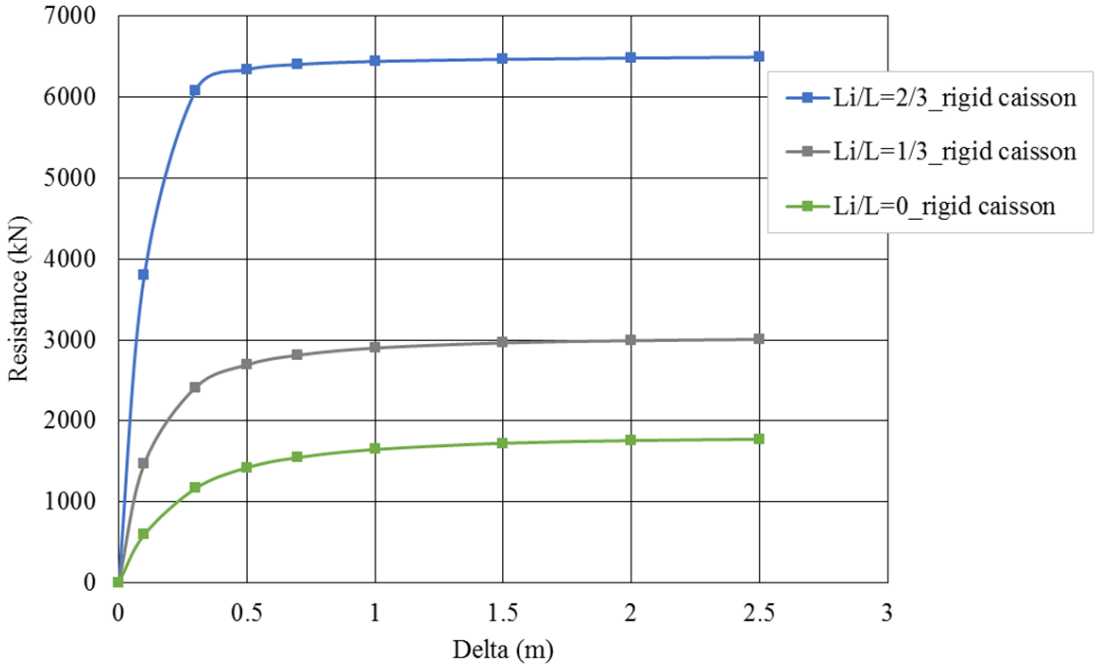

Figure 5.4 P-y curve of the rigid caisson, aspect ratio of 3, linearly increasing soil strength, and RI=300

The results of p-y curves of flexible caisson with different caisson shell thickness are added to the Figure 5.4 and is shown in Figure 5.5.

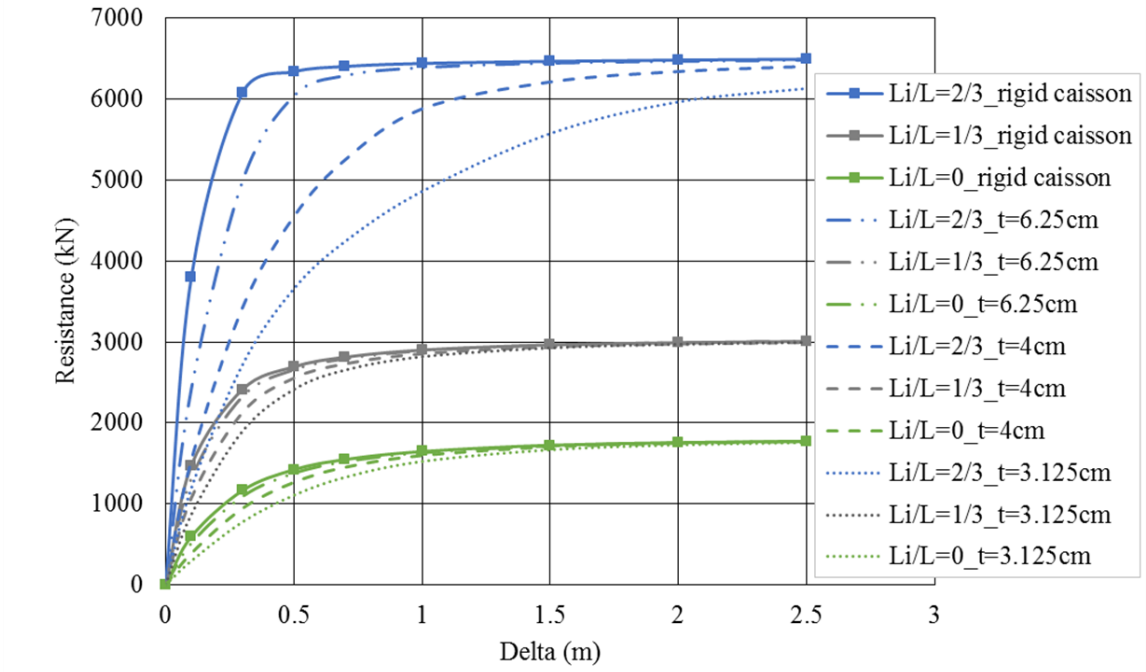

Figure 5.5 P-y curves of the rigid caisson and flexible caisson with different shell thickness, aspect ratio of 3, linearly increasing soil strength, and RI=300

These results indicate that the optimal load attachment point is at Li/L=2/3 for an aspect ratio of 5 caisson for both rigid and flexible caisson and that the capacity reduce with load attachment point moving up towards the caisson top.

These results also indicate that, although the ultimate capacity of rigid and flexible caissons are converging, the capacity of caisson at smaller displacement are quite different between rigid and flexible caisson and this difference is larger for load attachment point yielding larger capacity.

These result also indicate that when stiffened the caisson behaves stiffer at lower displacement level.

Effect of Soil Rigidity Index (RI)

The results of p-y curves of rigid caisson with different soil rigidity index with a caisson shell thickness of 4 cm are shown in Figure 5.6.

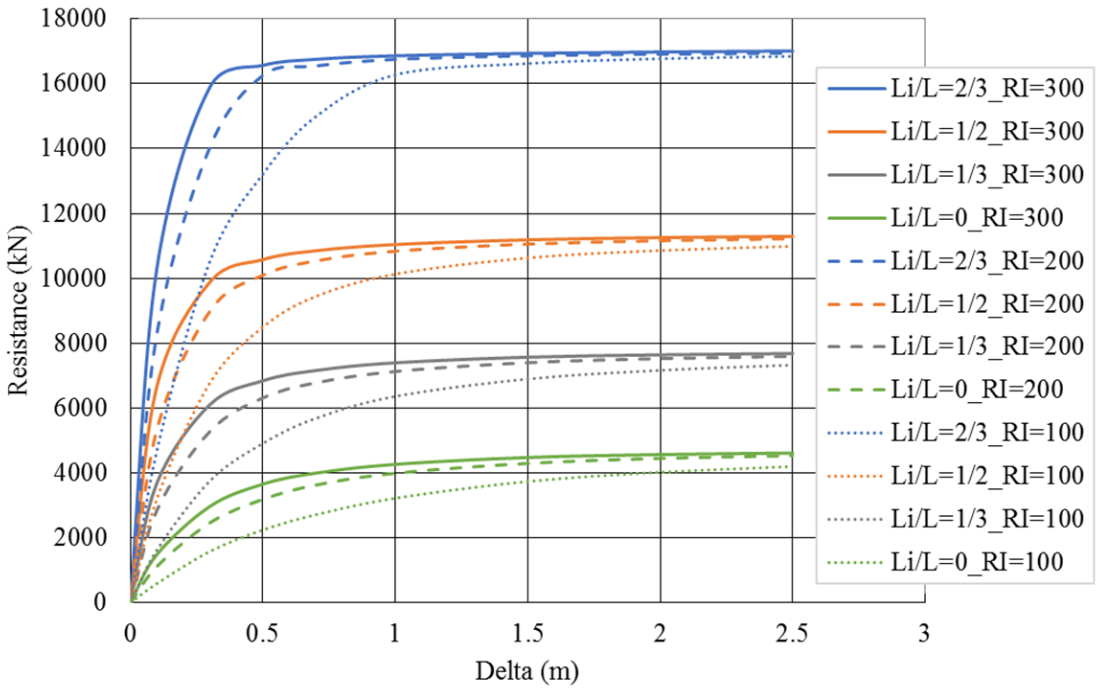

Figure 5.6 P-y curves of the rigid caisson with different RI, with shell thickness of 4 cm, aspect ratio of 5, linearly increasing soil strength

The results of p-y curves of flexible caisson with different soil rigidity index with a caisson shell thickness of 4 cm are shown in Figure 5.7.

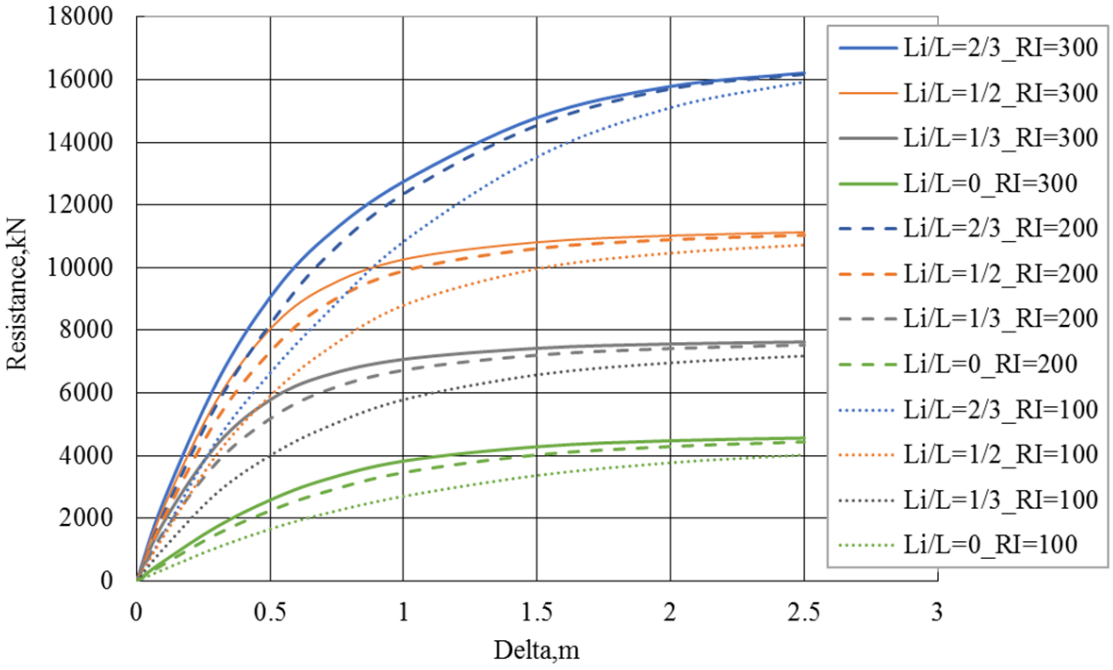

Figure 5.7 P-y curves of the flexible caisson with different RI, with shell thickness of 4 cm, aspect ratio of 5, linearly increasing soil strength

The results of p-y curves of rigid caisson with different soil rigidity index with a caisson shell thickness of 4 cm are shown in Figure 5.8.

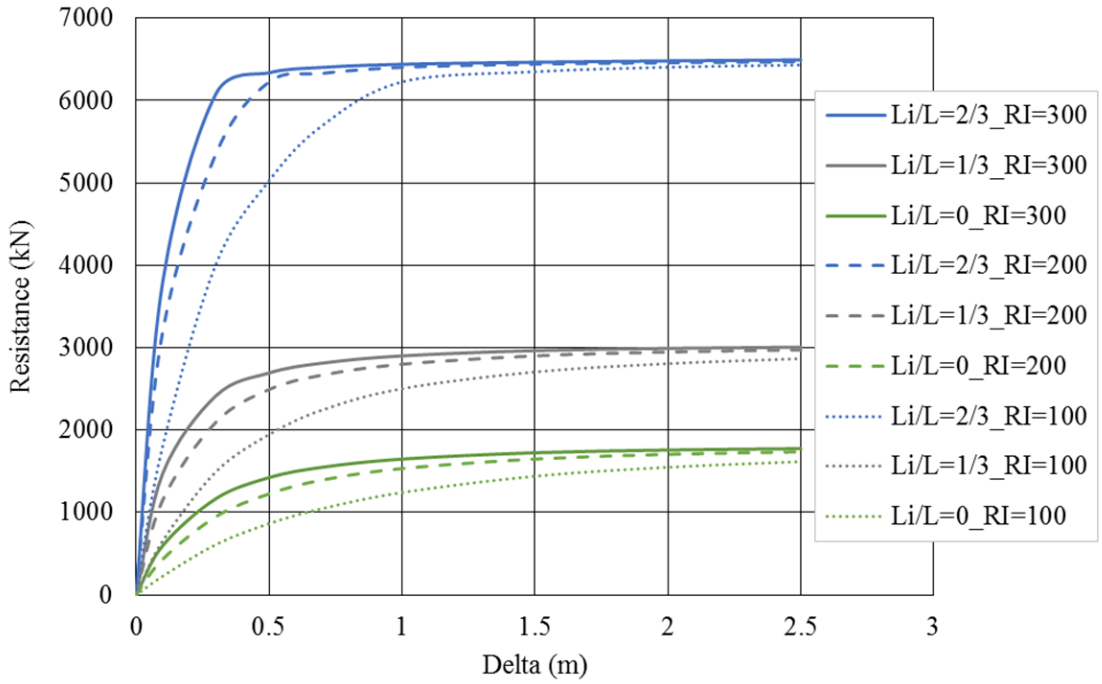

Figure 5.8 P-y curves of the rigid caisson with different RI, with shell thickness of 4 cm, aspect ratio of 3, linearly increasing soil strength

The results of p-y curves of flexible caisson with different soil rigidity index with a caisson shell thickness of 4 cm are shown in Figure 5.9.

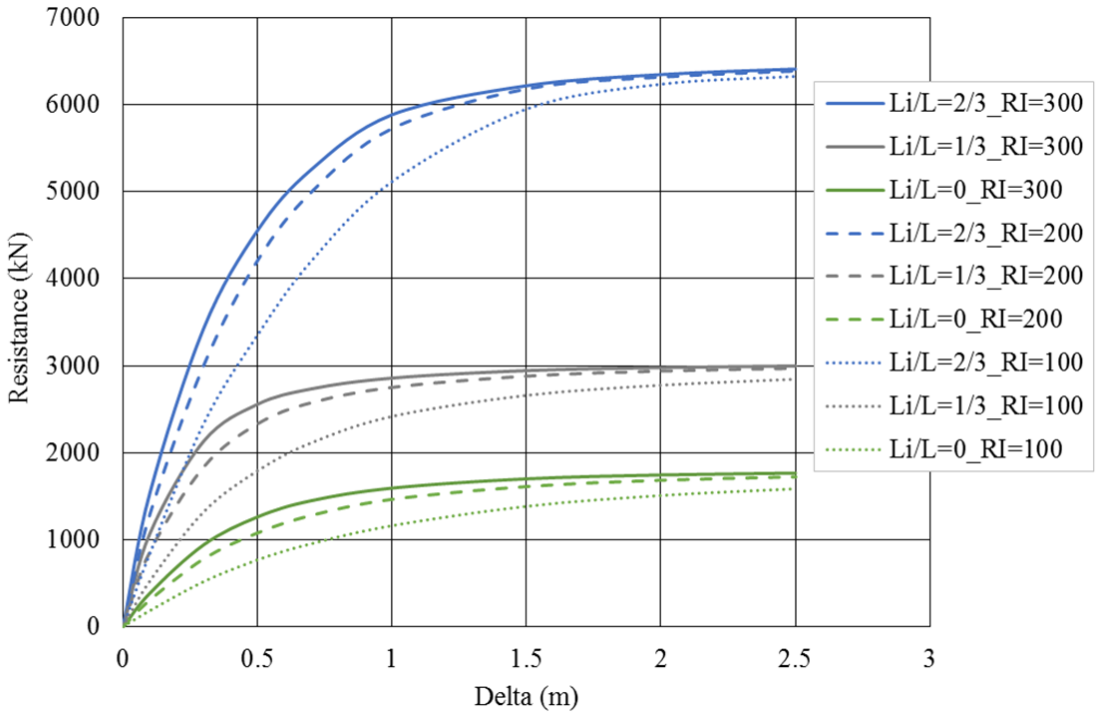

Figure 5.9 P-y curves of the flexible caisson with different RI, with shell thickness of 4 cm, aspect ratio of 3, linearly increasing soil strength

These results indicate that both rigid and flexible caissons have stiffer behavior when surrounded by soil with larger soil rigidity index. Also, all the previous analysis results indicate that a shorter caisson (lower aspect ratio) generally results in lower ultimate capacity than a longer caisson.

Effect of Soil Strength Profile

The results of p-y curves of rigid and flexible caisson in uniform strength soil, with different load attachment point, with a caisson aspect ratio of 5, shell thickness of 4 cm, and soil rigidity index of 300 are shown in Figure 5.10.

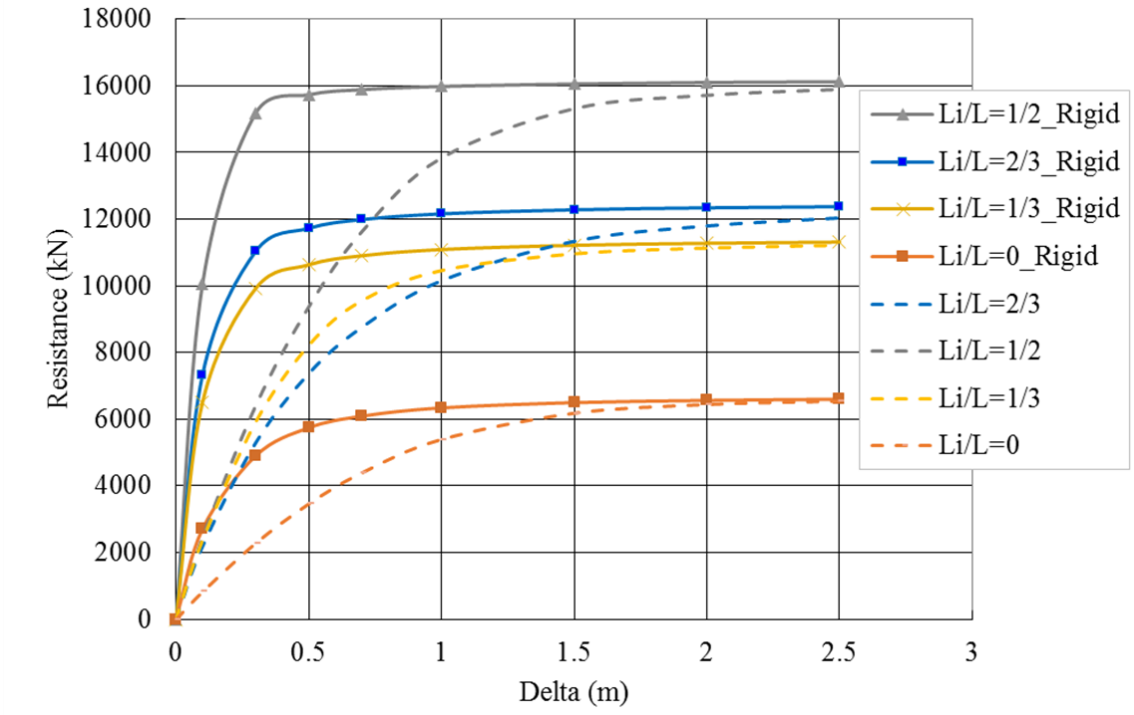

Figure 5.10 P-y curves of the rigid and flexible caissons in uniform strength soil, with different load attachment point, with caisson aspect ratio of 5, shell thickness of 4 cm, and soil rigidity index of 300

These results indicate that for a uniform soil strength the optimal load attachment point is at Li/L=1/2, and the second largest caisson capacity occurs at load attachment point of Li/L=2/3 and followed by the Li/L=1/3. The smallest capacity still occurs at caisson top, same as previous examples.

These results also reinforce the previous observation that the flexible caisson shows a more floppy behavior compared with rigid caisson and the ultimate capacity of these two types of caisson converges at larger displacement.

Effect of Stiffener

Effect of two types of stiffener-padeye stiffener and ring stiffener-is studied. Padeye stiffener, also called plate stiffener, is a steel plate supporting the front and back sides of the caisson and usually placed at the loading attachment level. A sketch of a padeye stiffener is shown below in Figure 5.11. In the analysis, the padeye stiffener is simulated with a rigid body.

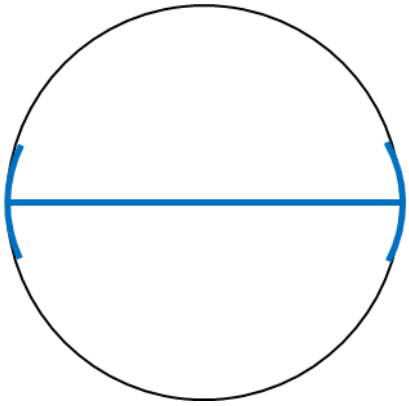

Figure 5.11 Cross section of a caisson with a padeye stiffener

A ring stiffener is a reinforced shell around the circumference of the caisson at certain location. In the analysis, the ring stiffener is simulated by doubling the shell thickness at the load attachment level.

The results of p-y curves of a caisson with aspect ratio of 5, shell thickness of 3.125 cm, in linearly increasing soil profile of RI=300 with padeye stiffener and ring stiffener is shown in Figure 5.12.

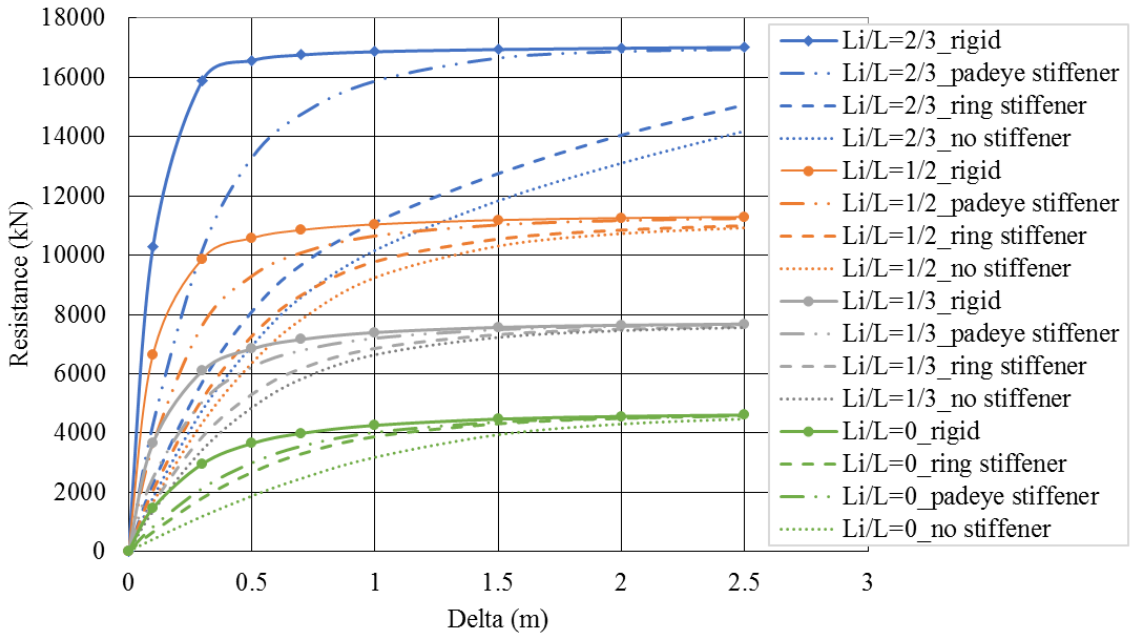

Figure 5.12 P-y curves of caisson with thickness of 3.125 cm with padeye stiffener and ring stiffener

The results of p-y curves of a caisson with aspect ratio of 5, shell thickness of 6.25 cm, in linearly increasing soil profile of RI=300 with padeye stiffener and ring stiffener is shown in Figure 5.13.

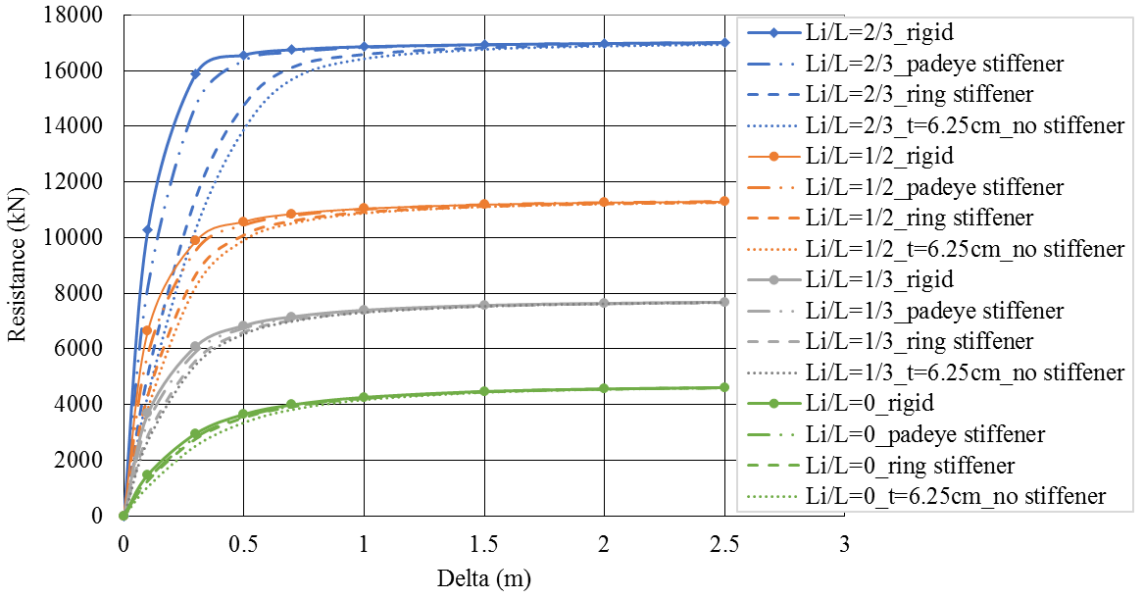

Figure 5.13 P-y curves of caisson with thickness of 6.25 cm with padeye stiffener and ring stiffener

The results indicate that both types of stiffener show benefit of increasing the stiffness of the caisson. A rigid padeye stiffener is more efficient on increasing the caisson stiffness than a ring stiffener. Generally, stiffeners are more efficiently increasing the caisson stiffness for a caisson with thinner shell. Thicker caisson is originally stiffer than a thinner caisson, and therefore benefits less from adding the stiffener.

Effect of Caisson Topcap

In practice, caisson can be connected to the superstructure directly on top of it. In this case, a topcap is usually used on top of the caisson to serve as a platform on which the superstructure is set. The topcap is considered a rigid cap, and the effect of this rigid confinement at caisson top on the p-y curves are investigated in this study.

The p-y curves showing effect of a rigid topcap for an aspect ratio of 5 and 3, shell thickness of 3.125 cm caissons in the linearly increasing soil profile with rigidity index of 300 are presented in Figure 5.14 and 5.15.

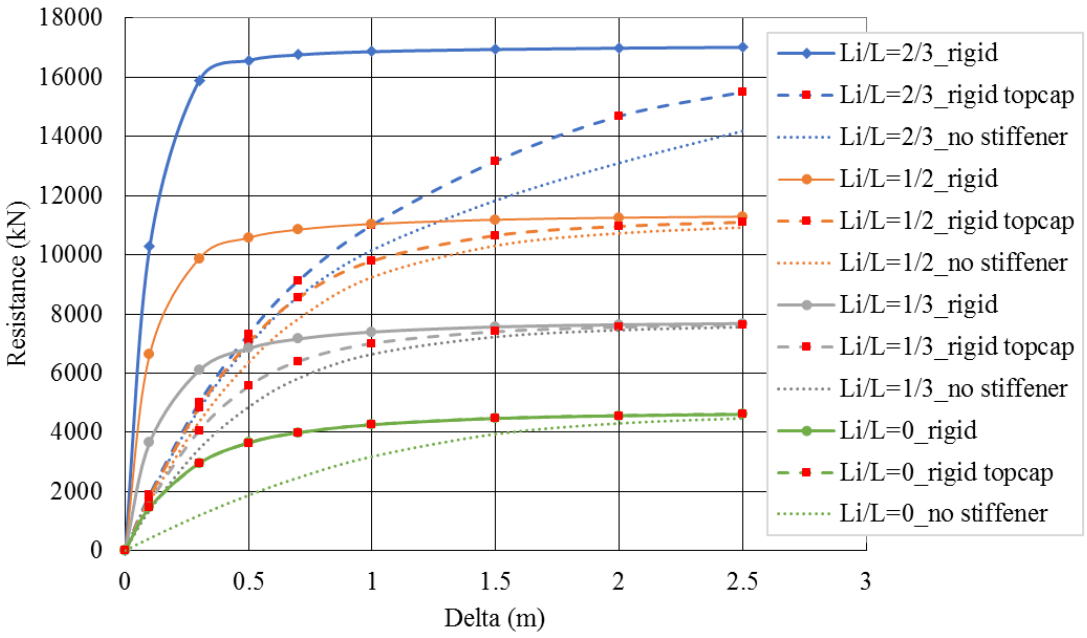

Figure 5.14 Effect of rigid topcap on p-y curves for aspect ratio of 5 caisson

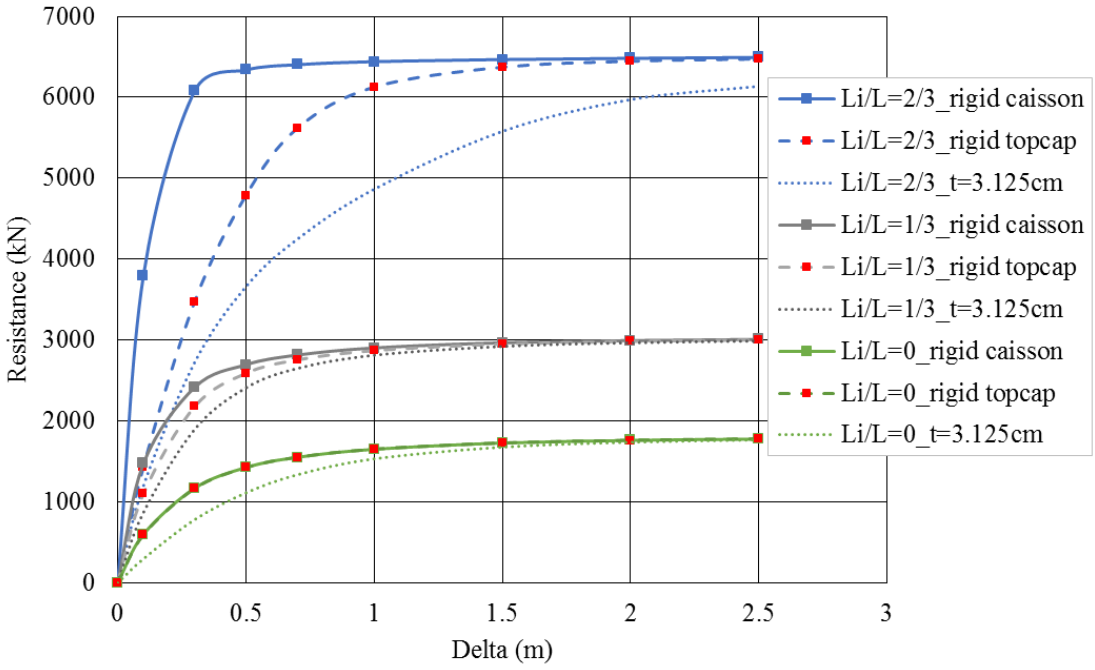

Figure 5.15 Effect of rigid topcap on p-y curves for aspect ratio of 3 caisson

For both long and short caissons, the rigid topcap increase the stiffness of caisson at all loading points. It seems that at optimal load attachment point, the rigid topcap on a short caisson showed more benefit in increasing caisson stiffness than on a long caisson. It is also noted that when loading at the caisson top, the effect of a rigid topcap is same as a rigid caisson.

Structural Assess of Caisson

The structural responses of caisson are investigate based on shell stress and bending moment. In this 3-D analysis, the largest stress (S11) and bending moment

(SM1) in caisson shell are investigated. Examples of caisson structural responses are presented and discussed below.

Caisson Shell Stress

The largest stress (S11) is in the direction that is perpendicular to the shell surface pointing outward the caisson. Therefore, the results for this radial shell stress, S_{11}, was presented in this study.

The radial stress of caisson at different depths with shell thickness of 3.125 cm and 6.25 cm, and a rigid caisson, with aspect ratio of 5, linearly increasing soil strength with RI=300, and loading at Li/L=2/3 are shown in Figures 5.16 to 518.

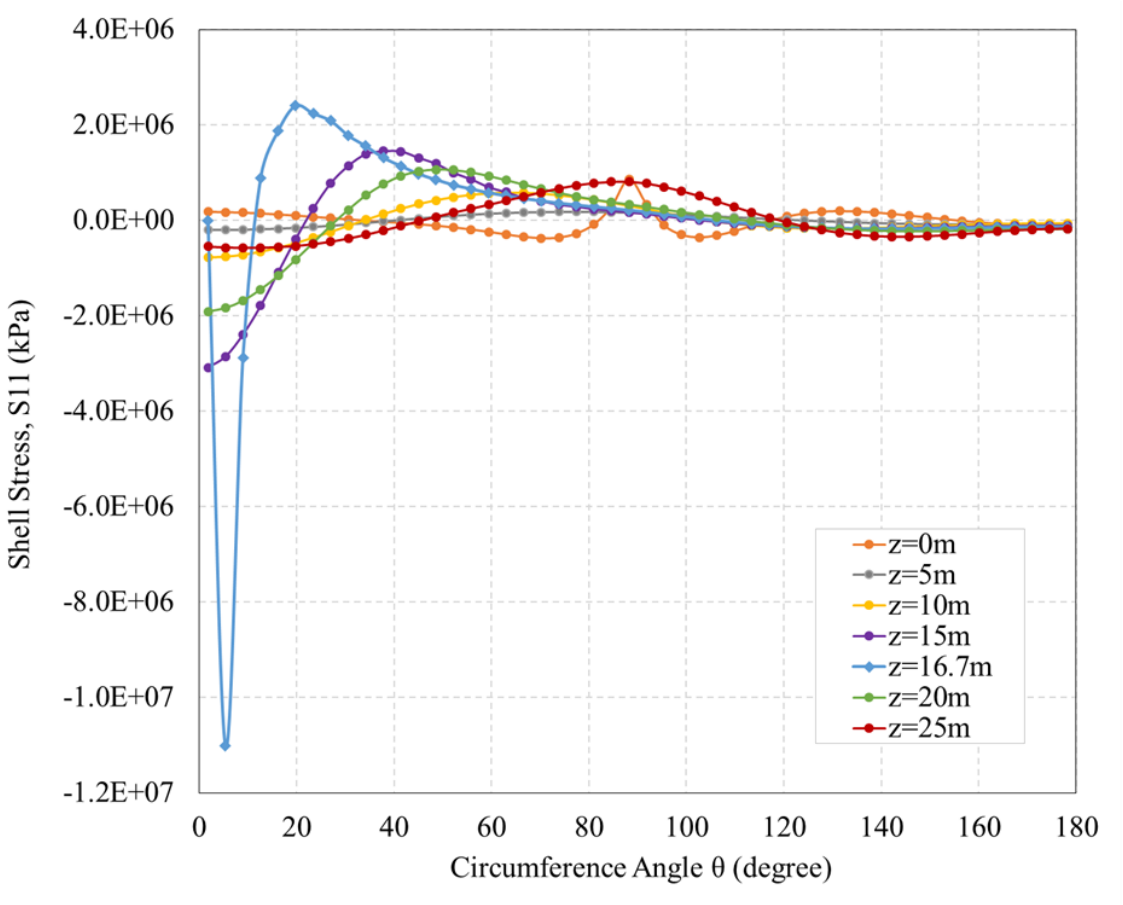

Figure 5.16 Radial stress of flexible caisson with shell thickness of 3.125 cm, with caisson aspect ratio of 5, linearly increasing soil strength, and loading at Li/L=2/3

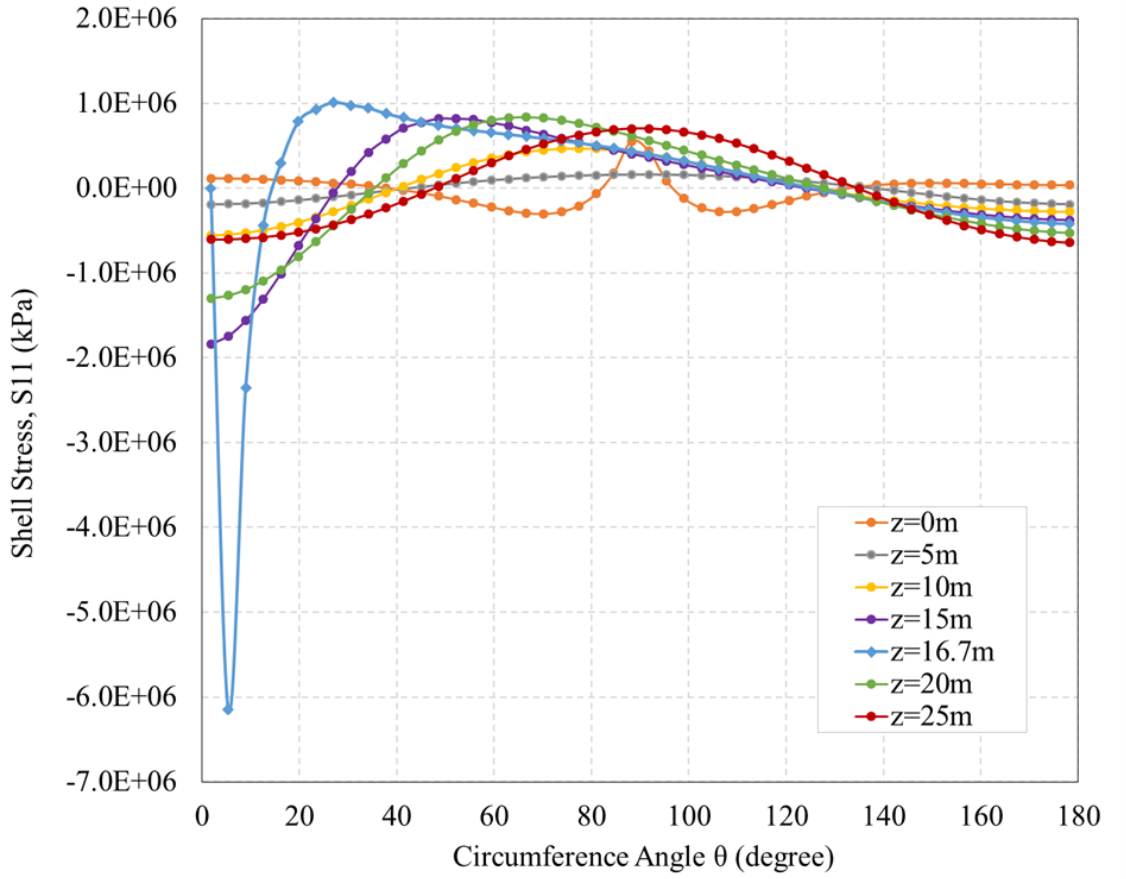

Figure 5.17 Radial stress of flexible caisson with shell thickness of 6.25 cm, with caisson aspect ratio of 5, linearly increasing soil strength, and loading at Li/L=2/3

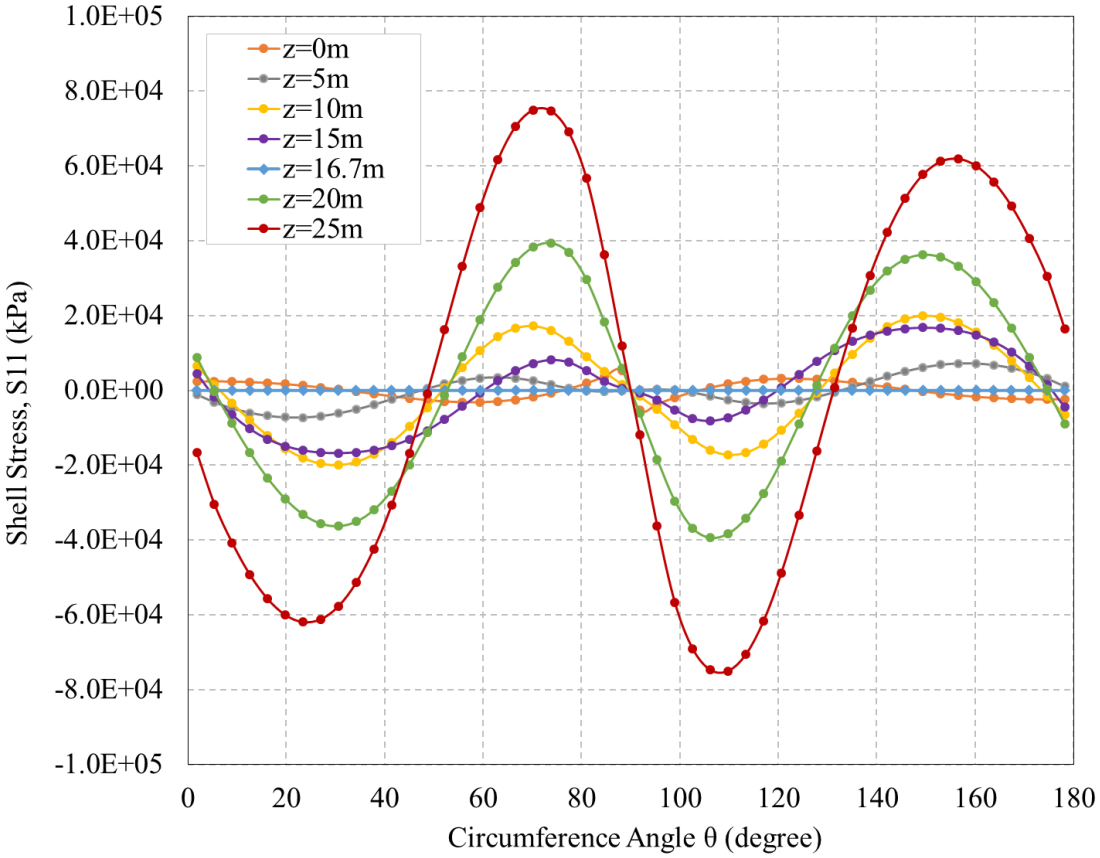

Figure 5.18 Radial stress of rigid caisson with aspect ratio of 5, linearly increasing soil strength, and loading at Li/L=2/3

The finite element results with stress contours for the above three cases are also shown in Figures 5.19 to 5.21 to show the stress distribution on the caisson.

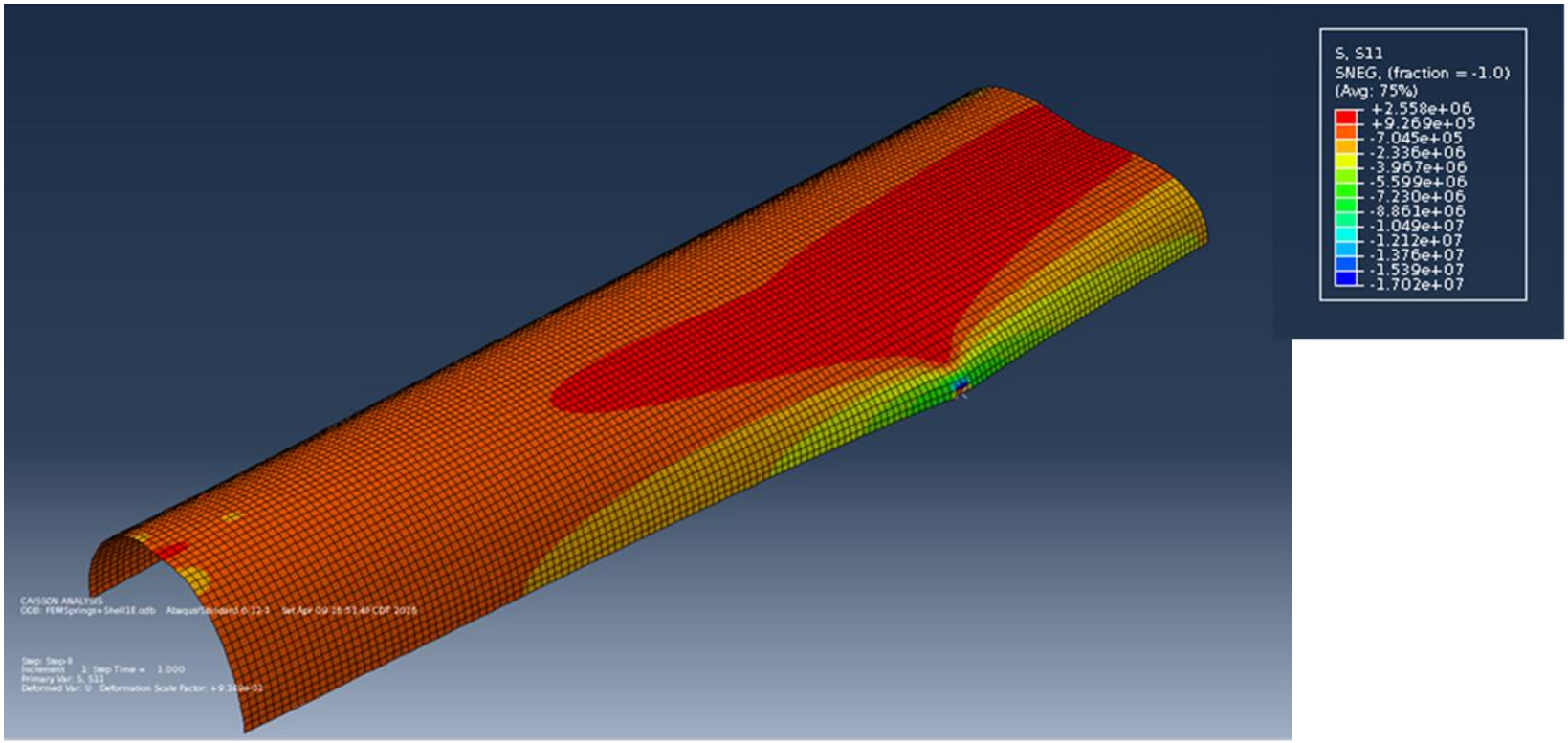

Figure 5.19 Stress (S11) distribution on caisson for caisson shell thickness of 3.125 cm

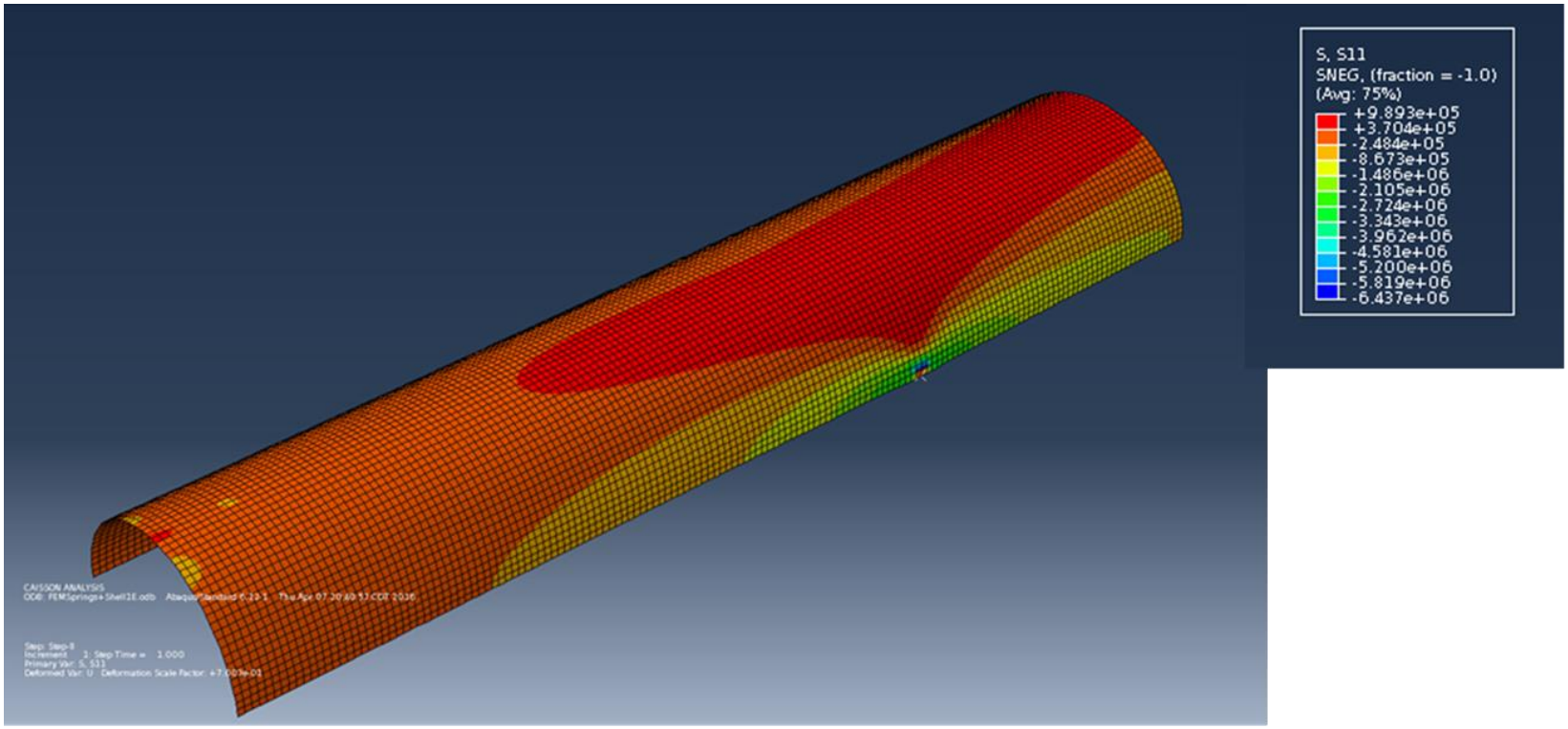

Figure 5.20 Stress (S11) distribution on caisson for caisson shell thickness of 6.25 cm

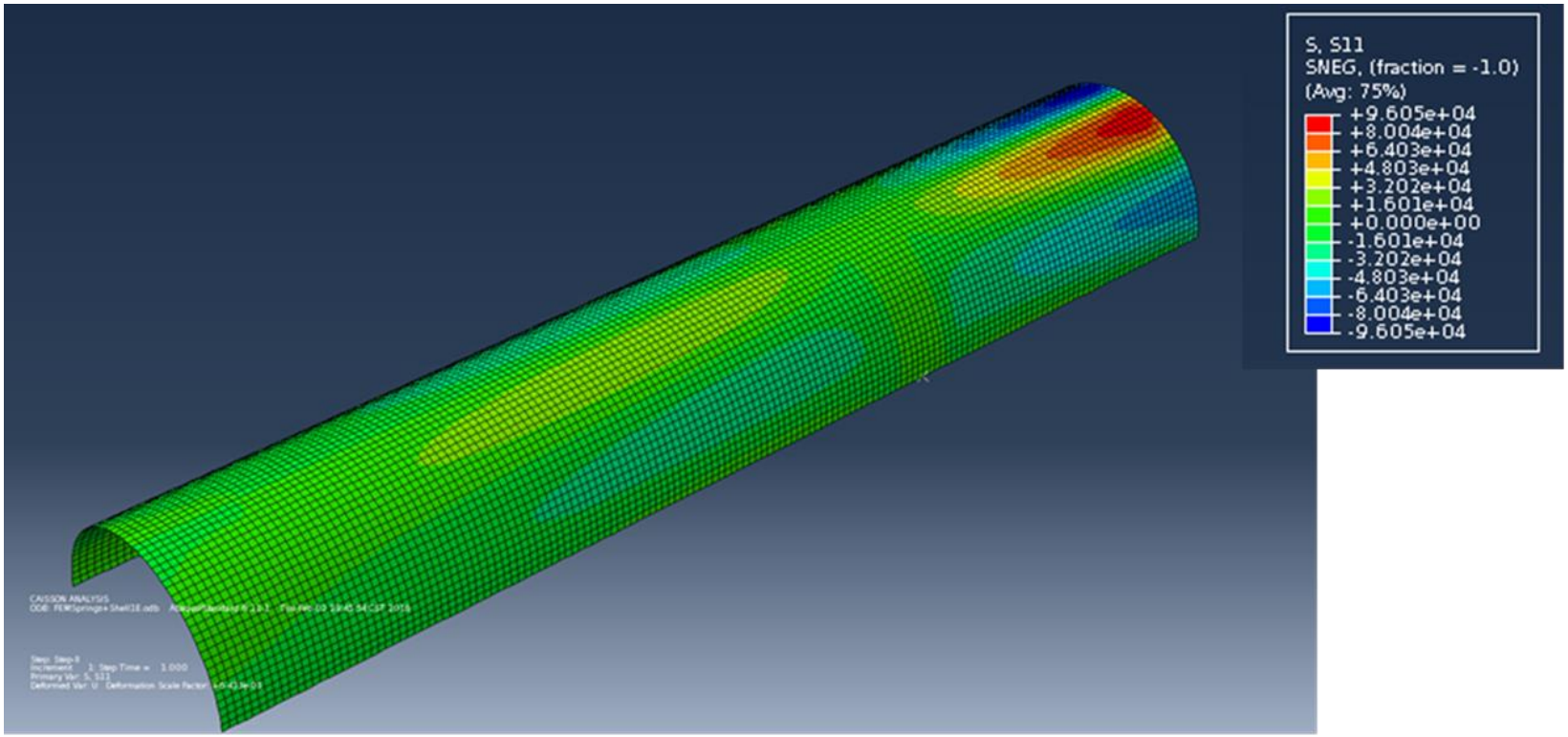

Figure 5.21 Stress (S11) distribution on caisson for rigid caisson

These results indicate that the larges stress occurs at the load attachment point in a flexible caisson and this maximum stress is larger in a caisson with thinner shell thickness, which mean that double the caisson shell thickness help to reduce the stress level in the caisson.

These results also indicate that however in a rigid caisson the larges stress occur at the bottom of caisson and the stress level is three magnitude and two magnitude smaller than the unstiffened caisson and ring stiffened caisson, respectively, based on this specific study.

Caisson Shell Bending Moment

The largest bending moment is about the local 2-direction that is tangential to the shell surface. Therefore, the results for this shell bending moment, SM1, was presented in this study.

The bending moment, SM1 of flexible caisson with shell thickness of 3.125 cm and 6.25 cm, and a rigid caisson, with the caisson aspect ratio of 5, linearly increasing soil strength with RI of 300, and loading at Li/L=2/3 are shown in Figure 5.22 to 5.24.

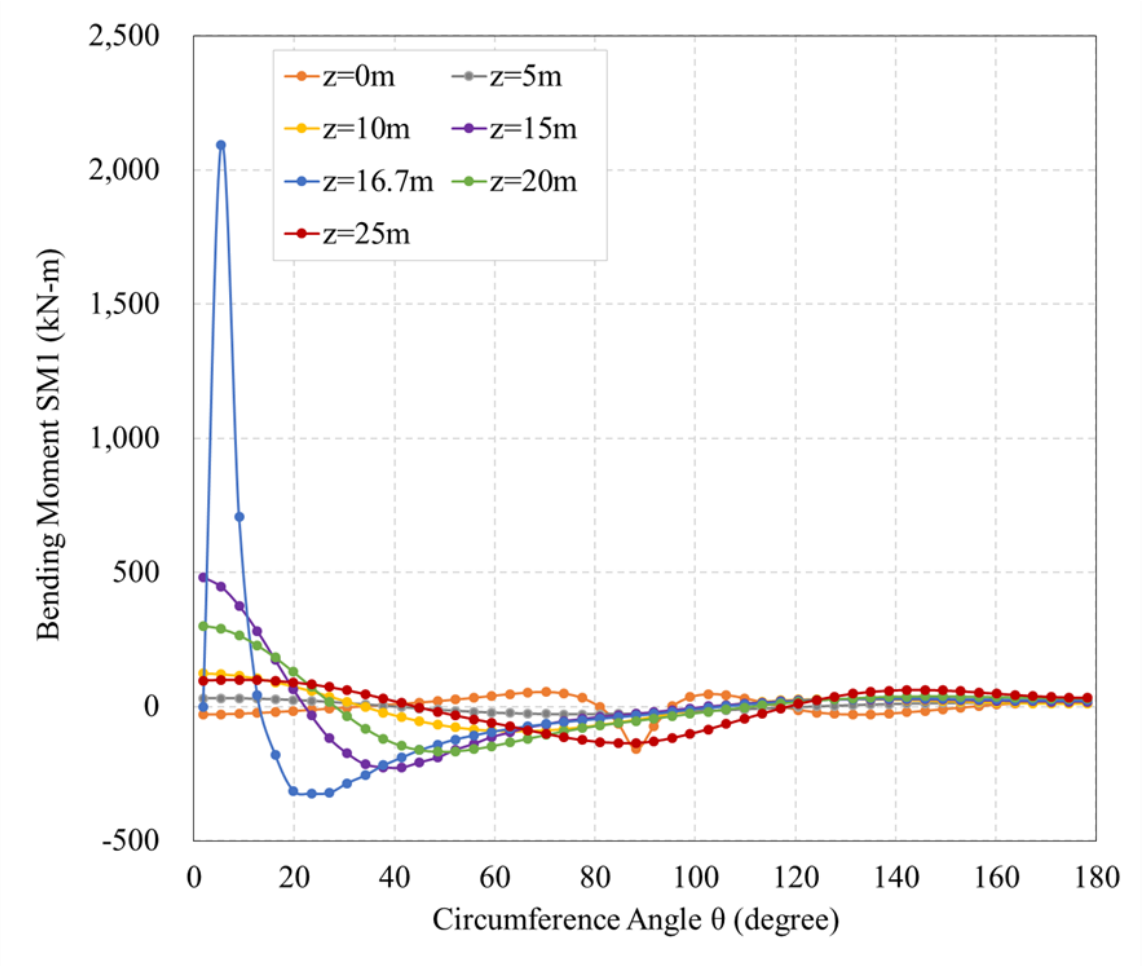

Figure 5.22 Bending moment of flexible caisson with shell thickness of 3.125 cm, with caisson aspect ratio of 5, linearly increasing soil strength, and loading at Li/L=2/3

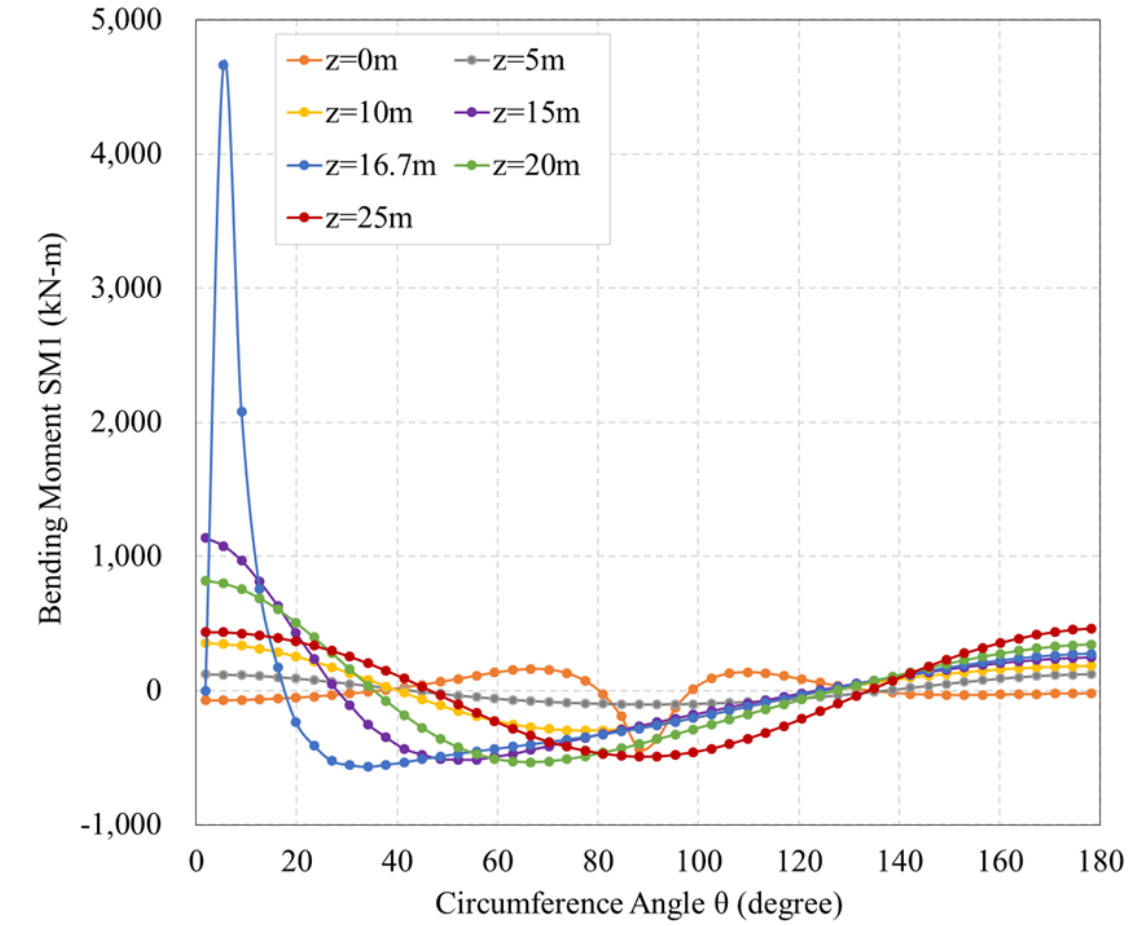

Figure 5.23 Bending moment of flexible caisson with shell thickness of 6.25 cm, with caisson aspect ratio of 5, linearly increasing soil strength, and loading at Li/L=2/3

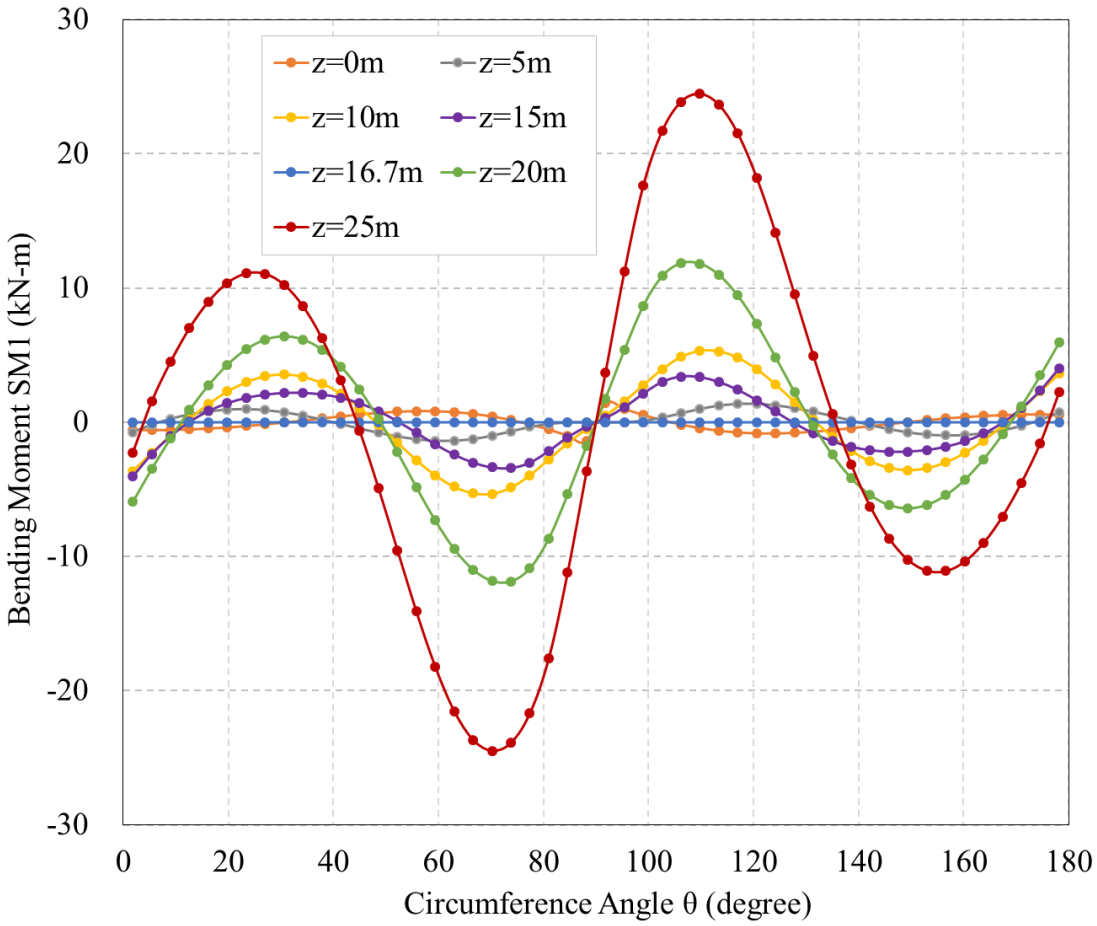

Figure 5.24 Bending moment of rigid caisson, with caisson aspect ratio of 5, linearly increasing soil strength, and loading at Li/L=2/3

These results indicate that in a flexible caisson the largest bending moment occurs at load attachment point and this maximum moment is larger in a caisson with thicker shell thickness.

These results also indicate that in a rigid caisson the largest bending moment occur at the bottom of caisson and the moment level is way less than that in a flexible

caisson by a factor of 10 compared with an unstiffened caisson based on this specific study.

CHAPTER VI

CONCLUSIONS AND RECOMMENDATIONS

The 3-D finite element analyses using a newly developed coupled caisson-springs model provided valuable results of elastic behavior of suction caisson foundations in typical soil profiles which was not investigated for a long time. The model also provided an efficient way of assessing the structural response of caisson in different soil and caisson properties. Based on this study, several important conclusions were reached which are outlined in this chapter. The finite element study did not account for all the factors that will also affect the results. Some of these factors are discussed in the final section in this chapter.

Conclusions

The most important observation in this study is that the elastic behavior of suction caisson is actually quite different from a rigid caisson. However, the previous researches had assume that the caisson was rigid when loaded in soft soils. The ultimate capacity is unaffected by elastic effects; however, at lower displacement or loading levels, the flexible caisson has a markedly more compliant behavior compared with a rigid caisson. This finding is very valuable for caisson design when under service loads instead of strength or ultimate load conditions.

The structural response of caisson also significantly affected by elasticity of the caisson. The maximum shell stress and bending moment in a flexible caisson occur at

the loading point. The stress and moment level obtained from an analysis that considers the elastic interaction between soil and caisson is much higher than that which occurs when structural analysis of the caisson is based on soil stress distributions corresponding to a rigid caisson.

In addition, this study presented a very time-efficient finite element method of using springs elements instead of continuum soil elements. By using the newly developed caisson-springs model, a 3-D analysis computing time reduced dramatically from hours to a few minutes, which greatly enhance the efficiency of evaluations. Taking the advantage of the caisson-springs model, it can be easily used to assess caisson structural response under different soil and caisson properties.

Recommendations

Potential for gap at the back side of the caisson

In this study, the spring properties were developed based on that assumption that there was no gap forming on the back side of the caisson. However, at shallow soil depth, it is very possible that the gap can be formed at the back side of the caisson particularly under long duration of monotonic loading. Studies need to be conducted to take this into consideration to generate springs that is useful to better evaluate the elastic behavior under this condition.

Effect of caisson tip resistance

The soil resistance at caisson tip could contribute significantly to overall load capacity for short caisson (small L/D). The short caisson studied in this analysis (L/D=3) did not take this into account. Therefore, it is not clear that how this factor will affect the elastic behavior of caisson compared with a rigid one. Studies need to be conducted to including this factor in the analysis for short caisson to understand the effect of tip resistance.

Calibration of the spring properties

The results of finite element analysis using coupled caisson-springs model under other setups, including soil profile, caisson stiffness, caisson dimensions, etc., need to be further confirmed with other continuum finite element analyses, laboratory testing results, or field testing results. Calibration of spring properties is a possible step if the results using springs based on the methodology described in this study are not in favorable agreement.

Complex spring properties for other loading conditions

The spring properties in this study were developed based on the 2-D finite element analysis. Therefore, the spring properties are valid for lateral direction, which means the coupled model is only appropriate to evaluate laterally loaded caisson and the vertical response cannot be simulated. However, the suction caisson foundation is very often under inclined and possibly torsional loading in real world practice. In order to

evaluate the suction caisson under more complex loading conditions and to take advantage of the efficiency of caisson-springs model, more complex springs with both lateral and vertical direction properties are needed.

As mentioned previously, in order to include the caisson tip resistance, the more complex mechanism and spring properties at caisson tip need to be investigated.

REFERENCES

Ahn, J., Lee, H., and Kim, Y.-T. (2014). "Holding capacity of suction caisson anchors embedded in cohesive soils based on finite element analysis." *International Journal for Numerical and Analytical Methods in Geomechanics,* 38(15), 1541-1555.

Allersma, H.G.B., Plenevaux, F.J.A, and Wintgens, J.-F.P.C.M.E. (1997). "Simulation of suction pile installation in sand in a geocentrifuge." *Proceedings of the 7th International Offshore and Polar Engineering Conference, May 25-30, 1997,* Honolulu, USA, 761-766.

Anderson, K.H., Jeanjean, P., Luger, D., and Jostad, H.P. (2005). "Centrifuge tests on installation of suction anchors in soft clay." *Ocean Engineering,* 32(7), 845-863.

Andréasson, B., Christophersen, H.P., and Kvalstad, T.J. (1988). "Field model tests and analyses of suction installed long-skirted foundations." *Proceedings of International Conference on Behavior of Offshore Structures, June, 1988,* Trondheim, Norway, Vol. 1, 243-257.

Aubeny, C.P., Han, S.W., and Murff, J.D. (2003a). "Inclined load capacity of suction caissons." *International Journal for Numerical and Analytical Methods in Geomechanics,* 27(14), 1235-1254.

Aubeny, C.P., Han, S.W., and Murff, J.D. (2003b). "Refined model for inclined load capacity of suction caissons." *Proceedings of the 22nd International Conference on Offshore Mechanics and Arctic Engineering, June 8-13, 2003,* Cancun, Mexico, 1-5.

Aubeny, C.P., Moon, S.K., and Murff, J.D. (2001b). "Lateral undrained resistance of suction caisson anchors." *International Journal of Offshore and Polar Engineering,* 11(3), 211-219.

Aubeny, C.P. And Murff, J.D. (2005). "Simplified limit solutions for the capacity of suction anchors under undrained conditions." *Ocean Engineering,* 32(7), 864-877.

Audibert, J.M.E., Clukey, E., and Huang, J. (2003). "Suction caisson installation at Horn Mountain - A case study history." *Proceedings of the 13th International Offshore and Polar Engineering Conference, May 25-30, 2003,* Honolulu, Hawaii, 762-769.

Bang, S. and Cho, Y. (2002). "Ultimate horizontal loading capacity of suction piles." *International Journal of Offshore and Polar Engineering,* 12(1), 56-63.

Bang, S., Jones, K., Kim, Y.S., and Kim, K.O., and Cho, Y. (2006). "Vertical pullout capacity of embedded suction anchors in sand." *Proceedings of the 16th International Offshore and Polar Engineering Conference, May 28-June 2, 2006,* San Francisco, California, 469-474.

Bemben, S.M., Kalajian, E.H., and Kupferman, M. (1973). "The vertical holding capacity of marine anchors in sand and clay subjected to static and cyclic loading." *Offshore Technology Conference, OTC 1912, April 30-May 2, 1973,* Houston, Texas, 871-880.

Broms, B.B. (1964). "Lateral resistance of piles in cohesive soils." *Journal of the Soil Mechanics and Foundations Division,* 90(2), 27-63.

Brown, G.A. And Nacci, V.A. (1971). "Performance of hydrostatic anchors in granular soils." *Offshore Technology Conference, OTC 1472, April 19-21, 1971,* Houston, Texas, 533-542.

Cao, J., Phillips, R., Popescu, R., Al-Khafaji, Z., and Audibert, J.M.E. (2002). "Penetration resistance of suction caissons in clay." *Proceedings of the 12th International Offshore and Polar Engineering Conference, May 26-31, 2002,* Kitakyushu, Japan, 800-806.

Cao, J., Phillips, R., Popescu, R., Audibert, J.M.E., and Al-Khafaji, Z. (2003). "Numerical analysis of the behavior of suction caissons in clay." *International Journal of Offshore and Polar Engineering,* 13(2), 154-159.

Cho, Y. and Bang, S. (2002). "Inclined loading capacity of suction piles." *Proceedings of the 12th International Offshore and Polar Engineering Conference, May 26-31, 2002,* Kitakyushu, Japan, 827-832.

Cho, Y., Bang, S., Karnoski, S.R., and Taylor, R.J. (2002). "Field validation of soil frictiontransition during suction pile installation." *International Journal of Offshore and Polar Engineering,* 12(4), 311-315.

Cho, Y., Bang, S., and Preber, T., (2002). "Transition of soil friction during suction pile installation." *Canadian Geotechnical Journal,* 39(5), 1118-1125.

Cho, Y., Lee, T.H., Park, J.B., Kwag, D.J., and Chung, E.S. (2002). "Field validation of suction pile installation in clay." *Proceedings of the Twelfth International Offshore and Polar Engineering Conference, May 26-31, 2002,* Kitakyushu, Japan, 815-819.

Cho, Y., Lee, T.H., Chung, E.S., and Bang, S. (2003). "Field tests on pullout loading capacity of suction piles in clay." *Proceedings of OMAE03, 22nd International Conference on Offshore Mechanics and Arctic Engineering, June 8-13, 2003,*

Cancun, Mexico, 1-7.

Clukey, E.C., Aubeny, C.P., and Murff, J.D. (2004). "Comparison of analytical and centrifuge model tests for suction caissons subjected to combined loads." *Journal of Offshore Mechanics and Arctic Engineering*, 126(4), 364-367.

Clukey, E.C., Gilbert, R.B., Andersen, K.H., and Dahlberg, R. (2013). "Reliability of suction caissons for deep water floating facilities." *Foundation Engineering in the Face of Uncertainty,* 456-474.

Clukey, E.C. and Morrison, M.J. (1993). "A centrifuge and analytical study to evaluate suction caissons for TLP applications in the Gulf of Mexico." *Geotechnical Special Publication (GSP)*, No. 38, 141-156.

Coffman, R.A., El-Sherbiny, R.M., Rauch, A.F., and Olson, R.E. (2004). "Measured horizontal capacity of suction caissons." *Offshore Technology Conference, OTC 16161, May 3-6, 2004,* Houston, Texas, 1-10.

Colliat, J.L. (2012). "Driven and suction anchor piles for two deepwater FPSO moorings." Offshore Site Investigation and Geotechnics: I*ntegrated Technologies – Present and Future, September 12-14*, London, UK, 607-612.

Colliat, J.L., Boisard, P., Sparrevik, P., and Gramet, J.-C. (1998). "Design and installation of suction anchor piles at soft clay site." *Journal of Waterway, Port, Coastal, and Ocean Engineering,* 124(4), 179-188.

Colliat, J.L. and Colliad, D. (2011). "Set-up of suction piles in deepwater Gulf of Guinea clays." *Proceedings of the 2nd International Symposium on Frontiers in Offshore Geotechnics, November 8-10,* Perth, Australia, 723-727.

Colliat, J.L., Dendani, H., and Schroeder, K. (2007). "Installation of suction piles at deepwater sites in Angola." *Proceedings of the 6th International Offshore Site Investigation and Geotechnics Conference: Confronting New Challenges and Sharing Knowledge, November 11-13, 2007*, London, UK, 413-420.

Dendani, H. And Colliat, J.L. (2002). "Girassol: Design analysis and installation of the suction anchors." *Offshore Technology Conference, OTC 14209, May 6-9, 2002,* Houston, Texas, 1-7.

Deng, W. and Carter, J.P. (2000). "Inclined uplift capacity of suction caissons in sand." *Offshore Technology Conference, OTC 12196, May 1-4, 2000,* Houston, Texas, 1-12.

Deng, W. and Carter, J.P. (2002). "A theoretical study of the vertical uplift capacity of suction caissons." *International Journal of Offshore and Polar Engineering,* 12(2),

89-97.

Dendani, H. (2003). "Suction anchors: Some critical aspects for their design and installation in clayey soils." *Offshore Technology Conference, OTC 15376, May 5-8, 2003,* Houston, Texas, 1-7.

El-Gharbawy, S.L. (2007). "Verification of suction caisson design model using the finite element method." *Offshore Technology Conference, OTC 18813, April 30-May 3, 2007,* Houston, Texas, 1-11.

El-Gharbawy, S.L., and Olson, R.E. (1998). "Laboratory modeling of suction caisson foundations." *Proceedings of the 8th International Offshore and Polar Engineering Conference, May 24-29, 1998,* Montréal, Canada, 537-542.

El-Gharbawy, S.L., and Olson, R.E. (1999). "The cyclic pullout capacity of suction caisson foundations." *Proceedings of the 9th International Offshore and Polar Engineering Conference, May 30-June 4, 1999,* Brest, France, 660-667.

El-Gharbawy, S.L. And Olson, R.E. (2000). "Modeling of suction caisson foundations." *Proceedings of the 10th International Offshore and Polar Engineering Conference, May 28-June 2, 2000,* Seattle, Washington, 670-677.

El-Gharbawy, S.L., Olson, R.E., and Scott, S.A. (1999). "Suction anchor installations for deep Gulf of Mexico applications." *Offshore Technology Conference, OTC 10992, May 3-6, 1999,* Houston, Texas, 1-8.

Fakharian, K. And Iraji, A. (2010). "Numerical modeling of suction pile installation in Caspian Sea clay effective and total stress analyses." *International Journal of Offshore and Polar Engineering,* 20(4), 313-320.

Gao, Y., Qiu, Y., Li, B., Li, D., Sha, C., and Zheng, X. (2013). "Experimental studies on the anti-uplift behavior of the suction caissons in sand." *Applied Ocean Research,* 43, 37-45.

Hansen, J.B. (1961). "The ultimate resistance of rigid piles against transversal forces." *Geoteknisk Institut,* Bulletin No. 12, 5-9.

Helfrich, S.C., Brazill, R.L., and Richards, A.F. (1976). "Pullout characteristics of a suction anchor in sand." *Offshore Technology Conference, OTC 2469, May 3-6, 1976,* Houston, Texas, 501-506.

Hogervorst, J.R. (1980). "Field trails with large diameter suction piles." *Offshore Technology Conference, OTC 3817, May 5-8, 1980,* Houston, Texas, 217-224.

Houlsby, G.T., Kelly, R.B., Huxtable, J., and Byrne, B.W. (2005). "Field trial of suction caissons in clay for offshore windturbine foundations." *Géotechnique 55, No.4,* 287-296.

House, A.R., Randolph, M.F., and Borbas, M.E. (1999). "Limiting aspect ratio for suction caisson installation in clay." *Proceedings of the 9th International Offshore and Polar Engineering Conference, May 30-June 4, 1999,* Brest, France, 676-683.

Jeanjean, P. (2006). "Setup characteristics of suction anchors for soft Gulf of Mexico clays: Experience from field installation and retrieval." *Offshore Technology Conference, OTC 18005, May 1-4, 2006,* Houston, Texas, 1-9.

Jiao, B., Lu, X., Zhao, J., Wang, A., Shi, Z., and Zeng, X.H. (2009). "Experimental study on the bearing capacity of suction caissons in saturated sand." *Proceedings of the 9th International Offshore and Polar Engineering Conference, June 21-26, 2009,* Osaka, Japan, 202-206.

Kim, K.S., Kwon, O., Oh, M., and Kim, T. (2013). "Penetration mechanism of suction bucket foundation in laboratory model test." *Proceedings of the 23rd International Offshore and Polar Engineering Conference, June 30-July 5, 2013,* Anchorage, Alaska, 461-464.

Kim, Y., Kim, S., Park, J., Kim. S., Kim, H., and Kim, K. (2001). "A centrifuge study of suction pile installation in sand." *Proceedings of the 11th International Offshore and Polar Engineering Conference, June 17-22, 2001,* Stavanger, Norway, 615-619.

Kim, Y., Kim, T., Kim, K., Lee, J., and Bak, J. (2013). "Centrifugal model behavior of laterally loaded suction pile." *Proceedings of the 23rd International Offshore and Polar Engineering Conference, June 30-July 5, 2013,* Anchorage, Alaska, 444-447.

Larsen, P. (1989). "Suction anchors as an anchoring system for floating." *Offshore Technology Conference, OTC 6029, May 1-4, 1989,* Houston, Texas, 535-540.

Luke, A.M., Rauch, A.F., Olson, R.E., and Mecham, E.C. (2005). "Components of suction caisson capacity measured in axial pullout tests." *Ocean Engineering,* 32(7), 878-891.

Murff, J.D. And Hamilton, J.M. (1993). "P-ultimate for undrained analyses of laterally loaded piles." *Journal of Geotechnical Engineering,* Vol. 119, No. 1, 91-107.

Newlin, J.A. (2003a). "Suction anchor piles for the Na Kika FDS mooring system, Part 1: Site characterization and design." *Deepwater Mooring System,* 28-54.

Newlin, J.A. (2003b). "Suction anchor piles for the Na Kika FDS mooring system,

Part 2: Installation performance." *Deepwater Mooring System,* 55-75.

Randolph, M.F. and Houlsby, G.T. (1984). "The limiting pressure on a circular pile loaded laterally in cohesive soil." *Géotechnique,* 34(4), 613-623.

Randolph, M.F. And House, A.R. (2002). "Analysis of suction caisson capacity in clay." *Offshore Technology Conference, OTC 14236, May 6-9, 2002,* Houston, Texas, 1-11.

Rao, S.N., Ravi, R., and Ganapathy, C. (1997). "Pullout behavior of model suction anchors in soft marine clays." *Proceedings of the 7th International Offshore and Polar Engineering Conference, May 25-30, 1997,* Honolulu, USA, 740-744.

Senpere, D. and Auvergne, G.A. (1982). "Suction anchor piles - A proven alternative to driving or drilling." *Offshore Technology Conference, OTC 4206, May 3-6, 1982,* Houston, Texas, 483-493.

Sparrevik, P. (2002). "Suction pile technology and installation in deep water." *Offshore Technology Conference, OTC 14241, May 6-9, 2002,* Houston, Texas, 1-9.

Supachawarote, C., Randolph, M, and Gourvence, S. (2004). "Inclined pull-out capacity of suction caissons." *Proceedings of the 14th International Offshore and Polar Engineering Conference, May 23-28, 2004,* Toulon, France, 500-509.

Taiebat, H.A. And Carter, J.P. (2005). "Interaction of forces on caissons in undrained soils." *Proceedings of the 15th International Offshore and Polar Engineering Conference, June 19-24, 2005,* Seoul, Korea, 625-632.

Tjelta, T.I. (1995). "Geotechnical experience from the installation of the Europipe jacket with bucket foundations." *Offshore Technology Conference, OTC 7795, May 1-4, 1995,* Houston, Texas, 897-908.

Tjelta, T.I. (2001). "Suction piles: Their position and application today." *Proceedings of the 11th International Offshore and Polar Engineering Conference, June 17-22, 2001,* Stavanger, Norway, 1-6.

Tjelta, T.I. and Guttormsen, T.R. (1986). "Large-scale penetration test at a deepwater site." *Offshore Technology Conference, OTC 5103, May 5-8, 1986,* Houston, Texas, 201-212.

Vásquez, L.F.G., Maniar, D.R., and Tassoulas, J.L. (2010). "Installation and axial pullout of suction caissons: Numerical modeling." *Journal of Geotechnical and Geoenvironmental Engineering,* Vol. 136, No. 8, 1137-1147.

Villalobos, F.A., Byrne, B.W., and Houlsby, G.T. (2010). "Model testing of suction

caissons in clay subjected to vertical loading." *Applied Ocean Research,* 32(4), 414-424.

Whittle, A.J and Germaine, J.T. (1998). "Behavior of miniature suction caissons in clay." *Offshore Site Investigation and Foundation Behavior, September 22-24, 1998,* London, UK, 279-300.

Zhou, H. and Randolph, M.F. (2006). "Numerical simulation of caissons installation in clay by suction and by jacking." *Proceedings of the 16th International Offshore and Polar Engineering Conference, May 28-June 2, 2006,* San Francisco, California, 588-595.